LOW POWER ENERGY HARVESTING WITH PIEZOELECTRIC GENERATORS

by

Sunghwan Kim

B.S. in Mechanical Engineering, Inha University, 1992

M.S. in Mechanical Engineering, University of Pittsburgh, 1996

Submitted to the Graduate Faculty of

School of Engineering in partial fulfillment

of the requirements for the degree of

Doctor of Philosophy

University of Pittsburgh

2002

UNIVERSITY OF PITTSBURGH

SCHOOL OF ENGINEERING

This dissertation was presented

by

Sunghwan Kim

It was defended on

December 11, 2002

and approved by

Dr. Qing-Ming Wang, Assistant Professor of Mechanical Engineering Department

Dr. Roy D. Marangoni, Associate Professor of Mechanical Engineering Department

Dr. Jeffrey S. Vipperman, Assistant Professor of Mechanical Engineering Department

Dr. Marlin H. Mickle, Professor of Electrical Engineering Department

Dissertation Director: Dr. William W. Clark, Associate Professor of Mechanical Engineering Department

ABSTRACT

LOW POWER ENERGY HARVESTING WITH PIEZOELECTRIC GENERATORS

Sunghwan Kim, PhD

University of Pittsburgh, 2002

Energy harvesting using piezoelectric material is not a new concept, but its generation capability has not been attractive for mass energy generation. For this reason, little research has been done on the topic.

Recently, concepts such as wearable computers, as well as small portable electrical devices have re-ignited the study of piezoelectric energy harvesting. The theory behind cantilever type piezoelectric elements is well known, but transverse moving diaphragm elements, which can be used in pressure type energy generation have not been yet fully developed. Power generation in a diaphragm depends on several factors. Among them, the thickness of each layer, the poling direction, and stress distribution are most important. In this thesis, unimorph and triple-morph diaphragm structures with various poling configurations were considered. Their energy generation was calculated with varying thickness ratios and poling directions at various locations using piezoelectric constitutive equations. The results of this analysis are presented, along with experimental results that indicate that an optimal electrode pattern will result in maximum electrical energy generation.

TABLE OF CONTENTS

LIST OF TABLES

LIST OF FIGURES

NOMENCLATURE

Notation	Description	Units
g_{ij}	Piezoelectric constant, Voltage constants,	*Vm/N*
d_{ij}	Piezoelectric constant, Charge constant, or Strain constant	*m/V, C/N*
h	piezoelectric constant	*V/m*
β_{ij}	Impermeability constant	*m/F*
s_{ijkl}	Elastic compliance constant	m^2/N
c_{ijkl}	Elastic stiffness constant	N/m^2
T_{ij}	Mechanical stress	N/m^2
S_{ij}	Mechanical strain	
E_i	Electric field strength	*V/m*
D_i	Electric charge density	C/m^2
E, superscript	Constant electric field	
D, superscript	Constant charge density	
S, superscript	Constant strain	
T, superscript	Constant stress	
ε	Mechanical strain	
σ	Mechanical stress	N/m^2
ϵ_{o}	Permittivity in free space, dielectric constant in vacuum	*F/m*
ϵ_{ij}	Permittivity constant, dielectric constant	*F/m*

Notation	Description	Units
U	Energy	J
C	Capacitance	F
h_p	Piezoelectric layer thickness	m
h_m	Substrate layer thickness	m
Q	Charge	C
F	Force	N
M	Moment	$N\,m$
A	Area	m^2
ρ	Curvature	$1/m$
x,y,z	Axis	m
z_o	Location of neutral surface	m
W,L	Width and Length	m
a	Radius of the diaphragm	m
b	Width of the electrode	m

1.0 INTRODUCTION

Energy has been essential in building up modern society. It is required everywhere from the household light bulb to a mission to Mars. Some energy can be seen, light for example, but most does not have a visible form. Energy is defined in several ways, such as mechanical, electrical, and chemical. All of these definitions are based on where the energy is stored.

Energy is stored everywhere. Heat, electricity, dynamic, chemical, photo and biomass forms of energy are all stored differently, but these can be converted from one to the other. Among many types of energy, electricity is the most commonly used form for modern devices because it is easy to convert to other types. The term “power generation” commonly refers to energy conversion from other energy forms to electrical energy.

There are many ways to complete electrical conversions. Photocells convert light to electricity, thermocouples convert heat to electricity, and magneto-electric generators convert mechanical energy to electricity. These are all called power generators and are frequently used in electricity generation. Similar to magneto-electric generators, piezoelectric generators (PEG) can also convert mechanical energy to electrical energy.

Piezoelectric power generators (PEG) have many advantages over other conversion methods. PEG’s consist of piezoelectric ceramics, and electrodes which cover them. Because of their simplicity, PEG’s can even be made small enough to fit inside of micro electromechanical systems (MEMS). Another advantage is that the lifetime of the system is almost unlimited if the applied force and external temperature are within the operational range. Unlike the power generation methods that rely on heat conversion, a PEG presents no problems such as heat isolation. In addition, the mechanical energy required for conversion can conceivably be obtained from the PEG's environment. Even with these advantages, PEG's have been neglected for power generation because of the small electrical output.

Recently, PEG is have regained interest in the power generation field for portable and low power consuming devices. The merit of applying PEG's to these devices is that they can reduce the battery weight and possibly make the device self-powered by harvesting mechanical energy. To maximize these advantages, there are problems to resolve such as how to design the PEG in order to optimize its electrical energy production. To answer this question, the electrical-mechanical characteristics of piezoelectric materials must be revisited.

In this research, investigations of mechanical elements such as stacks, beams, and circular plates will be carried out to analyze their suitability for piezoelectric energy generation. Our interest is in determining the factors that lead to maximum electrical energy generation in relation to a given volume of material or applied mechanical force, pressure, or stress.

In the next chapter, we will briefly discuss previous research in the general area of energy generation and harvesting. Next we will survey different possible configurations of piezoelectric energy generators, followed by detailed mathematical modeling of these configurations that result in relationships between applied force (or pressure) and generated electrical energy. Following the mathematical modeling will be a discussion of the models, including some numerical results that highlight the strengths and weaknesses of the various PEG configurations.

A set of experiments was completed which support the theoretical results for a diaphragm PEG. These tests are presented, along with their results. Finally some conclusions are presented from the research, along with some discussion of reasonable future research directions.

2.0 LITERATURE REVIEW

The piezoelectric effect was first discovered by Curie. As a word described by itself, piezo means pressure, while electric refers to electricity. That is, when crystals are pressurized, an electric field is generated. Curie found that voltage can be seen when the crystals are pressed, this is called the piezoelectric effect. These electric fields were quite small and not very useful until the LiTiBa ceramic was found. After the introduction of the LiTiBa ceramic, the piezoelectricity performance was increased and widely used as an electric device. One of the most common areas is resonators.

Piezoelectric material works both ways. The electric power can be used to generate force or deflection and also, deflection or force can generate electric power. With a usual piezoelectric ceramic, the deflection with an electrical energy input is almost invisible to the naked eye. To increase the deflection, a stacked device, or bender device, is used. In the sensor application, conventional diaphragm designs or sometimes spring mass damper designs are used. They are only used to measure the voltage generation.

Until recently, the piezoelectric generator (PEG) was not popular as a power generator because of its small power generation. Modern electrical devices are getting smaller and require smaller amounts of electrical energy. Before too long, people will be wearing computers like hats, and these wearable computers will not require much power.

With current technology, the power requirement for low power microprocessors is only about 1mW [21], and is possible with PEGs. Unfortunately, design problems still remain.

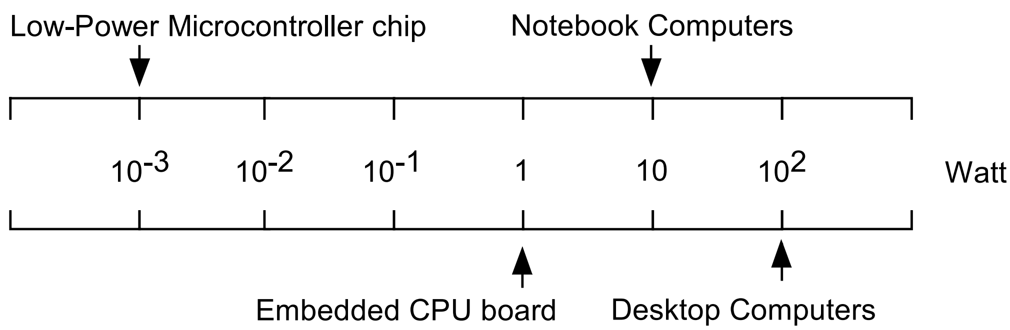

Figure 1. Energy Requirements [21]

Humans themselves are also involved with energy converters. We convert food to energy for body requirements such as breathing and walking. Theoretically, humans can generate sufficient electrical power with ordinary movements. With effective means of utilizing energy harvesting devices, people will not need batteries to operate portable electrical devices. This will be a tremendous help for those patients who require an operation just to replace a battery. For example, walking can generate 5.0-8.3 W, while breathing creates 0.2W of power [21].

Power generation

Power generation is the act of collecting electrons at a useful electric potential. Free electrons, which can be collected, are found everywhere inside of conductive material. There is an almost infinite number of free electrons in even small sizes of conductive material. In common power generation, power is not actually generated, but converted to electrical energy from other energy forms. The following are major energy conversion methods that are currently being used.

Thermal to electrical

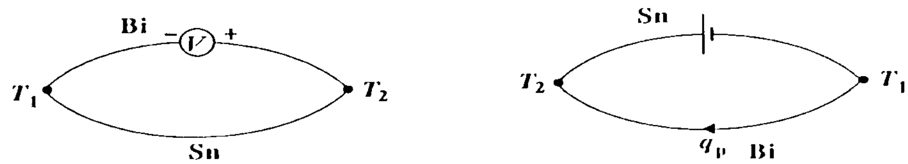

Figure 2. Left : Seebeck Effect, Right: Peltier Effect

Thermocouple effects were first found to convert the heat difference between two conjunctions of two different materials to electrical energy. This effect was discovered by T.J. Seebeck (1770-1881) and is called the Seebeck effect or the thermocouple effect. The opposite is also true and was discovered by J. Peltier (1785-1845). These thermocouples are currently built with P type and N type silicon to make either a cooling device or an energy harvesting device such as a power source of a pacemaker using nuclear battery[12].

One other famous heat converter is the Alkali Metal Thermal to Electric Converter (AMTEC). AMTECs were recently developed by J.T. Kummer and N. Weber in 1968. Its performance is comparable to the thermocouple (TE) or thermo photo voltaic (TPV). Currently, much research has been done to replace old thermocouple applications where large heat energies are available[17]. Most commonly mentioned applications are large power required remote missions such as those in space programs and remote military installation with radioisotope as a heat source[18]. This AMTEC technology has already been adopted by US space program, and some are already operational[10]. AMTEC is also replacing solar cell applications such as solar cell powered satellites and solar cell power stations[11].

AMTECs are very good for generating energy from a heat source, but it requires large amounts of heat and complex mechanisms. From the DOE standard, the AMTEC heat source requirement is around $900^{O}C$ [10].

Photon to electrical

Photovoltaic cells (PV) are commonly known as solar cells. When the photon hits the PV, electrons move to a high potential and create energy. PVs are well developed and are widely used in applications from wristwatches to power stations. PVs can also be fabricated in small sizes, but require an open window for a photon source. There is another type, TPV, that is a combination with a TE. Those photovoltaic cells and thermocouples are used to convert both photo and heat source to electrical energy. The efficiency is higher compared to the photovoltaic or the thermo voltaic cell. Even those TPV cell's efficiency is higher than its predecessors, it requires a higher operating temperature. Usual operation temperatures range from $1000^{O}C \sim 1300^{O}C$ [32] and mostly used for the space applications

Chemical to electrical

The most common electrical energy sources for current daily life are batteries. Chemical reactions create electrons, and some batteries are able to store these electrons. Other than batteries, another source is the fuel cell. Fuel cells convert fuel (eg. H_2) and O_2 gas to electrical energy and water. Mechanisms are complex, yet great for large power generation. Fuelcells have only recently been applied to industries to generate energy, and require more research.

Mechanical to electrical

There are not many energy conversion techniques for dynamic energy. The most common power generation is a turbine type electro magnetic generator. Almost all current power stations have this facility. Nuclear, coal, gas, and hydraulic power station convert heat energy to a turbine rotating dynamic energy. This energy is then converted to electrical energy. Magneto electrical devices can be used in MEMS technology using micro-turbine; but require a complex design and also requires fuel.

Other than magneto electrical energy conversion, there is a theoretical magneto hydrodynamic power generator (MHD) and a piezoelectric generator (PEG). MHDs were invented by M. Faraday. It is not useful as a portable power source because of its very high temperature requirement (2000K)[23]. Meanwhile, PEGs have not been considered until recently because of their low power generation capabilities. Usually, piezoelectric ceramics are used for active devices (eg. diaphragm) or signal devices (sensor, resonator). Among the previous energy conversion techniques, PV, TE, and PZT are good for the portable wearable devices, which do not require large amounts of power.

PVs and TEs have been studied for large applications and are currently being used. Solar panels are a well known PV, and are used for small hand calculators to huge powers station. TE applications are not used often because of the operational temperature requirements. A currently researched TE application is the hand held personal scheduler (PAM). As we know, PZT devices are not complex. All that is needed is the electrode on the PZT and a mechanical energy source. For this reason, it is very good for the micro or nano scale devices.

PVs and TEs can be a good power source for wearable computers[16], but the PEG is more attractive for the embedded devices such as MEMS. Even though PEGs are a sufficient energy harvesting device, there are still problems that exist. These problems are design and performance oriented.

Both piezoelectric ceramics and magneto electrical devices can convert kinetic energy to electrical energy, but PEGs have more advantages as long as power requirements are met. Initially, PEGs do not have a complex system as a turbine does. Secondly PEGs can be packaged in a closed form. Finally, no fuel or no rotating shafts are required to convert energy.

Previously, research has been conducted about various loading conditions, such as impact and resonance. They claim that PEGs lose performance under the resonance forcing condition [6] or the impact forcing condition [1,4, 8].

Actual implementation about energy harvesting from human movement was applied [5, 7]. They attached thunder™ actuators to sneakers to harvest energy. Polymer type piezoelectric material (PVF_2) was also investigated for the electrical energy conversion purpose [31]

Some research was also done for acoustic isolator application. They used two diaphragms to control noise. One was for energy harvesting, while the other was a control actuator which uses harvested energy from the other diaphragm [30].

For numerical calculations, a great amount of research has been done. The constitutive equations established the electrical and mechanical coupling in the PZT ceramics [29] and multiple layered cantilever beams equations for actuators [24,26,27] and sensors [25].

3.0 A SURVEY OF PIEZOELECTRIC ENERGY GENERATOR CONFIGURATIONS

In this chapter, we review the many different forms of piezoelectric generators. Many of these configurations are motivated by existing actuator designs. They are presented here to provide a working foundation for the mathematical modeling in the next chapter, and to highlight important features that distinguish each design.

It should be pointed out that while there are many piezoelectric materials from which to choose for a PEG, we plan to use lead zirconite titanate (PZT). So from this point on, the words PZT and piezoelectric may be used interchangeably, although, it is understood that except when referring to specific PZT material constants, other piezoelectric materials could be assumed to be used.

3.1 Charge Generation with Piezoelectric Material

Electro magnetic generators use electro magnetic force to move free electrons in a coil around the permanent magnet rotator. Piezoelectric material, which is used as a non-conductive material, does not have free electrons, and therefore electrons cannot pass freely through the material. Piezoelectric ceramics do not have free electrons, but are made up of crystals that have many "fixed" electrons. These fixed electrons can move slightly as the crystals deform by an external force. This slight movement of electrons alters the equilibrium status in adjacent conductive materials and creates electric force. This force will push and pull the electrons in the electrodes attached to the piezoelectric crystal as shown in Figure 3.

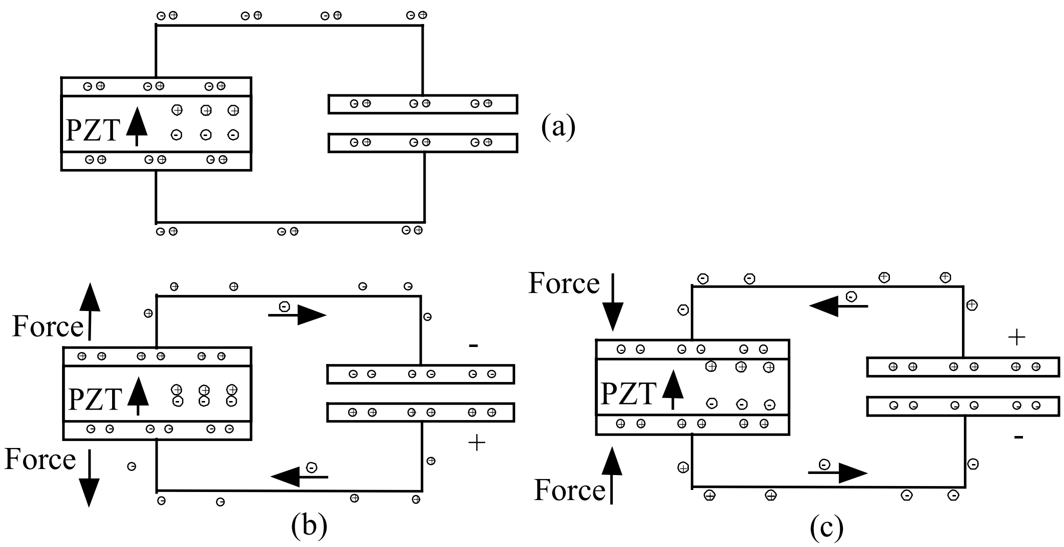

Figure 3 Schematics of The PEG Illustrating The Movement of Charge Due to Applied Force: (a) when no force applied (b) when tensile force applied (c) when compressive force applied

Both magnetic and piezoelectric generators work similarly (Figure 4). Magnetic generators use mechanical energy to change the magnetic field. This changing magnetic field creates force to move the free electrons. In piezoelectric generators, free electrons move by changing the electric field "inside" of the crystal.

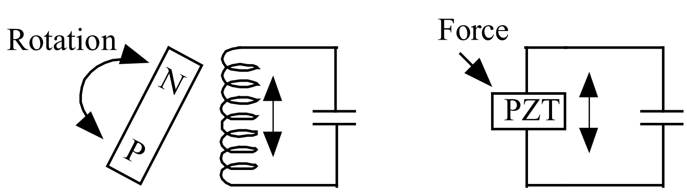

Figure 4. Magneto Electric Generator vs. Piezoelectric Generator (PEG)

Dielectric properties are observed on piezoelectric ceramics. Those positively charged atoms are not in the center of the crystal, creating a charge dipole. The direction from the center to the positively charged atom is called the poling direction and in general is randomly distributed throughout the polycrystalline piezoceramic, as shown in Figure 5 (a). This poling direction can be modified by heat and voltage conditions. Piezoelectric crystals have their own temperature characteristics, known as Curie temperature. Common piezoelectric material has its own specific Curie temperature. Once the piezoelectric material is heated above Curie temperature, it loses its polarity and a new poling direction will appear by the application of the voltage across the piezoelectric material. The new poling direction appears along the applied voltage (Figure 5 (b)).

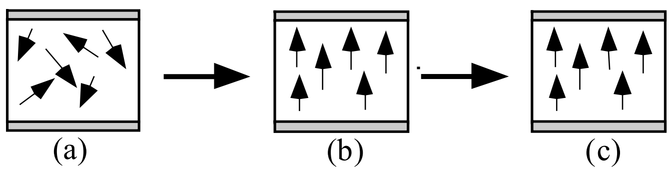

Figure 5. Poling process: (a) Before poling (b) Apply voltage through the electrode at above Curie temperature (c) Remove external voltage and cool down

The polling direction is a very important property in piezoelectric material. Depending upon the poling direction, the input-output relations change.

The most important relation for piezoelectric energy harvesting is between stress and charge, and is defined as a constant d. This "d" value is constant when static loading is applied, but changes when near a resonance application. For the static case, the open circuit charge generation relation is

$$D_{ij} = d_{ijk}\sigma_{lk} \tag{3.1}$$

where D is the charge per area, and σ is the applied stress. The subscripts i and j range from 1 through 6 and can be replaced by certain rules. When longitudinal stresses are in the system, the above relation can be rewritten as

$$D_3 = d_{31}\sigma_{11} \tag{3.2}$$

The first subscript stands for the surface, while the second subscript stands for the direction as defined in the general elasticity subscription rule. For piezoelectric constants, the first subscript shows the polling direction and the second subscript shows the direction of the applied force or field. Finally, the subscript of *D* represents the surface direction of the electrode. D_3 means that charge is collected on the electrodes, that are covering the surface of piezoelectric material normal to the 3-direction (shown in Figure 6, where P represents the poling direction).

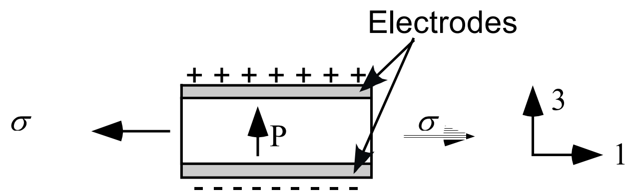

Figure 6. 31-Direction: Force at 1-direction and electrode on 3-surface

Common piezoelectric materials (4mm or 6mm class crystal) have 5 piezoelectric (*d* or *g*) constants (d_{31}, d_{32}, d_{33}, d_{15}, d_{24}). Other than these directions, all the remaining constants are zero. In a 4mm class ceramic (which will be considered in this work), there are more constraints. The constant d_{31} is the same as d_{32}, while d_{15} is the same as d_{24}. Therefore, there are only three distinct piezoelectric constants. The magnitude relation of these three constants is $d_{15} > d_{33} > d_{31}$. In a common piezoelectric material, d_{33} is about twice as large as d_{31}, and d_{15} is five times larger than d_{31}. Even though d_{15} is the largest number, which means that the 15 shear force can generate more energy than other force applications, this 15 direction is the shear stress as shown in Figure 7, which is difficult to realize in a real structure.

$$D_1 = d_{15}\sigma_{13} \tag{3.3}$$

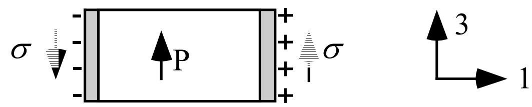

Figure 7. 15-Direction: Electrodes on 1-surface and shear stress

The next largest number is the 33 direction shown in Figure 8 and is also difficult to implement in a real structure.

$$D_3 = d_{33}\sigma_{33} \tag{3.4}$$

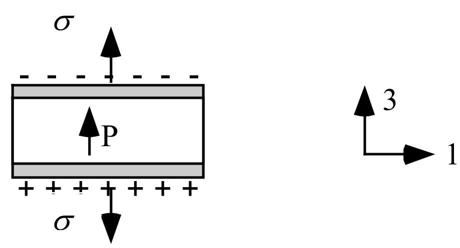

Figure 8. 33-Direction: Electrodes are on 3 surface and force along 3 axis

Currently available 33-direction devices are stack actuators and interdigital actuators. With a single plate of piezoelectric material, the displacement along the 3-direction is very small and is not good for the actuator purpose. On the other hand, using multi-layered 33-direction piezoelectric plates, the device can create a reasonable range of actuation by summing the effects of individual plates. This kind of actuator is called a stack actuator. Stack actuators use the 33-direction as shown in Figure 9, but the size is not good for small applications.

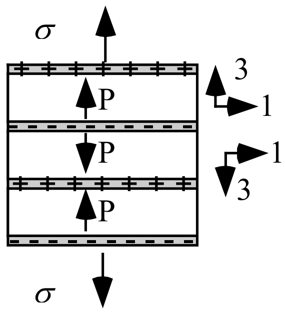

Figure 9. Poling direction and electrodes in piezoelectric stack

In a real structure, the constant stress conditions that are depicted in Figure 6-Figure 9 are rare. If the stress distribution is not constant, the electrical distribution will not be constant. For example, consider the following stress condition in Figure 10. Compression occurs at the upper electrode, while expansion occurs at the lower electrode.

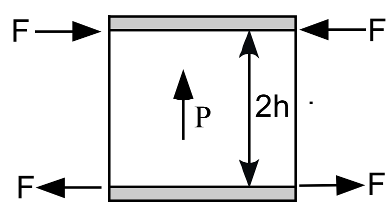

Figure 10. Piezoelectric material with complex stress condition (Bending)

If this system is symmetric and the applied forces are the same magnitude in opposite directions, both the upper and lower electrodes will have the same electric potential (Figure 11). That is, a voltage difference will not be seen between the electrodes. Thus, energy cannot be harvested using this force condition.

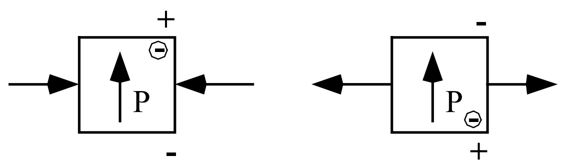

Figure 11. Relation between Voltage, Poling direction and Force

The numerical relation between the electric field and the stress is

$$E_3 = -g_{31}\sigma\left(x_3\right) \tag{3.5}$$

where g_{31} is the piezoelectric constant, and x_3 is thickness direction axis. Thus the voltage between these electrodes of Figure 10 is

$$V = \int_{-h}^{h} -g_{31}\sigma\left(x_3\right)dx_3 = 0 \tag{3.6}$$

This result must also agree with FEM results. Current FEM packages work well for actuator designs. Though, in the energy generation calculation, it becomes difficult because of the boundary conditions. Unlike the actuator design, the electric potential is unknown on the electrodes. Furthermore, the electric potential should have the same value on the corresponding electrode.

Generated electric potential on the piezoelectric material and the electric potential on the electrodes might have different values. This difference can act as another boundary condition to the piezoelectric material. Therefore, the electric potential is constant between electrodes whether there is a stress distribution or not.

3.2 33-type Stacked Piezoelectric Device

Generally piezoelectric devices cannot create large deformations. It is almost impossible to detect the deformation with the bare eye. And this normal size piezoelectric device produces relatively large strain at very high electric field. This small micro-scale deformation with very high electric field requirement and the material's brittle characteristic prevent popular use of the device material for strain generation. To overcome this disadvantage of piezoelectric devices, the stacked device was introduced. This stacked device can produce the same strain with a low electric field. A piezoelectric stack actuator is made of a large number of thin piezoelectric plates that are glued together and wired in parallel. The device actuation direction is the 33-direction (force and poling directions are the same). So n times more performance can be obtainable where n is the number of piezoelectric layers. For this reason, piezoelectric stack actuator is the most common force-generating device. The disadvantages in the stacked piezoelectric device are 1) lateral force must be avoided, and 2) volume is relatively large.

For the piezoelectric stack as a PEG, the stacked piezoelectric can convert only longitudinal direction compressive force to electric energy as shown in Figure 12. A stack PEG can generate charge only when pressed along the longitudinal direction. If a compressive prestress is applied to the stack to prevent fracture in both piezoelectric and glued layer, then the applied force can be either tensile or compressive. That means a stack piezoelectric can not generate electrical energy with bending lateral force, and if there are only lateral forces, PEG requires an external casing to convert the lateral force to longitudinal force. In addition, small sized stacked devices are hard to fabricate. For the power generation purpose, magneto electric generators perform better than same sized stack PEG.

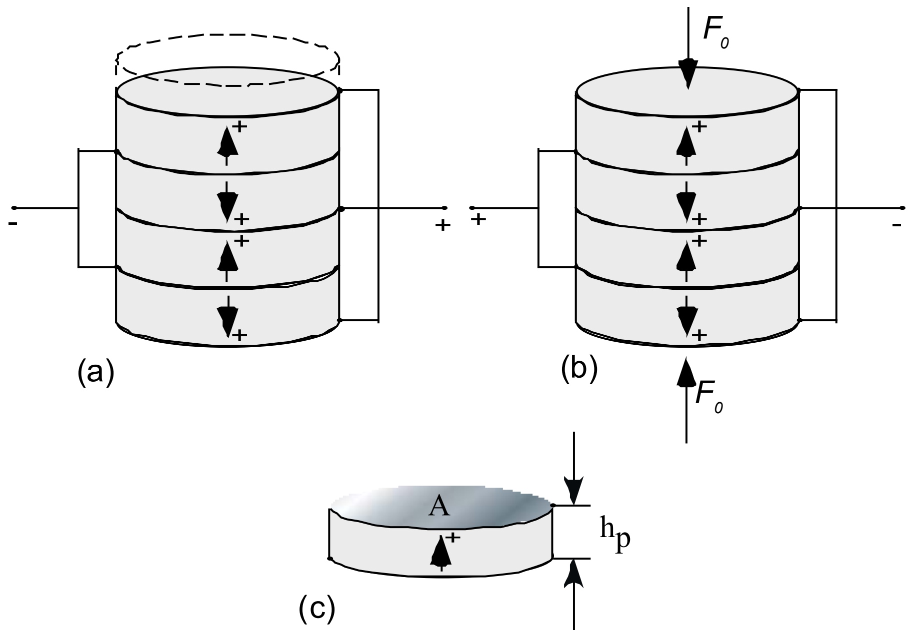

Figure 12. Piezoelectric stack actuator/generator configuration and poling direction (a)Actuator: Electrical to mechanical conversion (b) PEG: Mechanical to electrical conversion (c) Single layer

3.3 31-type Piezoelectric Device

Another common piezoelectric actuator/generator is the cantilever beam. Cantilever benders can generate significant deflection compared to the longitudinal direction cantilever actuators, and can be found in applications such as micro valves. For the energy harvesting purpose, cantilever benders can be good generators because it is easier to convert force into high stress compared to stack PEGs.

Multilayer cantilever beams are common mechanical bending elements and are widely used. They are usually called bimorph cantilever or triple morph cantilever depending on the number of layers. Bimorph cantilever (Figure 13) PEGs contain a piezoelectric layer that is bonded to a layer of non-piezoelectric material. A triple morph is made with two piezoelectric layers on the outside and one non-piezoelectric material in the middle. Note that Figure 13 shows both 31 and 33 type unimorphs.

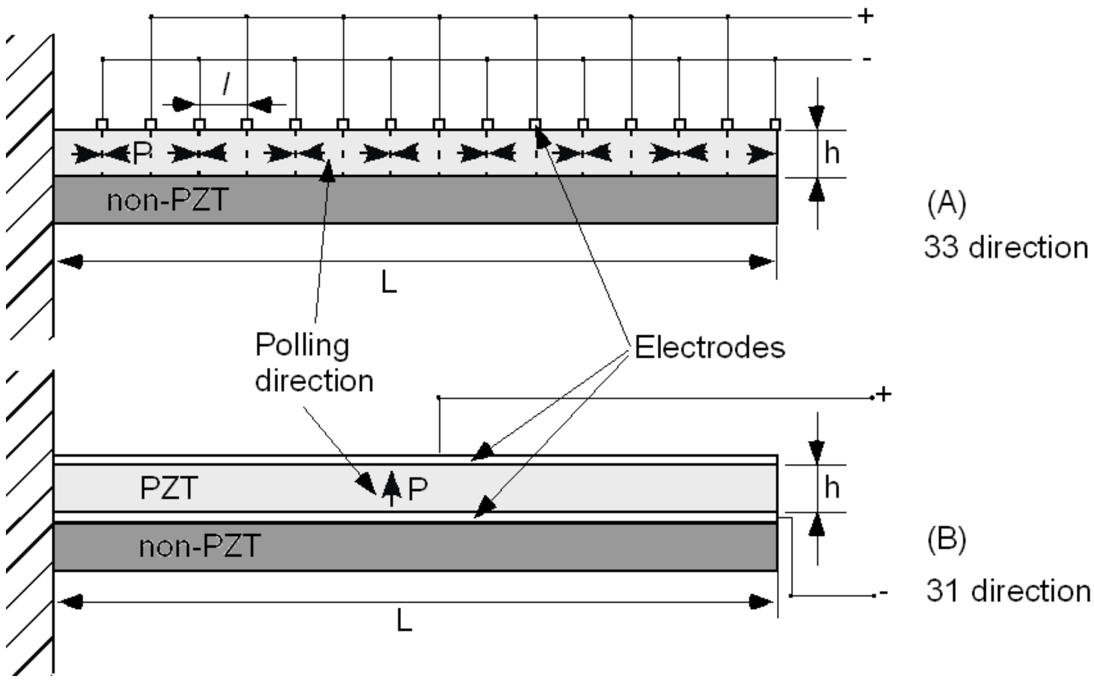

Figure 13. Unimorph cantilever bender

The mechanism of cantilever bender is simple. One layer is generally in tension and the other layer is in compression. One example of a unimorph cantilever example is a thermostat. Thermostats are made of two materials with different thermal expansion coefficients. Since one side of the beam is more sensitive to temperature changes, a unimorph cantilever will bend when temperature changes. In other words, one side expands or contracts more with temperature changes. In the piezoelectric unimorph cantilever beam, the piezoelectric layer side expands or contracts while the other non-piezoelectric side does not change with the applied electric field. The opposite effect is also true. When the unimorph cantilever beam undergoes bending, electric fields are generated between the electrodes of the piezoelectric layer. The PEG utilizes this opposite effect.

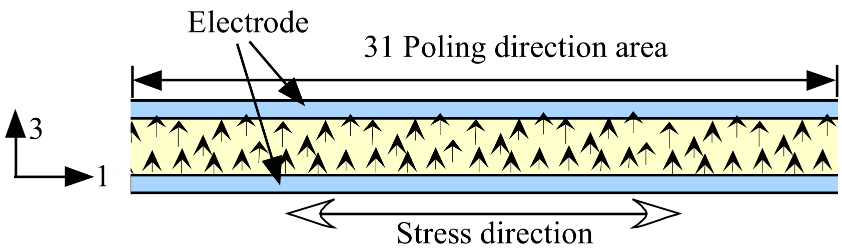

Figure 14. 31-Type conventional bulk PZT

General unimorph cantilevers and triple morph cantilevers are made of thin bulk piezoelectric patches. The poling direction of the bulk piezoelectric patch is perpendicular to the surface as shown in Figure 14 and Figure 13(B), thus the characteristics for the general cantilever beams are the 31-type piezoelectric. 31-type configuration is that the polling direction is perpendicular to the stress direction and electrode covers whole upper surface and bottom surface of the piezoelectric material. The 33 unimorph (Figure 13(A)) will be addressed specifically in the next two sections.

3.4 33-type Sliced Stack PZT

One way of making a 33-direction device and thereby obtain increased electromechanical coupling is to use existing stack actuators. A stack actuator's poling direction is 33, therefore it is a 33-direction device. These actuators operate in a longitudinal direction (orthogonal direction to layer). Common stack actuators are made with large numbers of thin piezoelectric disks that are glued together.

Each glued surface can be broken from an external twisting force. The triple layered bender can minimize this bonding break because the piezoelectric material can sustain large compression forces, but are very weak to extensional force conditions. By using the middle layer as a pre-stressed constraint layer, the piezoelectric layer undergoes compression all of the time.

Even though this 33 mode using bender is advantageous, it is almost impossible to fabricate into a long plate or beam because of the brittleness of the thin piezoelectric layer and also the bonding layer. For a thick plate, the slicing of a PZT stack actuator by mechanical means might be possible (Figure 15). Another disadvantage is that the sliced piezoelectric plate can only be used for a rectangular patch on certain structures such as cantilever bender, but cannot be used for diaphragm (circular plate) applications. An alternative option to this sliced stack PZT is a PZT plate with interdigitated electrodes.

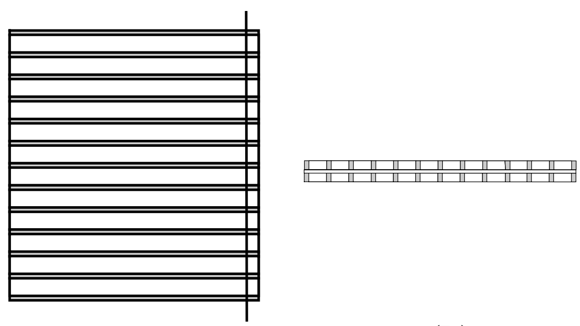

(A) (B)

Figure 15. (A) Cross section of PZT stack actuator, (B) Triple layered cantilever with sliced PZT stack actuator

3.5 Interdigitated Piezoelectric Device

Other than slicing and stacking piezoelectric, there is another way to make a 33-type device using polarization of the piezoelectric material. By using interdigitated electrodes, much of the material of a normal 31 patch can be made to act in the 33 mode. Interdigitated piezoelectric devices are a newly developed type, which are designed to increase the performance by changing the polling direction from 31 to 33. This kind of interdigitated piezoelectric device is currently available as a rectangular plate actuator.

In the interdigitated configuration, the polling direction is parallel to the stress direction and electrodes cover only a portion of the surface. Figure 16 shows the cross section of the interdigitated PEG segments.

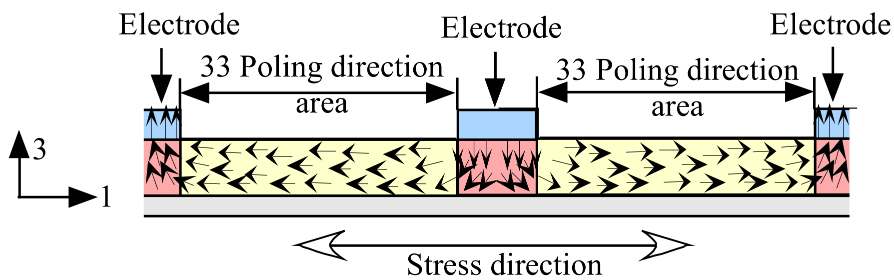

Figure 16. Interdigitated PZT (33-type)

As mentioned before, the 33-mode allows approximately twice the mechanical to electric energy conversion as the 31-mode of application. In the cantilever or diaphragm application, surface interdigitated electrodes are used to convert 31-polarization to 33-polarization and the same electrodes are used to generate electrical energy.

The mechanism of the interdigitated piezoelectric patch is quite simple, but the fabrication process will be described initially. This will be more helpful in understanding the mechanism. The poling direction is commonly perpendicular to the surface for most bulk piezoelectric thin plates. As illustrated in Figure 17, first, the original electrodes on the bulk piezoelectric plate are eliminated and rebuilt in an interlocking comb shape or interdigitated pattern on the surface. After the electrodes are generated, a high voltage is applied while maintaining a high temperature (above Curie temperature). During this period, the poling direction is changed according to the electric field conditions (Figure 17(b)). This piezoelectric device will have approximately the same poling direction after cooling down to normal temperature (Figure 17(c)).

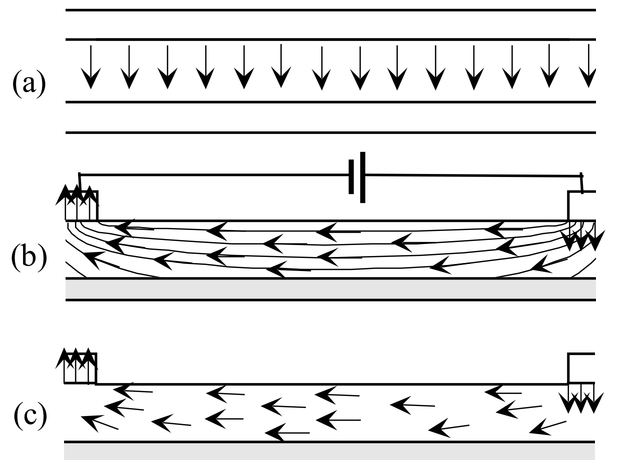

Figure 17. Procedure to convert bulk PZT plate to Interdigitated PZT. A) Un modified bulk PZT, b) remove electrode and create interdigitated electrodes on the surface and apply high voltage to the electrode while maintaining high temperature, c) Final poling direction in the interdigitated PZT

This interdigitated method can not generate a precise 33 poling direction throughout the material, because of non-uniform poling field directions, and incomplete depth of poling field in the material. In this work, however, it is assumed that the 33 poling is uniform and extends completely through the depth. This can be achieved to some extent by maintaining sufficient distance between electrodes. It is also assumed that 33 poling exists in all except the area directly below the electrodes.

Beneath the electrode, the poling direction is approximately 31 but changes to nearly 33 away from the electrode. It is generally difficult to determine the exact relationship between poling direction and the stress condition near the electrodes in this configuration. Also the generated power from the volumes under the electrodes is not big compared to the rest of the volume (however, it still generates power due to its 31 poling). If we assume that the electrode is very thin and the area below the electrode is small, then we can eliminate those volumes and obtain an accurate conservative estimate of generated power.

3.6 Surface Electrode Effect

Piezoelectric devices are covered with electrodes. These electrodes cause different electrical energy generation characteristics. The PEG with a fully covered electrode can use the generated electric energy from some (stressed) areas to change the materials shape in regions where no force applied. This effect will be seen in the bending structures such as the cantilever and diaphragm. In the cantilever beam, the electrode effect will not be significant but in the diaphragm case, the effect will be significant. As described in

Figure 18, diaphragm (circular plate) with clamped edge usually undergoes different stress direction between inner and outer region.

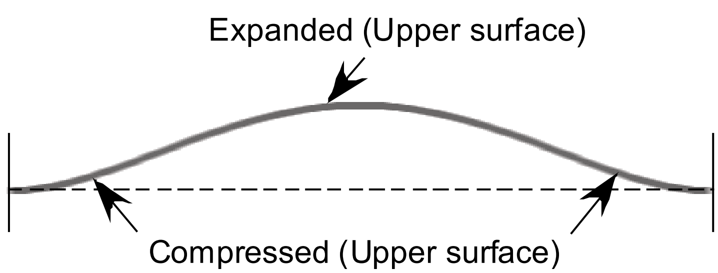

Figure 18. Deflection and stress of diaphragm

When constant pressure (or force) is applied upward, the inner region expands on the upper surface and the outer region is compressed on the upper surface. It will be shown later that this stress distribution lowers energy generation when the electrodes fully cover the surface. Because, the current can easily flow on the electrode covered surface and act as an external electric field. In other words, a fully covered system uses energy to reduce the system stiffness and therefore, electric power generation will be small. To prevent this, the surface electrodes in different stressed regions should be disconnected. A key contribution of this research, then, will be to analyze the effect of regrouping electrodes of some-stressed regions to increase power output.

4.0 MATHMATICAL MODELING

Mathematical relations of the piezoelectric materials are well developed and widely accepted in study of piezoelectricity. In this chapter, the electric power generation equations for cantilever beam and diaphragm with piezoelectric constitutive equation will be developed. Before that, the constitutive equations will be described briefly and a simple stack PEG will be described as a simple example. For each cantilever beam and diaphragm, electrical power generation characteristics of unimorph and triple morph structure will be shown. Also for those structures, interdigitated and non-interdigitated electrodes will be solved. Finally, another type of electrode configuration for a diaphragm structure will be followed. A total of 12 cases will be solved: four cantilever beam cases and eight diaphragm cases (Figure 19. Analyzed piezoelectric devices).

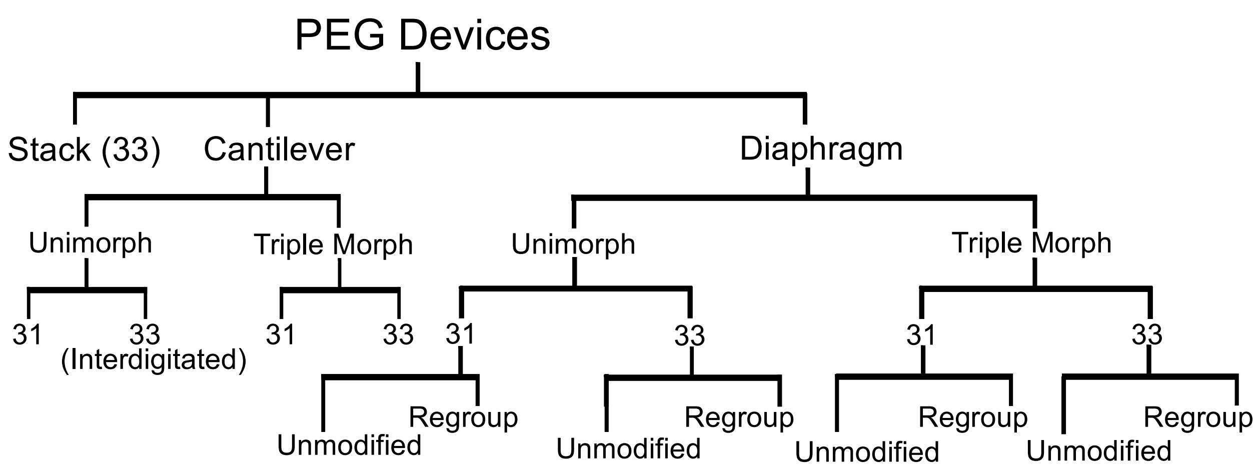

Figure 19. Analyzed piezoelectric devices

4.1 Constitutive Equation

The relation between stress and strain for the common material is described using the material's elastic properties. But in the piezoelectric material, there is an additional effect of strong electro-mechanical coupling that must be considered. The fully-coupled constitutive relations between stress, strain, electric field and charge are accepted as the standard way of describing piezoelectric materials, and can be written as [9].

$$T_{ij} = c^{E}_{ijkl} S_{kl} - e_{kij} E_k \tag{4.1}$$

$$D_i = e_{ikl} S_{kl} + \epsilon^{S}_{ik} E_k \tag{4.2}$$

$$S_{ij} = s^{E}_{ijkl} T_{kl} + d_{kij} E_k \tag{4.3}$$

$$D_i = d_{ikl} T_{kl} + \epsilon^{T}_{ik} E_k \tag{4.4}$$

$$S_{ij} = s^{D}_{ijkl} T_{kl} + g_{kij} D_k \tag{4.5}$$

$$E_i = -g_{ikl} T_{kl} + \beta^{T}_{ik} D_k \tag{4.6}$$

$$T_{ij} = c^{D}_{ijkl} S_{kl} - h_{kij} D_k \tag{4.7}$$

$$E_i = -h_{ikl} S_{kl} + \beta^{S}_{ik} D_k \tag{4.8}$$

where the notation used is defined in the nomenclature. The subscripts *i, j, k and l* are the indices which span 1 through 3 and show the direction within the material. These subscripts follow common tensor notations in elasticity and can be converted to common subscripts. The common subscript conversion rule is that the pair *i* and *j* or *k* and *l* convert to a single subscript which spans 1 through 6. Those rules are shown in Table 1.

Table 1. Subscript conversion table

Pair i,j or k,l	Single subscript
11	1
12 or 21	6
13 or 31	5
22	2
23 or 32	4
33	3

With those conversion rules, four tensor subscripts become two common subscripts, and two tensor subscript become one common subscript. Some of the parameters for piezoelectric materials in Eqs. 4.1-4.8 have three subscripts, and will be converted to two subscripts. Among the three, the first subscript is the surface indicator, and the other two indicate direction of the field. Only this direction pair is converted to a single subscript. As shown in Figure 20, the first subscript shows the surface (orthogonal to the axis) and the second subscript shows vector direction.

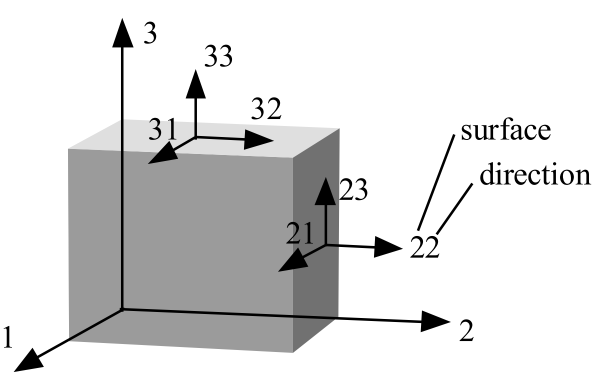

Figure 20. Subscript notation for piezoelectric constant

The Young's modulus used in the constitutive equations is also the same as the engineering elasticity matrix, which consists of 36 elements. As can be seen from the constitutive equations (Eqs. 4.1-4.8), 63 constants are needed: 36 elastic constants, 18 piezoelectric constants, and 9 permittivity constants. Fortunately almost half of those constants are zeros for the most frequently used materials. Common piezoelectric materials are 4mm crystal class and have 6 elastic, 3 piezoelectric and 2 permittivity constants. So a total of 11 distinct constants out of 63 are required to describe common piezoelectric material. For example, one of the constitutive equations (Eq.4.4) can be expanded as:

$$\begin{aligned} D_1 &= d_{11}T_{11} + d_{16}T_{12} + d_{15}T_{13} + d_{16}T_{21} + d_{12}T_{22} + d_{14}T_{23} + d_{15}T_{31} + d_{14}T_{32} + d_{13}T_{33} \\ &+\epsilon_{11}^T E_1 + \epsilon_{12}^T E_2 + \epsilon_{13}^T E_3 \end{aligned} \tag{4.9}$$

$$\begin{aligned} D_2 &= d_{21}T_{11} + d_{26}T_{12} + d_{25}T_{13} + d_{26}T_{21} + d_{22}T_{22} + d_{24}T_{23} + d_{25}T_{31} + d_{24}T_{32} + d_{23}T_{33} \\ &+\epsilon_{21}^T E_1 + \epsilon_{22}^T E_2 + \epsilon_{23}^T E_3 \end{aligned} \tag{4.10}$$

$$\begin{aligned} D_3 &= d_{31}T_{11} + d_{36}T_{12} + d_{35}T_{13} + d_{36}T_{21} + d_{32}T_{22} + d_{34}T_{23} + d_{35}T_{31} + d_{34}T_{32} + d_{33}T_{33} \\ &+\epsilon_{31}^T E_1 + \epsilon_{32}^T E_2 + \epsilon_{33}^T E_3 \end{aligned} \tag{4.11}$$

but for the 4mm class piezoelectric crystal, the above equations can be simplified as

$$D_1 = 2d_{15}T_5 + \epsilon_{11}^T E_1 \tag{4.12}$$

$$D_2 = 2d_{24}T_4 + \epsilon_{22}^T E_2 \tag{4.13}$$

$$D_3 = d_{31}(T_1 + T_2) + d_{33}T_3 + \epsilon_{33}^T E_3 \tag{4.14}$$

The general constitutive equation for the strain (Eq.4.3) is complex, but is simplified with 4mm crystals characteristics. The full strain equation is

$$\begin{aligned} S_{11} &= s_{11}^E T_{11} + s_{16}^E T_{12} + s_{15}^E T_{13} + s_{16}^E T_{21} + s_{12}^E T_{22} + s_{14}^E T_{23} + s_{15}^E T_{31} + s_{14}^E T_{32} + s_{13}^E T_{33} \\ &+d_{11}E_1 + d_{21}E_2 + d_{31}E_3 \end{aligned} \tag{4.15}$$

$$S_{12} = s_{61}^E T_{11} + s_{66}^E T_{12} + s_{65}^E T_{13} + s_{66}^E T_{21} + s_{62}^E T_{22} + s_{64}^E T_{23} + s_{65}^E T_{31} + s_{64}^E T_{32} + s_{63}^E T_{33} + d_{16} E_1 + d_{26} E_2 + d_{36} E_3 \tag{4.16}$$

$$S_{13} = s_{51}^E T_{11} + s_{56}^E T_{12} + s_{55}^E T_{13} + s_{56}^E T_{21} + s_{52}^E T_{22} + s_{54}^E T_{23} + s_{55}^E T_{31} + s_{54}^E T_{32} + s_{53}^E T_{33} + d_{15} E_1 + d_{25} E_2 + d_{35} E_3 \tag{4.17}$$

$$S_{22} = s_{21}^E T_{11} + s_{26}^E T_{12} + s_{25}^E T_{13} + s_{26}^E T_{21} + s_{22}^E T_{22} + s_{24}^E T_{23} + s_{25}^E T_{31} + s_{24}^E T_{32} + s_{23}^E T_{33} + d_{12} E_1 + d_{22} E_2 + d_{32} E_3 \tag{4.18}$$

$$S_{23} = s_{41}^E T_{11} + s_{46}^E T_{12} + s_{45}^E T_{13} + s_{46}^E T_{21} + s_{42}^E T_{22} + s_{44}^E T_{23} + s_{45}^E T_{31} + s_{44}^E T_{32} + s_{43}^E T_{33} + d_{14} E_1 + d_{24} E_2 + d_{34} E_3 \tag{4.19}$$

$$S_{33} = s_{31}^E T_{11} + s_{36}^E T_{12} + s_{35}^E T_{13} + s_{36}^E T_{21} + s_{32}^E T_{22} + s_{34}^E T_{23} + s_{35}^E T_{31} + s_{34}^E T_{32} + s_{33}^E T_{33} + d_{31} E_1 + d_{32} E_2 + d_{33} E_3 \tag{4.20}$$

and can be simplified as

$$S_{11} = S_1 = s_{11}^E T_{11} + s_{12}^E T_{22} + s_{13}^E T_{33} + d_{31} E_3 \tag{4.21}$$

$$S_{12} = S_6 = s_{66}^E (T_{12} + T_{21}) \tag{4.22}$$

$$S_{13} = S_5 = s_{55}^E (T_{13} + T_{31}) + d_{15} E_1 \tag{4.23}$$

$$S_{22} = S_2 = s_{21}^E T_{11} + s_{22}^E T_{22} + s_{23}^E T_{33} + d_{32} E_3 \tag{4.24}$$

$$S_{23} = S_4 = s_{44}^E (T_{23} + T_{32}) + d_{15} E_2 \tag{4.25}$$

$$S_{33} = S_3 = s_{31}^E (T_{11} + T_{22}) + s_{33}^E T_{33} + d_{33} E_3 \tag{4.26}$$

The energy equation for piezoelectric material consists of two parts. The one is elastic energy, and the other is electric energy. The general energy equation for piezoelectric material is described as

$$\text{Energy} = \frac{1}{2} * \text{Strain} * \text{Stress} + \frac{1}{2} * \text{Charge} * \text{Electric field} \tag{4.27}$$

and the general energy equation for 4mm class piezoelectric material is

$$Energy = \frac{1}{2}\left(S_1T_1 + S_2T_2 + S_3T_3 + S_4T_4 + S_5T_5 + S_6T_6\right) + \frac{1}{2}\left(D_1E_1 + D_2E_2 + D_3E_3\right) \quad (4.28)$$

Substituting strain (Eqs.4.21-4.26)and the charge density (Eqs.4.12-4.14), the energy equation in terms of stress and electric field becomes

$$Energy =$$

$$\frac{1}{2}\left(\begin{array}{l} \left(s_{11}^{E}T_1 + s_{12}^{E}T_2 + s_{13}^{E}T_3 + d_{31}E_3\right)T_1 + \left(s_{21}^{E}T_1 + s_{22}^{E}T_2 + s_{23}^{E}T_3 + d_{31}E_3\right)T_2 \\ +\left(s_{31}^{E}(T_1+T_2) + s_{33}^{E}T_3 + d_{33}E_3\right)T_3 + \left(2s_{44}^{E}T_4 + d_{15}E_2\right)T_4 + \left(2s_{55}^{E}T_5 + d_{15}E_1\right)T_5 + 2s_{66}^{E}T_6^{2} \\ +\left(\left(2d_{15}T_5 + \epsilon_{11}^{T}E_1\right)E_1 + \left(2d_{24}T_4 + \epsilon_{22}^{T}E_2\right)E_2 + \left(d_{31}(T_1+T_2) + d_{33}T_3 + \epsilon_{33}^{T}E_3\right)E_3\right) \end{array}\right)$$

$$= \frac{1}{2}\left(\begin{array}{l} s_{11}^{E}T_1^{2} + s_{22}^{E}T_2^{2} + s_{33}^{E}T_3^{2} + 2s_{44}^{E}T_4^{2} + 2s_{55}^{E}T_5^{2} + 2s_{66}^{E}T_6{}^{2}{}_{3} + 2s_{12}^{E}T_1T_2 + 2s_{31}^{E}(T_1T_3 + T_2T_3) \\ +2d_{31}\left(T_1E_3 + T_2E_3\right) + 2d_{33}T_3E_3 + 3d_{15}\left(T_4E_2 + T_5E_1\right) \\ +\epsilon_{11}^{T}E_1^{2} + \epsilon_{22}^{T}E_2^{2} + \epsilon_{33}^{T}E_3^{2} \end{array}\right) \quad (4.29)$$

The first line of the equation 4.29 contains pure mechanical energy terms and second line describes the mechanical-electrical coupled energy. The last line shows pure electrical energy applied to the structure.

In this research, 6mm class piezoelectric crystal (PZT5H) [19] will be considered and solved with 6mm class parameters. Common elasticity notation will be used instead of *T*s and *S*s, which were used in constitutive equations. From now on, σ and ε will be used to describe stress and strain.

4.2 PZT Stack as PEG

The generated charge on a piezoelectric stack from an applied load F_o can be calculated using piezoelectric constitutive equations. The constitutive equations are for an infinitesimal small volume, so it is easy to calculate the total power generation for a given physical stack by integrating throughout the volume.

For a compressive load, F_o, applied to the stack shown in Figure 12, energy in a single plate of the PZT stack PEG can be calculated with Eq. 4.29. There is only a compressive force, which is in the 3-direction, and is equated as $T_1 = T_2 = T_4 = T_5 = T_6 = 0$. Electrodes are only on the 3-surface, therefore, $E_1 = E_2 = 0$.

$$\begin{aligned} U_i &= \int_{volume} \left(\frac{1}{2} \varepsilon_3 \sigma_3 + \frac{1}{2} D_3 E_3 \right) dv \\ &= A h_p \left(\frac{1}{2} s_{33}^E {\sigma_3}^2 + d_{33} \sigma_3 E_3 + \frac{1}{2} \epsilon_{33}^T {E_3}^2 \right) \\ &= \frac{s_{33}^E h_p}{2A} {F_o}^2 + d_{33} F_o V + \frac{A \epsilon_{33}^T}{2 h_p} V^2 \end{aligned} \tag{4.30}$$

Where A is the area of the surface and h_p is the thickness of the layer.

Total energy in an n-layered stack PEG is (ignoring energy contained in the epoxy between layers)

$$U_{total} = \frac{n s_{33}^E h_p}{2A} {F_o}^2 + n d_{33} F_o V + \frac{n A \epsilon_{33}^T}{2 h_p} V^2 \tag{4.31}$$

There are three terms in Eq. 4.31. The first term shows the elastic energy and the last term shows electric energy. The middle term in the energy equation represents the coupled electromechanical energy. This coupled energy term is neither pure elastic energy nor pure electric energy, but it shows how much energy can be converted from mechanical to electrical.

Since the electrical energy is described by charge and voltage ($U_E = QV$), the partial derivative of the total energy with respect to the voltage will reveal the generated charge.

$$Q_{Gen} = \frac{\partial U_{total}}{\partial V} = n d_{33} F_o + \frac{n A \epsilon_{33}^T}{h_p} V \tag{4.32}$$

The charge equation 4.32 is described in terms of applied force and the electric field boundary condition. In the PEG application, supplied voltage is zero. Thus the actual generated charge from force is

$$Q_{Gen} = nd_{33}F_o \qquad (4.33)$$

Another term we can obtain from the charge equation 4.32 is the capacitance of piezoelectric material. The capacitance is a characteristic of the piezoelectric material and can be measured. Capacitance is the relation between the voltage and charge on the piezoelectric material. The last voltage term of the charge equation 4.32 shows the relation between the charge and the voltage, so the capacitance of this PEG can be found to be

$$C_{free} = \frac{nA\epsilon_{33}^{T}}{h_p} \qquad (4.34)$$

Knowing the PEG capacitance, the voltage at which charge is generated for a given applied force can be written as:

$$V_{Gen} = \frac{Q_{Gen}}{C_{free}} = \frac{d_{33}h_p}{\epsilon_{33}^{T}A}F_o \qquad (4.35)$$

Note here that the voltage in the equations above and the calculated voltage in equation 4.35 are different. Voltage used in equations 4.30-4.32 are from the boundary applied electric field, whereas the calculated voltage in Eq. 4.35 is the voltage that appears on the PEG due to the applied load. Therefore, the calculated electrical energy generation with force F_o in the piezoelectric stack PEG is

$$QV = \frac{nd_{33}^{\ 2}h_p}{\epsilon_{33}^{T}A}F_o^{\ 2} \qquad (4.36)$$

All the electric field and the stresses are constant at the steady state and the simple calculation is enough to describe charge generation.

4.3 PEG Cantilever Beam

In the analysis of the stack PEG, the stress fields were constant. But in the cantilever analysis, stress distribution is not a constant. In this analysis, it is assumed that there is only a stress along the longitudinal direction. This assumption is included in the classical analytical solution of the cantilever beam.

The energy methods are the best way of solving complex problems of this type. This calculation using energy method for unimorph cantilever beam has been done by Smith [28]. In the charge calculation using energy methods, first the whole structure energy is calculated and then differentiated with respect to voltage to obtain charge generation.

Cantilever beams are common mechanical elements whose exact solution is available in many text books.

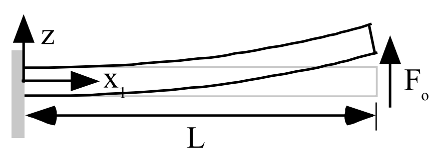

Figure 21. Cantilever beam

When point force F_o is applied to the end of the cantilever beam (Figure 21), the moment can be calculated as

$$M\left(x_1\right) = F_o\left(L - x_1\right) \tag{4.37}$$

and the strain is

$$\varepsilon\left(x_1, z\right) = -\frac{z}{R\left(x_1, M, E_3\right)} = -\rho\left(x_1, M, E_3\right) z \tag{4.38}$$

where, $R\left(x_1, M, E_3\right)$ is the radius of curvature and $\rho\left(x_1, M, E_3\right)$ is the curvature. At any given point along the beam, the moment equation 4.37 should be same as the moment calculated from stresses on a cross-section,

$$M = \int \sigma\left(\varepsilon\left(x_1, z\right), E_3\right) z dz \tag{4.39}$$

Since the stresses inside of piezoelectric layers are coupled with strain and electric field, and this strain can be described as curvature times distance from the neutral layer as shown in Eq. 4.38, the moment equation will now be the function of curvature and electric field.

$$M = \int \sigma\left(\rho\left(x_1, M, E_3\right), E_3\right) z dz \tag{4.40}$$

From Eqs. 4.37 and 4.40, curvature equation can be obtained in terms of force and electric field as variables.

$$\rho\left(x_1, F_o, E_3\right) = f_1\left(x_1, F_o\right) + f_2\left(x_1, E_3\right) \tag{4.41}$$

Therefore, the system's total energy equation 4.29 also can be described with curvature and electric field. With this energy equation, we can find charge generation by differentiating with respect to the voltage because energy in electrical system is described charge times voltage.

The electric power generation for the 31-type and interdigitated type cantilever beams will follow in next subsections. For each case, unimorph and triple morph cantilever beams will be used as PEG structure.

4.4 Cantilever Bender

The most important difference in unimorph benders from other benders is that the neutral surface where no stresses are generated by the external bending force in the unimorph structures is not necessarily in the middle of the beam because the Young's moduli of each of the layers are different. Thus the stress distribution is also different from a unimorph structure shown in Figure 22. The neutral surface can be calculated using following equation.

$$z_c = \frac{\Sigma zA}{\Sigma A} = \frac{z_1 A_1 - \frac{E_2}{E_1} z_2 A_2}{\frac{E_2}{E_1} A_2 + A_1} = \frac{h_p^2 s_m - h_m^2 s_{11}^E}{2\left(h_m s_{11}^E + h_p s_m\right)} \tag{4.42}$$

where A's are areas of each layer's cross section, h's are each layer's thickness, and E's are the young's moduli of each layer. Subscripts 1 and 2 show upper and lower layer. z is the distance from the center (or boundary between different material). The neutral surface z_c is the distance from z=0. The subscript p shows piezoelectric parameters and m shows non-piezoelectric parameters and. h is the thickness of each layer. In the Eq. 4.42, there is negative sign in numerator. This negative sign is because 2nd layer lies below the center surface.

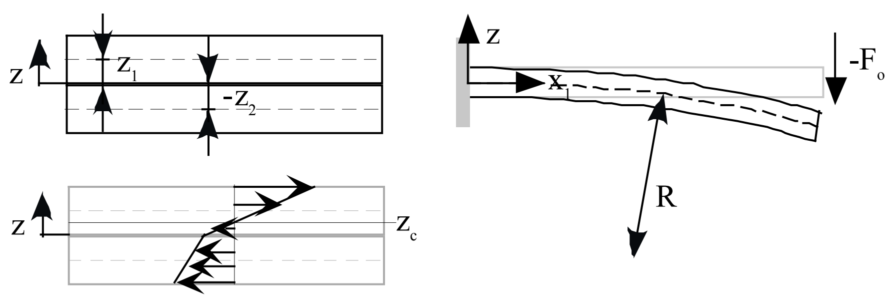

Figure 22. neutral surface. Upper left: neutral surface of each layer. Lower left: stress distribution of unimorph and neutral surface z_c. Right: radius of curvature and force.

With this neutral surface, strain can be described in terms of the curvature

$$\varepsilon_1 = -\frac{z - z_c}{R} = -\rho\left(z - z_c\right) \tag{4.43}$$

This relationship between neutral surface z_c, curvature ρ, and strain ε_1 will be used in the following subsections to solve the unimorph cantilever case.

4.4.1 31 Unimorph Cantilever Bender

A 31-cantilever unimorph beam is made up of a piezoelectric layer that operates in the 31-mode, and a second material such as aluminum. In this calculation, the global axes are located in the fixed middle surface of the cantilever and positive forcing direction is upward. Throughout the research, upper layers will be set to have positive electric field to prevent confusion. To get the positive charge and voltage when the direction of tip force is down ward, the electrodes of piezoelectric device are connected to have negative electric field (Figure 23).

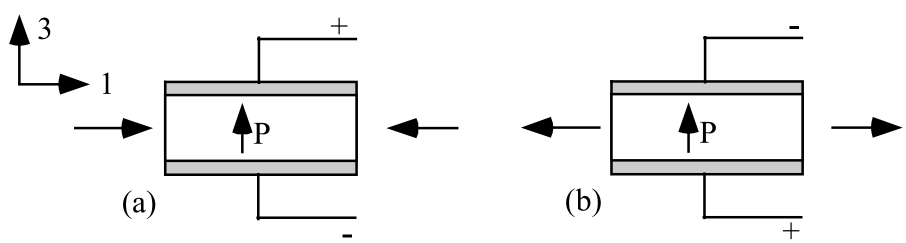

Figure 23. Electric field direction. (a) Positive electric field (b) Negative electric field

Because, according to the constitutive Equation. 4.6, positive volts will be shown when negative stresses are applied. Then, the constitutive equations for unimorph cantilever beam with negative electric field are, for the piezoelectric layer

$$\begin{Bmatrix} \varepsilon_1 = s_{11}^E \sigma_1 - d_{31} E_3 \\ D_3 = -d_{31}\sigma_1 + \epsilon_{33}^T E_3 \end{Bmatrix} \tag{4.44}$$

and for the non piezoelectric layer, simple stress – strain relation can be used. If young's modulus of non-piezoelectric layer is $1/s_m$, the relation is

$$\varepsilon_1 = s_m \sigma_1 \tag{4.45}$$

Throughout this research, subscript *m* stands for the parameters of non-piezoelectric. As shown above, Each layer's energy is described differently. After substituting into energy

Equation 4.27 with Equations 4.44 and 4.45, energies in the system can be described in terms of stress and electric field only. The total energy in the structure is the sum of those energies in each layer. For the piezoelectric layer,

$$dU_p = \frac{1}{2}\left(s_{11}^E \sigma_1 - d_{31}E_3\right)\sigma_1 + \frac{1}{2}\left(-d_{31}\sigma_1 + \epsilon_{33}^T E_3\right)E_3$$

$$= \frac{1}{2}s_{11}^E \sigma_1^2 - d_{31}\sigma_1 E_3 + \frac{1}{2}\epsilon_{33}^T E_3^2 \tag{4.46}$$

and for the non piezoelectric layer, there is only elastic energy, which is described as

$$dU_m = \frac{1}{2}s_m \sigma_1^2 \tag{4.47}$$

The stresses in Equation 4.46 and 4.47 can be calculated from the moment equation. The moment equation for the unimorph beam with width W is also stress equation and is

$$M = \int_{Area} \sigma_1 \left(z - z_c\right) dydz = \int_z \sigma_1 \left(z - z_c\right) W dz \tag{4.48}$$

The stresses in the moment equation can be replaced with the constitutive equations (4.44 and 4.45)

$$\left.\begin{array}{ll} \sigma_1 = \dfrac{1}{s_{11}^E}\left(\varepsilon_1 + d_{31}E_3\right) & \text{for piezoelectric layer} \\ \sigma_1 = \dfrac{1}{s_m}\varepsilon_1 & \text{for non-piezoelectric layer} \end{array}\right\} \tag{4.49}$$

and the strain of the stress equation can be replaced using the radius of curvature relation shown in equation. 4.43.

Combining equations (4.48-4.49), the moment equation in terms of curvature and electric field is now

$$M = \int_0^{h_p} \frac{1}{s_{11}^E}\left(-\rho\left(z - z_c\right) + d_{31}E_3\right) W \left(z - z_c\right) dz + \int_{-h_m}^{0} -\frac{1}{s_m} W \rho \left(z - z_c\right)^2 dz \tag{4.50}$$

We have two unknowns, the moment and curvature. Since the curvature is not the function of z, moment equation 4.50 can be easily solved.

$$M = -\frac{\rho W B_{11}}{12 s_m s_{11}^E \left(s_{11}^E h_m + s_m h_p \right)} + \frac{d_{31} h_p h_m \left(h_m + h_p \right) W}{2 \left(s_{11}^E h_m + s_m h_p \right)} E_3 \tag{4.51}$$

where $B_{11} = s_m{}^2 h_p{}^4 + 4 s_{11}^E s_m h_m h_p{}^3 + 6 s_m s_{11}^E h_p{}^2 h_m{}^2 + 4 s_{11}^E s_m h_p h_m{}^3 + s_{11}^{E\,2} h_m{}^4$.

After substitute M with Equation 4.37, which is elastic solution, the above equation is converted to the equation with three unknowns.

$$F_o \left(L - x_1 \right) = -\frac{\rho W B_{11}}{12 s_m s_{11}^E \left(s_{11}^E h_m + s_m h_p \right)} + \frac{d_{31} h_p h_m \left(h_m + h_p \right) W}{2 \left(s_{11}^E h_m + s_m h_p \right)} E_3 \tag{4.52}$$

After rearranging equation 4.52, the curvature equation for this unimorph cantilever beam will be solved in terms of applied Force (F_o) and electric field (E_3).

$$\rho = -\frac{12 s_m s_{11}^E \left(s_{11}^E h_m + s_m h_p \right) \left(L - x_1 \right)}{B_{11} W} F_o + \frac{6 d_{31} s_m s_{11}^E h_p h_m \left(h_m + h_p \right)}{B_{11}} E_3 \tag{4.53}$$

Using this curvature, we can find the strains and stresses in the structure. Rewrite equation 4.49 with strain-curvature relation and get

$$\left. \begin{aligned} \sigma_1 &= \frac{1}{s_{11}^E} \left(-\rho \left(z - z_c \right) + d_{31} E_3 \right) && \text{for piezoelectric layer} \\ \sigma_1 &= -\frac{1}{s_m} \rho \left(z - z_c \right) && \text{for non piezoelectric layer} \end{aligned} \right\} \tag{4.54}$$

Therefore, the energy in a differential volume of each layer can be rewritten as

$$\left. \begin{aligned} dU_p &= \frac{1}{2} s_{11}^E \left(\frac{-\rho \left(z - z_c \right) + d_{31} E_3}{s_{11}^E} \right)^2 - d_{31} \left(\frac{1}{s_{11}^E} \left(-\rho \left(z - z_c \right) + d_{31} E_3 \right) \right) E_3 + \frac{1}{2} \epsilon_{33}^T E_3^2 \\ dU_m &= \frac{1}{2} \left(s_m \sigma_1 \right) \sigma_1 = \frac{1}{2} s_m \left(-\rho \left(z - z_c \right) \right)^2 \end{aligned} \right\} \tag{4.55}$$

Thus the total system energy in this Unimorph cantilever beam can be obtained by integrating over the whole structure.

$$
\begin{aligned}
U &= \int_0^L \int_0^W \left(\int_0^{h_p} dU_p dz + \int_{-h_m}^{0} dU_m dz \right) dydx \\
&= \frac{2 s_{11}^{E} s_m s_h L^3}{W B_{11}} F_o^{\,2} - \frac{3 d_{31} s_{11}^{E} s_m h_p h_m \left(h_m + h_p\right) L^2}{B_{11}} E_3 F_o \\
&\quad + \frac{\epsilon_{33}^{T} W L h_p}{2} \left(1 + \left(\frac{3 s_{11}^{E2} s_m h_m^{\,2} h_p \left(h_m + h_p\right)^2}{s_h B_{11}} - 1 \right) K_{31}^{\,2} \right) E_3^{\,2}
\end{aligned} \tag{4.56}
$$

where, $s_h = s_{11}^{E} h_m + s_m h_p$ and $K_{31} = {d_{31}} \big/ {\sqrt{\epsilon_{33}^{T} s_{11}^{E}}}$.

Since electrical energy is described as charge times voltage (*QV*), charge generation can be calculated by differentiating total energy with respect to *V*. However, there are no voltage terms in equation 4.56 and only electric field terms exist. Electric field is defined by

$$
\text{Electric field } \left(E\right) = \frac{\text{Voltage across electrode } \left(V\right)}{\text{PZT thickness between electrode}} \tag{4.57}
$$

Thus, the electric field in this unimorph cantilever is $E_3 = V / h = V / h_p$. Substitute electric field and differentiate the energy equation 4.56 with respect to voltage.

$$
\begin{aligned}
Q &= \frac{\partial U}{\partial V} \\
&= -\frac{3 d_{31} s_m s_{11}^{E} h_m \left(h_m + h_p\right) L^2}{B_{11}} F_o + \frac{\epsilon_{33}^{T} W L}{h_p} \left(1 + \left(\frac{3 s_{11}^{E2} s_m h_p h_m^2 \left(h_m + h_p\right)^2}{S_h B_{11}} - 1 \right) K_{31}^2 \right) V
\end{aligned} \tag{4.58}
$$

Equation 4.58 is the general charge output equation when both force and electric field exists. *F* is the external force input and *V* is the external voltage input. The charge generation from the only mechanical force input is

$$
Q_{Gen} = -\frac{3 d_{31} s_m s_{11}^{E} h_m \left(h_m + h_p\right) L^2}{B_{11}} F_o \tag{4.59}
$$

and from the relation $Q=CV$, the open circuit capacitance is

$$C_{free} = \frac{\epsilon_{33}^T WL}{h_p}\left(1+\left(\frac{3s_{11}^{E2} s_m h_p h_m^2 \left(h_m + h_p\right)^2}{S_h B_{11}} - 1\right) K_{31}^2\right) \quad (4.60)$$

From Eqs. 4.59 and 4.60, the voltage that appears on the electrodes is

$$V_{Gen} = \frac{Q_{Gen}}{C_{free}} = -\frac{3d_{31} s_{11}^E s_m h_p h_m \left(h_m + h_p\right) L}{\epsilon_{33}^T W B_{11}\left(1+\left(\frac{3s_{11}^{E2} s_m h_p h_m^2 \left(h_m + h_p\right)^2}{S_h B_{11}} - 1\right) K_{31}^2\right)} F_o \quad (4.61)$$

Thus the total electric energy generation from only force F_o is

$$U_{Gen} = Q_{Gen} V_{Gen} = \frac{9d_{31}^2 s_{11}^{E2} s_m^2 h_p h_m^2 \left(h_m + h_p\right)^2 L^3}{\epsilon_{33}^T W {B_{11}}^2 \left(1+\left(\frac{3s_m s_{11}^{E2} h_p h_m^2 \left(h_m + h_p\right)^2}{S_h B_{11}} - 1\right) K_{31}^2\right)} {F_o}^2 \quad (4.62)$$

4.4.2 Interdigitated Unimorph Cantilever Bender

The interdigitated cantilever unimorph beam shown in Figure 24 is a unimorph piezoelectric structure that utilizes the 33-mode.

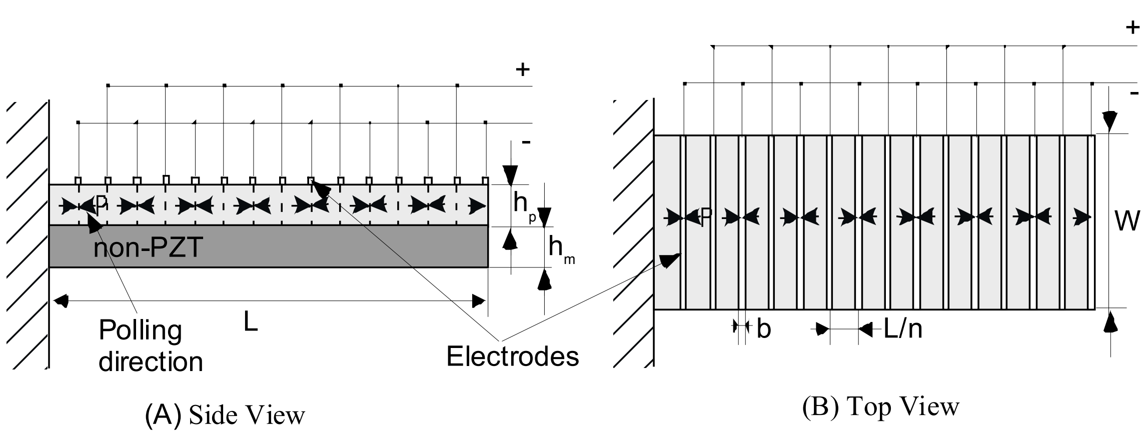

Figure 24. Interdigitated unimorph cantilever PEG

The constitutive equations for the piezoelectric layer of this interdigitated unimorph cantilever beam for the area where no electrodes are covered are slightly different from the 31-type unimorph cantilever beam. The piezoelectric layer's poling direction is changed and their constitutive equation is

$$\begin{Bmatrix} S_1 = s_{33}^E \sigma_1 - d_{33} E_3 \\ D_3 = -d_{33} \sigma_1 + \epsilon_{33}^T E_3 \end{Bmatrix} \tag{4.63)}$$

and for the non piezoelectric layer, the stress-strain relation is the same as for the 31-type Eq. 4.45, thus equation 4.45 can be used without modification. The energy in the interdigitated piezoelectric structure can be described as

$$dU_p = \frac{1}{2}\left(s_{33}^E \sigma_1 - d_{33} E_3\right)\sigma_1 + \frac{1}{2}\left(-d_{33}\sigma_1 + \epsilon_{33}^T E_3\right)E_3$$

$$= \frac{1}{2} s_{33}^E \sigma_1^2 - d_{33}\sigma_1 E_3 + \frac{1}{2}\epsilon_{33}^T E_3^2 \tag{4.64}$$

The neutral surface in the interdigitated cantilever beam is not the same as for the 31 type as mentioned before. The elastic properties also change when poling direction changes. The neutral surface for this interdigitated unimorph is also changed. From Eq. 4.42, the neutral surface for interdigitated unimorph cantilever beam is

$$z_{c3} = \frac{h_p^2 s_m - h_m^2 s_{33}^E}{2\left(h_m s_{33}^E + h_p s_m\right)} \tag{4.65}$$

The moment at a certain cross section with the stress from the constitutive equation is almost same as 31-type

$$M = \int_0^{h_p} \frac{1}{s_{33}^E}\left(-\rho\left(z - z_{c3}\right) + d_{33}E_3\right)W\left(z - z_{c3}\right)dz + \int_{-h_m}^{0} -\frac{1}{s_m} W\rho\left(z - z_{c3}\right)^2 dz \tag{4.66}$$

As before, equation 4.66 should be the same as for the elasticity solution 4.37. Then the curvature can be solve in terms of Force (F_o) and electric field (E_3)

$$\rho = -\frac{12 s_m s_{33}^E \left(s_{33}^E h_m + s_m h_p\right)\left(L-x\right)}{B_{33}W} F_o + \frac{6 d_{33} s_{33}^E s_m h_p h_m \left(h_m + h_p\right)}{B_{33}} E_3 \qquad (4.67)$$

where $B_{33} = s_m{}^2 h_p{}^4 + 4 s_{33}^E s_m h_m h_p{}^3 + 6 s_m s_{33}^E h_p{}^2 h_m{}^2 + 4 s_{33}^E s_m h_p h_m{}^3 + s_{33}^{E\,2} h_m{}^4$. Using this curvature, all the stress and strain information can be obtained. The stress equation for the PZT layer in the function of curvature is

$$\sigma_1 = \frac{1}{s_{33}^E}\left(-\rho\left(z - z_{c3}\right) + d_{33}E_3\right) \qquad (4.68)$$

The energy equation 4.64 is now described as

$$dU_p = \frac{1}{2} s_{33}^E \left(\frac{-\rho\left(z-z_{c3}\right) + d_{33}E_3}{s_{33}^E}\right)^2 - d_{33}\left(\frac{1}{s_{33}^E}\left(-\rho\left(z-z_{c3}\right) + d_{33}E_3\right)\right)E_3 + \frac{1}{2}\epsilon_{33}^T E_3^2 \quad (4.69)$$

The total system energy in the interdigitated Unimorph cantilever beam is the summation of each segment between the electrodes. If there are n+1 electrodes on the surface and their width is b like in Figure 24 then the total energy in the structure is

$$\begin{aligned} U &= \sum_{i=1}^{n} \int_{\frac{(i-1)L}{n}+\frac{b}{2}}^{\frac{iL}{n}-\frac{b}{2}} \int_0^W \left(\int_0^{h_p} dU_p dz + \int_{-h_m}^{0} dU_m dz\right) dy dx \\ &= \frac{s_{h3} s_{33}^E s_m \left(L - nb\right)\left(4nL^2 + nb^2 - 2bL\right)}{2nWB_{33}} F_o{}^2 - \frac{3 d_{33} s_{33}^E s_m h_m h_p \left(h_m + h_p\right)\left(L-nb\right)L}{B_{33}} F_o E_3 \\ &\quad + \frac{\epsilon_{33}^T h_p W \left(L - nb\right)}{2}\left(1 + \left(\frac{3 s_{33}^{E\,2} s_m h_m{}^2 h_p \left(h_m + h_p\right)^2}{S_{h3} B_{33}} - 1\right) K_{33}^2\right) E_3{}^2 \end{aligned} \qquad (4.70)$$

where, $K_{33}{}^2 = \frac{d_{33}{}^2}{\epsilon_{33}^T s_{33}^E}$, and $S_{h3} = s_{33}^E h_m + s_m h_p$.

Substitute above equation 4.70 with $E_3 = V/h = V/\left(L/n\right)$ and differentiate with respect to *V*.

$$Q = -\frac{3nd_{33}s_{33}^{E}s_m h_m h_p\left(h_m + h_p\right)\left(L - nb\right)}{B_{33}}F_o + \frac{n^2\epsilon_{33}^{T}h_p W\left(L - nb\right)}{L^2}\left(1 + \left(\frac{3s_{33}^{E\,2}s_m h_m{}^2 h_p\left(h_m + h_p\right)^2}{S_{h3}B_{33}} - 1\right)K_{33}^2\right)V \tag{4.71}$$

then the generated charge from force is

$$Q_{Gen} = -\frac{3nd_{33}s_{33}^{E}s_m h_m h_p\left(h_m + h_p\right)\left(L - nb\right)}{B_{33}}F_o \tag{4.72}$$

and the open circuit capacitance is

$$C_{free} = \frac{n^2\epsilon_{33}^{T}h_p W\left(L - nb\right)}{L^2}\left(1 + \left(\frac{3s_{33}^{E\,2}s_m h_m{}^2 h_p\left(h_m + h_p\right)^2}{S_{h3}B_{33}} - 1\right)K_{33}^2\right) \tag{4.73}$$

The voltage that appears on the electrode is

$$V_{Gen} = \frac{Q_{Gen}}{C_{free}} = -\frac{3d_{33}s_{33}^{E}s_m h_m\left(h_m + h_p\right)L^2}{n\epsilon_{33}^{T}WB_{33}\left(1 + \left(\frac{3s_{33}^{E\,2}s_m h_p h_m^2\left(h_m + h_p\right)^2}{S_{h3}B_{33}} - 1\right)K_{33}^2\right)}F_o \tag{4.74}$$

and the total generated electrical energy from force F_o is

$$U_{Gen} = Q_{Gen}V_{Gen} = \frac{9d_{33}^2 s_{33}^{E\,2}s_m^2 h_p h_m^2\left(h_m + h_p\right)^2\left(L - nb\right)L^2}{\epsilon_{33}^{T}WB_{33}{}^2\left(1 + \left(\frac{3s_{33}^{E\,2}s_m h_p h_m^2\left(h_m + h_p\right)^2}{S_{h3}B_{33}} - 1\right)K_{33}^2\right)}F_o{}^2 \tag{4.75}$$

4.4.3 Triple-morph Cantilever Bender

A triple morph cantilever beam consists of two piezoelectric outer layers and non-piezoelectric middle layer. The polarities of the two piezoelectric layers are in opposite directions of each other to obtain performance. This triple morph cantilever is symmetric along the cross section, and thus the neutral surface lies on the middle surface of the beam. The triple morphed cantilever bender was solved previously and in this section, Wang's[25] solution will be resolved.

4.4.4 31 Triple-morph Cantilever Bender

The upper two layers, the piezoelectric and non piezoelectric layer, are the same as for the 31-type cantilever beam and their Eqs. 4.44 and 4.45 can be used here. To make the bender work, the upper and lower piezoelectric layer's electric fields should be opposite each other. Therefore, the lower piezoelectric layer is connected to have positive electric field.

$$\begin{Bmatrix} S_1 = s_{11}^E \sigma_1 + d_{31} E_3 \\ D_3 = d_{31} \sigma_1 + \epsilon_{33}^T E_3 \end{Bmatrix} \tag{4.76}$$

The total energy in the structure can be obtained by the summation of these three layers. The upper two layers have the same energy equation as the 31-type unimorph cantilever beam, and the lower layer's energy equation is

$$\begin{aligned} dU_p &= \frac{1}{2}\left(s_{11}^E \sigma_1 + d_{31} E_3\right)\sigma_1 + \frac{1}{2}\left(d_{31}\sigma_1 + \epsilon_{33}^T E_3\right)E_3 \\ &= \frac{1}{2} s_{11}^E \sigma_1^2 + d_{31}\sigma_1 E_3 + \frac{1}{2}\epsilon_{33}^T E_3^2 \end{aligned} \tag{4.77}$$

The stress is calculated from the moment equation. The moment equation is shown in Eq. 4.37. Using the stresses from the constitutive equations, the moment at any certain cross section is

$$M = \int_{h_m/2}^{h_m/2+h_p} \frac{1}{s_{11}^E}\left(-\rho z + d_{31}E_3\right)Wzdz + \int_{-h_m/2}^{h_m/2} -\frac{1}{s_m} W\rho z^2 dz$$
$$+\int_{-h_m/2-h_p}^{-h_m/2} \frac{1}{s_{11}^E}\left(-\rho z - d_{31}E_3\right)Wzdz \tag{4.78}$$

From the elasticity moment solution 4.37, we can solve for curvature in terms of force (F_o) and electric field (E_3)

$$\rho = -\frac{12 s_m s_{11}^E \left(L-x\right)}{X_{11}W}F_o + \frac{12 d_{31} s_m h_p \left(h_m + h_p\right)}{X_{11}}E_3 \tag{4.79}$$

and $X_{11} = 12 s_m h_p{}^2 h_m + 8 s_m h_p{}^3 + 6 s_m h_p h_m{}^2 + s_{11}^E h_m{}^3$

Using this curvature, we can figure out the strains in the structure. Using the constitutive equation, the stress can be calculated using the curvature just solved and then the total energy can be found. Using the previous 31-type stress equation for the upper two layers, and for the lower layer, we have

$$\sigma_1 = \frac{1}{s_{11}^E}\left(-\rho z - d_{31}E_3\right) \tag{4.80}$$

Using the stress equation, the energy equation can be calculated. The upper two layer's energy equation is the same as for the 31-type unimorph case except for the difference in curvature. The energy equation for the lower layer is described as

$$dU_{lo} = \frac{1}{2}\left(-\rho z - d_{31}E_3\right)^2 + d_{31}\left(\frac{1}{s_{11}^E}\left(-\rho z - d_{31}E_3\right)\right)E_3 + \frac{1}{2}\epsilon_{33}^T E_3^2 \tag{4.81}$$

Thus, when U_{up} is upper layer's energy and U_m is middle layer's energy, the total system energy in this triple morph cantilever beam is

$$U = \int_0^L \int_0^W \left(\int_{h_m/2}^{h_m/2+h_p} U_{up} dz + \int_{-h_m/2}^{h_m/2} U_m dz + \int_{-h_m/2-h_p}^{-h_m/2} U_{lo} dz \right) dy dx$$

$$= \frac{2 s_{11}^E s_m L^3}{X_{11} W} F_o^{\,2} - \frac{6 d_{31} s_m h_p \left(h_m + h_p\right) L^2}{X_{11}} F_o E_3 + \epsilon_{33}^T W L h_p \left(1 + \frac{\left(6 s_m h_p \left(h_m + h_p\right)^2 - X_{11}\right)}{X_{11}} K_{31}^2 \right) E_3^2 \quad (4.82)$$

Substituting $E_3 = V / h = V / \left(2h_p\right)$ into the above Eq. 4.82 and differentiate with respect to V gives

$$Q = -3 \frac{d_{31} s_m \left(h_m + h_p\right) L^2}{X_{11}} F_o + \frac{\epsilon_{33}^T W L}{2h_p} \left(1 + \frac{\left(6 s_m h_p \left(h_m + h_p\right)^2 - X_{11}\right)}{X_{11}} K_{31}^2 \right) V \quad (4.83)$$

thus the generated charge from the force is

$$Q_{Gen} = -3 \frac{d_{31} s_m \left(h_m + h_p\right) L^2}{X_{11}} F_o \quad (4.84)$$

and the open circuit capacitance is

$$C_{free} = \frac{\epsilon_{33}^T W L}{2h_p} \left(1 + \left(\frac{6 s_m h_p \left(h_m + h_p\right)^2}{X_{11}} - 1 \right) K_{31}^2 \right) \quad (4.85)$$

The generated voltage is then

$$V_{Gen} = \frac{Q_{Gen}}{C_{free}} = -\frac{6 d_{31} s_m h_p \left(h_m + h_p\right) L}{\epsilon_{33}^T W X_{11} \left(1 + \left(\frac{6 s_m h_p \left(h_m + h_p\right)^2}{X_{11}} - 1 \right) K_{31}^2 \right)} F_o \quad (4.86)$$

Finally, the total generated electric energy from force F_o is

$$U_{Gen} = Q_{Gen} V_{Gen} = \frac{18 d_{31}^2 s_m^2 h_p \left(h_m + h_p\right)^2 L^3}{\epsilon_{33}^T W X_{11}{}^2 \left(1 + \left(\frac{6 s_m h_p \left(h_m + h_p\right)^2}{X_{11}} - 1\right) K_{31}^2\right)} F_o{}^2 \tag{4.87}$$

4.4.5 Interdigitated Triple-morph Cantilever Bender

The analytical solution here assumes that most of the piezoelectric material is poled in the 33-direction, and the piezoelectric effect of the small uncertain volume of the piezoelectric layer under the electrodes can be neglected. The configuration for the interdigitated triple bender also consists of 3 layers. The upper and lower layers are the piezoelectric layers and mid layer is a non-piezoelectric layer. The upper and lower layers' polarities are opposite each other as shown in Figure 25.

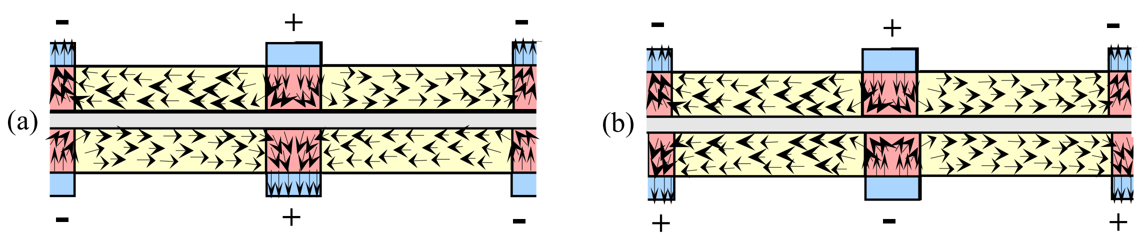

Figure 25. Triple layered Interdigitated PEG

The constitutive equations for the upper and lower layers for the interdigitated device are the same as for the unimorph case. The lower layer should have a positive electric field to perform and the constitutive equation for positive electric field is

$$\begin{Bmatrix} S_1 = s_{33}^E \sigma_1 + d_{33} E_3 \\ D_3 = d_{33} \sigma_1 + \epsilon_{33}^T E_3 \end{Bmatrix} \tag{4.88}$$

The lower layer's energy is described as

$$dU_{pl} = \frac{1}{2}\left(s_{33}^{E}\sigma_1 + d_{33}E_3\right)\sigma_1 + \frac{1}{2}\left(d_{33}\sigma_1 + \epsilon_{33}^{T}E_3\right)E_3$$

$$= \frac{1}{2}s_{33}^{E}\sigma_1^2 + d_{33}\sigma_1 E_3 + \frac{1}{2}\epsilon_{33}^{T}E_3^2 \tag{4.89}$$

To obtain curvature information, the moment equation is to be used. For this triple interdigitated cantilever beam, the moment is described as

$$M = \int_{h_m/2}^{h_m/2+h_p} \frac{1}{s_{33}^{E}}\left(-\rho z + d_{33}E_3\right)Wzdz + \int_{-h_m/2}^{h_m/2} -\frac{1}{s_m}W\rho z^2 dz$$

$$+\int_{-h_m/2-h_p}^{-h_m/2} \frac{1}{s_{33}^{E}}\left(-\rho z - d_{33}E_3\right)Wzdz \tag{4.90}$$

Using elasticity solution 4.37, the curvature equation can be found in terms of the force (F_o) and electric field (E_3)

$$\rho = -\frac{12 s_m s_{33}^{E}\left(L-x\right)}{X_{33}W}F_o + \frac{12 d_{33} s_m h_p\left(h_m + h_p\right)}{X_{33}}E_3 \tag{4.91}$$

With this curvature, the stress relation can be found. The upper two layer's stress equation is the same as that for the unimorph case except for the difference in curvature. The lower layer's stress equation can be described as

$$\sigma_1 = \frac{1}{s_{33}^{E}}\left(-\rho z - d_{33}E_3\right) \tag{4.92}$$

The total system energy in this triple morph cantilever beam can be found by substituting all the stresses in the form of curvature into each layer's energy equation. The system energy, excluding the electrode area is

$$U = \sum_{i=1}^{n}\int_{\frac{(i-1)L}{n}+\frac{b}{2}}^{\frac{iL}{n}-\frac{b}{2}}\int_0^W\left(\int_{h_m/2}^{h_m/2+h_p} dU_{pu}dz + \int_{-h_m/2}^{h_m/2} dU_m dz + \int_{-h_m/2-h_p}^{-h_m/2} dU_{pl}dz\right)dydx$$

$$= \frac{s_{33}^E s_m \left(nb^2 + 4nL^2 - 2Lb\right)\left(L - nb\right)}{2nX_{33}W} F_o^{\,2} - \frac{6d_{33}s_m h_p L\left(h_m + h_p\right)\left(L - nb\right)}{X_{33}} F_o E_3$$

$$+\epsilon_{33}^T W h_p \left(L - nb\right)\left(1 - \frac{\left(2s_m h_p^3 + h_m^3 s_{33}^E\right)}{X_{33}} K_{33}^2\right) E_3^2 \qquad (4.93)$$

where dU_{pu}, dU_m, dU_{pl} are the upper, middle, and lower layer's energy, n is the number of segments, b is the electrode width, L is the length of cantilever beam and W is the width of the beam.

Substituting into Eq. 4.93 for the electric field, $E_3 = V/h = V/\left(L/n\right)$, and differentiating with respect to V yields

$$Q = \frac{\partial U}{\partial V}$$

$$= -\frac{6nd_{33}s_m h_p \left(h_m + h_p\right)\left(L - nb\right)}{X_{33}} F_o + \frac{2n^2 \epsilon_{33}^T W h_p \left(L - nb\right)}{L^2}\left(1 - \frac{\left(2s_m h_p^3 + h_m^3 s_{33}^E\right)}{X_{33}} K_{33}^2\right) V \qquad (4.94)$$

where $X_{33} = 12 s_m h_p^{\,2} h_m + 8 s_m h_p^{\,3} + 6 s_m h_p h_m^{\,2} + s_{33}^E h_m^{\,3}$ and $K_{33} = d_{33} \Big/ \sqrt{\epsilon_{33}^T s_{33}^E}$

Thus the generated charge from force is

$$Q_{Gen} = -\frac{6nd_{33}s_m h_p \left(h_m + h_p\right)\left(L - nb\right)}{X_{33}} F_o \qquad (4.95)$$

and the open circuit capacitance is

$$C_{free} = \frac{2n^2 \epsilon_{33}^T W h_p \left(L - nb\right)}{L^2}\left(1 - \frac{\left(2s_m h_p^3 + h_m^3 s_{33}^E\right)}{X_{33}} K_{33}^2\right) \qquad (4.96)$$

The generated voltage is

$$V_{Gen} = \frac{Q_{Gen}}{C_{free}} = -\frac{3s_m d_{33} L^2 \left(h_m + h_p\right)}{n\epsilon_{33}^T W X_{33}\left(1 - \left(\frac{2s_m h_p^3 + s_{33}^E h_m^3}{X_{33}}\right) K_{33}^2\right)} F_o \tag{4.97}$$

Finally, the total generated electric energy from force F_o is

$$U_{Gen} = Q_{Gen} V_{Gen} = \frac{18 d_{33}^2 s_m^2 h_p \left(h_m + h_p\right)^2 \left(L - nb\right) L^2}{\epsilon_{33}^T W X_{33}{}^2 \left(1 - \left(\frac{2s_m h_p^3 + s_{33}^E h_m^3}{X_{33}}\right) K_{33}^2\right)} F_o{}^2 \tag{4.98}$$

4.5 Diaphragm (Circular Plate) with Constant Pressure

A diaphragm structure is a common structure for pressure sensors such as those that detect acoustic pressure or hydraulic pressure (Figure 27). The analytical solution exists for a circular disk with clamped edges. This solution follows some restriction. From the general elasticity description of thick plate, it is known that there is no shear strain and no stress along thickness direction (*z*-dir). Another restriction is that the deflection is much smaller than thickness of the plate. Again, the energy method will be used to calculate the generated charge. The conventional 31 and interdigitated configurations will be solved for each unimorph and triple morph case.

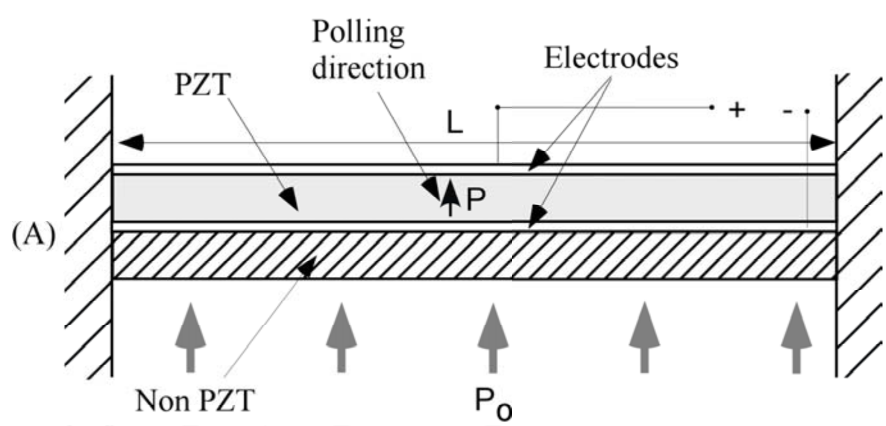

Figure 26. . Unimorph PZT Circular plate with electrode configuration and it's polling direction

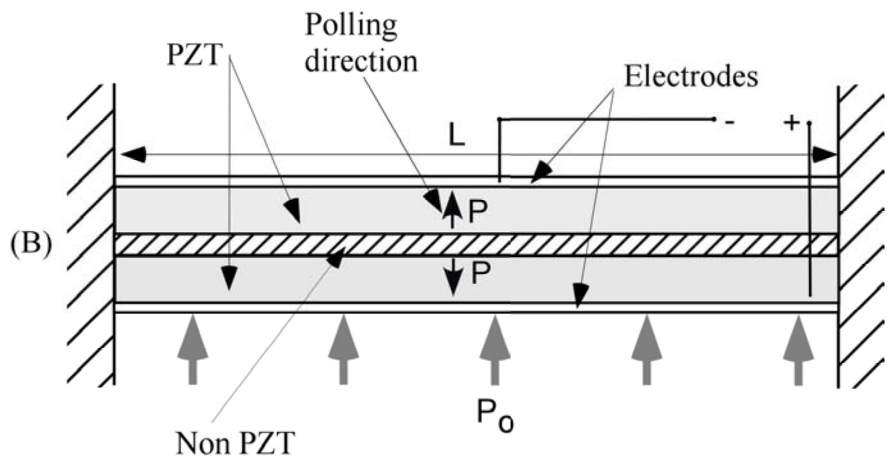

Figure 27. Triple-morph PZT Circular plate with electrode configuration and it's polling direction

The moment equation which we need for the calculation of the curvature is from the elasticity solution [20] for the clamped circular diaphragm.

$$W_r = \frac{P_o\left(a^4 - 2a^2r^2 + r^4\right)}{64D} \tag{4.99}$$

$$\left.\begin{aligned} M_r &= -D\left(\frac{\partial^2 W_r}{\partial r^2} + \frac{1}{r}\frac{\partial W_r}{\partial r}\right) = \frac{P_o}{16}\left(a^2 - 3r^2 + \nu a^2 - \nu r^2\right) \\ M_\theta &= -D\left(\frac{1}{r}\frac{\partial W_r}{\partial r} + \nu\frac{\partial^2 W_r}{\partial r^2}\right) = \frac{P_o}{16}\left(a^2 - r^2 + \nu a^2 - 3\nu r^2\right) \end{aligned}\right\} \tag{4.100}$$

where W_r is the deflection of the diaphragm in the z direction, r is the distance from the center of the diaphragm to the point of deflection, and a is the radius of the diaphragm. The constant D is related to the structure property but is not important here because we need moments and the D will be canceled out at the moment equation.

Not like cantilever beams, there are two moment terms. One is radial direction and the other is angular direction. Thus, there will be two curvatures and each curvature equation will be in terms of both moment terms. However, for the 31-type diaphragm, there is only one neutral surface, since the surface depends only on the cross-section of the bender and the elastic properties are the same for radial and angular direction. Therefore, strain-curvature equation for the 31-type diaphragm is described as

$$\varepsilon_r = -\rho_r \left(z - z_c \right) , \qquad \varepsilon_\theta = -\rho_\theta \left(z - z_c \right) \tag{4.101}$$

In the 33-type diaphragm case, the elastic properties are different from each direction. The elastic property for the angular direction does not change, but for the radial direction, the elastic property is changed from $1/s_{11}^E$ to $1/s_{33}^E$. Therefore, the neutral surface for the each direction should be different. The strain-curvature equation for the interdigitated diaphragm is

$$\varepsilon_r = -\rho_r \left(z - z_{c3} \right), \quad \varepsilon_\theta = -\rho_\theta \left(z - z_c \right) \tag{4.102}$$

In this section, energy generation for all 4 types will be developed as cantilever PEG. 31-type unimorph diaphragm, interdigitated unimorph diaphragm, 31-type triple morph diaphragm, and interdigitated triple morph diaphragm will be shown here.

4.5.1 Unimorph Circular Plate

As in the unimorph cantilever beam, the neutral surface of the unimorph diaphragm is not on the middle surface. Also the neutral surface moves by the electric field changes but this change is assumed to be small enough to be neglected. Only elastic properties of the PZT will be considered to calculate neutral surface for the unimorph diaphragm.

4.5.2 Unimorph 31 Circular Plate

The moment in the diaphragm is calculated using equation 4.39 which was used in the cantilever beam. This time, the constitutive equation is a little bit more complex than the cantilever beam case. The constitutive equation 4.3 and 4.4 can be written for diaphragm and is

$$\left.\begin{aligned} \varepsilon_r &= s_{11}^E\left(\sigma_r - \nu\sigma_\theta\right) - d_{31}E_3 \\ \varepsilon_\theta &= s_{11}^E\left(\sigma_\theta - \nu\sigma_r\right) - d_{31}E_3 \\ D_3 &= -d_{31}\left(\sigma_r + \sigma_\theta\right) + \epsilon_{33}^T E_3 \end{aligned}\right\} \tag{4.103}$$

where $\nu\left(= -s_{12}^E / s_{11}^E\right)$ is poison's ratio and the poling direction is downward. Radial direction is 1, angular direction is 2, and perpendicular to the surface is 3. The subscript r and θ are used instead of 1 and 2. Using this piezoelectric constitutive equation, stress can be described as strains and electric field.

For the piezoelectric, the upper layer is

$$\left.\begin{aligned} \sigma_r &= \frac{1}{s_{11}^E\left(1-\nu^2\right)}\left(\varepsilon_r + \nu\varepsilon_\theta + \left(1+\nu\right)d_{31}E_3\right) \\ \sigma_\theta &= \frac{1}{s_{11}^E\left(1-\nu^2\right)}\left(\nu\varepsilon_r + \varepsilon_\theta + \left(1+\nu\right)d_{31}E_3\right) \end{aligned}\right\} \tag{4.104}$$

and for the non-piezoelectric lower layer

$$\left.\begin{aligned} \sigma_r &= \frac{1}{s_m\left(1-\nu^2\right)}\left(\varepsilon_r + \nu\varepsilon_\theta\right) \\ \sigma_\theta &= \frac{1}{s_m\left(1-\nu^2\right)}\left(\nu\varepsilon_r + \varepsilon_\theta\right) \end{aligned}\right\} \tag{4.105}$$

To replace strain with pressure, the curvature equation should be found. As in the cantilever beam case, the curvature equation might be found from moment equation. The moment equation from the above stress equation is described as

$$\left.\begin{aligned} M_r &= \int_0^{h_p} \left(\frac{\varepsilon_r + \nu\varepsilon_\theta}{\left(1-\nu^2\right)S_{11}^E} + \frac{\left(1+\nu\right)d_{31}E_3}{\left(1-\nu^2\right)S_{11}^E} \right)\left(z - z_c\right)dz + \int_{-h_m}^0 \left(\frac{\varepsilon_r + \nu\varepsilon_\theta}{\left(1-\nu^2\right)S_m} \right)\left(z - z_c\right)dz \\ M_\theta &= \int_0^{h_p} \left(\frac{\nu\varepsilon_r + \varepsilon_\theta}{\left(1-\nu^2\right)S_{11}^E} + \frac{\left(1+\nu\right)d_{31}E_3}{\left(1-\nu^2\right)S_{11}^E} \right)\left(z - z_c\right)dz + \int_{-h_m}^0 \left(\frac{\nu\varepsilon_r + \varepsilon_\theta}{\left(1-\nu^2\right)S_m} \right)\left(z - z_c\right)dz \end{aligned}\right\} \quad (4.106)$$

The strain-curvature equations can be obtained by substituting equation 4.101 into the equation 4.106 gives the strain-curvature equations. After rearranging the curvature is

$$\left.\begin{aligned} \rho_r &= -\frac{12S_{11}^E S_m\left(s_{11}^E h_m + s_m h_p\right)}{B_{31}}\left(M_r - \nu M_\theta\right) + \frac{6d_{31}s_{11}^E s_m h_p h_m\left(h_m + h_p\right)}{B_{31}}E_3 \\ \rho_\theta &= -\frac{12S_{11}^E S_m\left(s_{11}^E h_m + s_m h_p\right)}{B_{31}}\left(M_\theta - \nu M_r\right) + \frac{6d_{31}s_{11}^E s_m h_p h_m\left(h_m + h_p\right)}{B_{31}}E_3 \end{aligned}\right\} \quad (4.107)$$

where $B_{31} = h_p{}^4 s_m{}^2 + 4s_{11}^E s_m h_m h_p{}^3 + 6s_{11}^E s_m h_m{}^2 h_p{}^2 + 4s_{11}^E s_m h_m{}^3 h_p + h_m{}^4 s_{11}^2$

Energies of each layer are described differently. For the diaphragm structure, the energies in a small volume can be described as

$$\left.\begin{aligned} dU_p &= \frac{1}{2}\varepsilon_r\sigma_{rp} + \frac{1}{2}\varepsilon_\theta\sigma_{\theta p} - \frac{d_{31}\left(\sigma_{rp} + \sigma_{\theta p}\right)}{2}E_3 + \frac{1}{2}\epsilon_{33}^T E_3^2 \quad &&\text{for piezoelectric} \\ dU_m &= \frac{1}{2}\varepsilon_r\sigma_{rp} + \frac{1}{2}\varepsilon_\theta\sigma_{\theta p} &&\text{for non-piezoelectric} \end{aligned}\right\} \quad (4.108)$$

The stresses used in above equation 4.108 can be replaced with equation 4.104 and 4.105. Then, using the strain-curvature equation 4.101 and 4.107, above energy equations can be a function of moment and electric field. This moment can also be replaced by equation 4.100. Therefore, total system energy can be written in pressure and electric field.

$$U = \int_0^a \int_0^{2\pi} \left(\int_0^{h_p} dU_p dz + \int_{-h_m}^0 dU_m dz \right) r d\theta dr$$

$$= \frac{\pi a^6 s_{11}^E s_m s_h \left(1-\nu^2\right)}{32 B_{31}} P_o^{\ 2} +$$

$$\frac{\epsilon_{33}^T \pi a^2 h_p}{2} \left(1 - \frac{2}{(1-\nu)} \left(1 - \frac{3 s_{11}^{E2} s_m h_m^{\ 2} h_p \left(h_p + h_m\right)^2}{S_h B_{31}} - 1\right) K_{31}^2\right) E_3^{\ 2} \tag{4.109}$$

Electric field is constant throughout the structure, since the electrodes cover the whole surface. Therefore, the field is constant throughout the diaphragm structure. After integrating, the total energy Equation 4.109, electric field (E_3) can be replaced by V/h_p. The general charge from the external condition can be found by differentiating total energy with respect to the voltage (V) which gives

$$Q = \frac{\epsilon_{33}^T \pi a^2}{h_p} \left(1 - \frac{2}{(1-\nu)} \left(1 - \frac{3 s_{11}^{E2} s_m h_m^{\ 2} h_p \left(h_p + h_m\right)^2}{S_h B_{31}}\right) K_{31}^2\right) V \tag{4.110}$$

This is the general equation of the charge generation. When converting mechanical energy to electrical energy, there is no applied voltage. Thus the converted energy from pressure is only described with the pressure term.

Generated charge

$$Q_{Gen} = 0 \tag{4.111}$$

Open circuit capacitance will be

$$C_{free} = \frac{\epsilon_{33}^T \pi a^2}{h_p} \left(1 - \frac{2}{(1-\nu)} \left(1 - \frac{3 s_{11}^{E2} s_m h_m^{\ 2} h_p \left(h_p + h_m\right)^2}{S_h B_{31}}\right) K_{31}^2\right) \tag{4.112}$$

Generated voltage

$$V_{gen} = \frac{Q_{gen}}{C_{free}} = 0 \tag{4.113}$$

Generated electrical energy

$$U_{Gen} = Q_{Gen} * V_{Gen} = 0 \tag{4.114}$$

4.5.3 Unimorph Interdigitated Circular Plate

In this interdigitated case, the moment equation is almost the same as for the 31 case except for the elastic and piezoelectric parameter. s_{11}^E has been changed to s_{33}^E and d_{31} has been changed to d_{33}. Of course, the neutral surface has been changed too. For the interdigitated diaphragm, the constitutive equation is

$$\left.\begin{aligned} \varepsilon_r &= s_{33}^E\left(\sigma_r - \nu\sigma_\theta\right) - d_{33}E_3 \\ \varepsilon_\theta &= s_{33}^E\left(\sigma_\theta - \nu\sigma_r\right) - d_{33}E_3 \\ D_3 &= -d_{33}\left(\sigma_r + \sigma_\theta\right) + \epsilon_{33}^T E_3 \end{aligned}\right\} \tag{4.115}$$

Here, radial direction is poling direction which is 3, angular direction is 2. The Poisson ratio is now $\nu = -s_{32}^E / s_{33}^E$. Stresses in the circular plate can be found by rearranging above constitutive Equation 4.115. The stresses in the interdigitated piezoelectric layer can be described as

$$\left.\begin{aligned} \sigma_{rl} &= \frac{1}{(1-\nu^2)s_{33}^E}\left(\varepsilon_r + \nu\varepsilon_\theta - (1+\nu)d_{33}E_3\right) \\ \sigma_{\theta l} &= \frac{1}{(1-\nu^2)s_{33}^E}\left(\nu\varepsilon_r + \varepsilon_\theta - (1+\nu)d_{33}E_3\right) \end{aligned}\right\} \tag{4.116}$$

and the stress in the non piezoelectric layer is the same as the 31 type unimorph diaphragm case in Eq. 4.105. Again, the moment equations for this interdigitated unimorph structure are

$$\left.\begin{aligned} M_r &= \int_0^{h_p}\left(\frac{\varepsilon_r + \nu\varepsilon_\theta}{\left(1-\nu^2\right)s_{33}^E} + \frac{\left(1+\nu\right)d_{33}E_3}{\left(1-\nu^2\right)s_{33}^E}\right)\left(z - z_{c3}\right)dz + \int_{-h_m}^{0}\left(\frac{\varepsilon_r + \nu\varepsilon_\theta}{\left(1-\nu^2\right)S_m}\right)\left(z - z_{c3}\right)dz \\ M_\theta &= \int_0^{h_p}\left(\frac{\nu\varepsilon_r + \varepsilon_\theta}{\left(1-\nu^2\right)s_{33}^E} + \frac{\left(1+\nu\right)d_{33}E_3}{\left(1-\nu^2\right)s_{33}^E}\right)\left(z - z_c\right)dz + \int_{-h_m}^{0}\left(\frac{\nu\varepsilon_r + \varepsilon_\theta}{\left(1-\nu^2\right)S_m}\right)\left(z - z_c\right)dz \end{aligned}\right\} \tag{4.117}$$

Substituting the strain - curvature Equation 4.102 into the above moment Equation 4.117 gives the curvature – moment equations. After rearranging, the curvatures are

$$\left.\begin{aligned}\rho_r &= -\frac{12 s_{33}^E s_m \left(s_{33}^E h_m + s_m h_p\right)}{B_{33}}\left(M_r - \nu M_\theta\right) + \frac{6 d_{33} s_{33}^E s_m h_p h_m \left(h_m + h_p\right)}{B_{33}} E_3 \\ \rho_\theta &= -\frac{12 s_{33}^E s_m \left(s_{33}^E h_m + s_m h_p\right)}{B_{33}}\left(M_\theta - \nu M_r\right) + \frac{6 d_{33} s_{33}^E s_m h_p h_m \left(h_m + h_p\right)}{B_{33}} E_3\end{aligned}\right\} \quad (4.118)$$

where $B_{33} = {h_p}^4 {s_m}^2 + 4 s_{33}^E s_m {h_p}^3 h_m + 6 s_{33}^E s_m {h_p}^2 {h_m}^2 + 4 s_{33}^E s_m h_p {h_m}^3 + {h_m}^4 s_{33}^{E\,2}$

The equation for the energy in the small volume of the piezoelectric layer is,

$$dU_p = \frac{1}{2}\varepsilon_r \sigma_{rp} + \frac{1}{2}\varepsilon_\theta \sigma_{\theta p} - \frac{d_{33}\left(\sigma_{rp} + \sigma_{\theta p}\right)}{2} E_3 + \frac{1}{2}\epsilon_{33}^T E_3^2 \quad (4.119)$$

The total energy can be obtained by integrating over the volume where no electrode is on the surface. As mentioned before, the area directly below the electrode is not poled in the 33 direction, and to ensure 33 poling between the electrodes, the electrodes should be located “far away” from each other and they should be narrow. Thus we can assume that the area below the electrode is small and can be neglected.

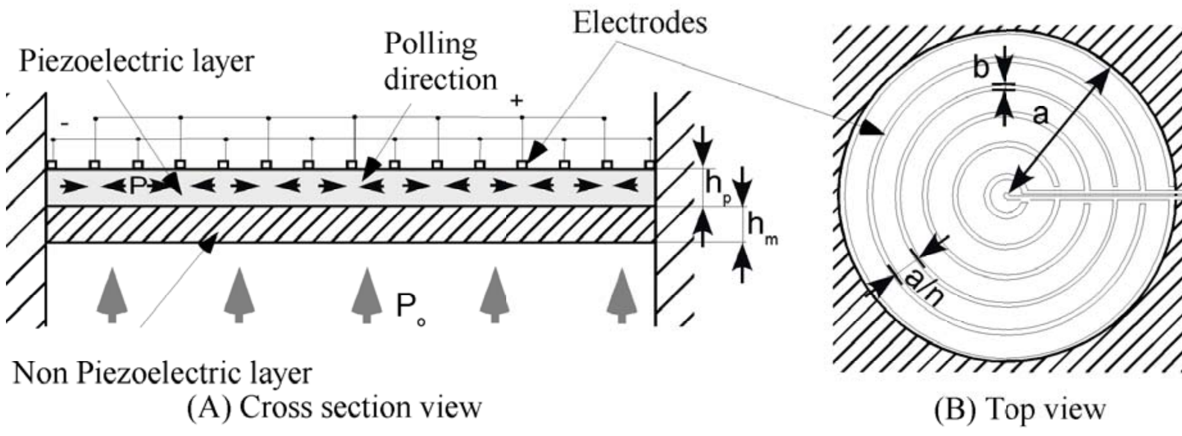

Figure 28. Interdigitated unimorph diaphragm

The total energy except the volume directly under the electrode is

$$U=\sum_{i=1}^{n}\int_{a(i-1)/n+b/2}^{ai/n-b/2}\int_{0}^{2\pi}\left(\int_{0}^{h_p}dU_p dz+\int_{-h_m}^{0}dU_m dz\right)rd\theta dr$$

$$=\frac{a\pi s_{33}^{E}s_m s_{h3}Y\left(1-\nu^2\right)\left(a-nb\right)}{1024n^3B_{33}}P_o^{\,2}-\frac{3}{8}\frac{\pi abd_{33}s_{33}^{E}s_m h_m h_p\left(h_m+h_p\right)\left(2a-nb\right)\left(a-nb\right)\left(1+\nu\right)}{nB_{33}}P_oE_3$$

$$+\frac{\epsilon_{33}^{T}\pi ah_p\left(a-nb\right)}{2}\left(1-\frac{2}{\left(1-\nu\right)}\left(1-\frac{3s_{33}^{E\,2}s_m h_m^{\;2}h_p\left(h_m+h_p\right)^2}{S_{h3}B_{33}}\right)K_{33}^{2}\right)E_3^{\;2} \quad (4.120)$$

where
$Y=32n^3a^4-8a^3b(13n^2-3\nu-5+3\nu n^2)+4na^2b^2(3\nu n^2+13n^2+6\nu+10)+(3b^4n^3-12ab^3n^2)(5+3\nu)$

Here, n is the number of the cluster (volume between electrodes) which means that there are $n+1$ electrodes on the surface. a is radius of the diaphragm and b is the width of the electrode.

dU_m is the energy of non piezoelectric layer and shown in equation 4.108. After substituting electric field (E_3) with $V/\left(a/n\right)$, this total energy equation will be described in terms of pressure and voltage. The general charge generation is the derivative of the total energy with respect to the voltage (V).

$$Q=\frac{\epsilon_{33}^{T}\pi n^2\left(a-nb\right)h_p}{a}\left(1-\frac{2}{\left(1-\nu\right)}\left(1-\frac{3s_{33}^{E\,2}s_m h_m^{\;2}h_p\left(h_m+h_p\right)^2}{S_{h3}B_{33}}\right)K_{33}^{2}\right)V$$

$$-\frac{3}{8}\frac{\pi abd_{33}s_{33}^{E}s_m h_m h_p\left(h_m+h_p\right)\left(2a-nb\right)\left(a-nb\right)\left(1+\nu\right)}{nB_{33}}P_o \quad (4.121)$$

with this general charge, the following solutions can be obtained. Thus the generated charge due to pressure is

$$Q_{Gen}=-\frac{3}{8}\frac{\pi abd_{33}s_{33}^{E}s_m h_m h_p\left(h_m+h_p\right)\left(2a-nb\right)\left(a-nb\right)\left(1+\nu\right)}{nB_{33}}P_o \quad (4.122)$$

and the open circuit capacitance is

$$C_{free} = \frac{\epsilon_{33}^{T} \pi n^2 \left(a - nb\right) h_p}{a} \left(1 - \frac{2}{\left(1-\nu\right)} \left(1 - \frac{3 s_{33}^{E\,2} s_m h_m{}^2 h_p \left(h_m + h_p\right)^2}{S_{h3} B_{33}}\right) K_{33}^2\right) \tag{4.123}$$

Therefore, the generated voltage is

$$V_{gen} = \frac{Q_{gen}}{C_{free}} = -\frac{3}{8} \frac{a^2 b d_{33} s_{33}^{E} s_m h_m \left(h_m + h_p\right)\left(2a - nb\right)\left(1+\nu\right)}{\epsilon_{33}^{T} n^3 B_{33} \left(1 - \frac{2}{\left(1-\nu\right)} \left(1 - \frac{3 s_{33}^{E\,2} s_m h_m{}^2 h_p \left(h_m + h_p\right)^2}{S_{h3} B_{33}}\right) K_{33}^2\right)} P_o \tag{4.124}$$

Thus, the energy generated by external pressure is

$$\begin{aligned} U_{Gen} &= Q_{Gen} * V_{Gen} \\ &= \frac{9}{64} \frac{\pi a^3 b^2 d_{33}{}^2 s_{33}^{E\,2} s_m{}^2 h_m{}^2 h_p \left(h_m + h_p\right)^2 \left(a - nb\right)\left(2a - nb\right)^2 \left(1+\nu\right)^2}{\epsilon_{33}^{T} n^4 B_{33}{}^2 \left(1 - \frac{2}{\left(1-\nu\right)} \left(1 - \frac{3 s_{33}^{E\,2} s_m h_m{}^2 h_p \left(h_m + h_p\right)^2}{S_{h3} B_{33}}\right) K_{33}^2\right)} P_o{}^2 \end{aligned} \tag{4.125}$$

4.5.4 Triple Layered Circular Plate

The deflection from the elasticity solution 4.99 is also true in the triple layered diaphragm. The difference from the unimorph case is that there is one more layer to calculate and the location of the neutral surface in on the middle surface. As triple morph cantilever, the electric field directions of the piezoelectric layers are opposite to each other to maximize the bending effect. In this section, the upper piezoelectric layer has negative electric field and the lower layer have positive electric field (refer to Figure 23). Both upper and lower piezoelectric layers' thicknesses are the same, h_p , and h_m is the thickness of the non-piezoelectric middle layer.

4.5.5 31 Triple-morph Circular Plate

The constitutive equations for the upper and middle layers are already shown in equation 4.103. The constitutive equation for the lower layer is

$$\left.\begin{aligned}\varepsilon_r &= s_{11}^E\left(\sigma_r - \nu\sigma_\theta\right) + d_{31}E_3\\ \varepsilon_\theta &= s_{11}^E\left(\sigma_\theta - \nu\sigma_r\right) + d_{31}E_3\\ D_3 &= d_{31}\left(\sigma_r + \sigma_\theta\right) - \epsilon_{33}^T E_3\end{aligned}\right\} \tag{4.126}$$

Except the electric field direction (E_3), this constitutive equation is exactly same as the piezoelectric layer of the 31-type unimorph case. The stresses are also the same as the 31-type unimorph case (Eqs. 4.104-4.105) except for the lower layer. The electric field of the lower layer is opposite to the upper layer, and stresses are described differently. The stress of the lower layer is

$$\left.\begin{aligned}\sigma_r &= \frac{1}{s_{11}^E\left(1-\nu^2\right)}\left(\varepsilon_r + \nu\varepsilon_\theta - \left(1+\nu\right)d_{31}E_3\right)\\ \sigma_\theta &= \frac{1}{s_{11}^E\left(1-\nu^2\right)}\left(\nu\varepsilon_r + \varepsilon_\theta - \left(1+\nu\right)d_{31}E_3\right)\end{aligned}\right\} \tag{4.127}$$

Using these stresses, the moments of each layer can be obtained. The moment equations for the triple layer is

$$\begin{aligned}M_r = &\int_{\frac{hm}{2}}^{\frac{hm}{2}+hp}\left(\frac{\varepsilon_r+\nu\varepsilon_\theta}{\left(1-\nu^2\right)s_{11}^E}+\frac{1+\nu}{\left(1-\nu^2\right)s_{11}^E}d_{31}E_3\right)z\ \ dz+\int_{-\frac{hm}{2}}^{\frac{hm}{2}}\left(\frac{\varepsilon_r+\nu\varepsilon_\theta}{\left(1-\nu^2\right)s_m}\right)z\ \ dz\\ &+\int_{-\frac{hm}{2}-hp}^{-\frac{hm}{2}}\left(\frac{\varepsilon_r+\nu\varepsilon_\theta}{\left(1-\nu^2\right)s_{11}^E}-\frac{1+\nu}{\left(1-\nu^2\right)s_{11}^E}d_{31}E_3\right)z\ \ dz\\ &=-\frac{X_{31}}{12(1-\nu^2)s_{11}^E s_m}(\rho_r+\nu\rho_\theta)+\frac{d_{31}h_p\left(h_p+h_m\right)}{s_{11}^E(1-\nu)}E_3\end{aligned} \tag{4.128}$$

$$M_{\theta r}=\int_{\frac{hm}{2}}^{\frac{hm}{2}+hp}\left(\frac{\varepsilon_\theta+\nu\varepsilon_r}{\left(1-\nu^2\right)s_{11}^E}+\frac{1+\nu}{\left(1-\nu^2\right)s_{11}^E}d_{31}E_3\right)z\quad dz+\int_{-\frac{hm}{2}}^{\frac{hm}{2}}\left(\frac{\varepsilon_\theta+\nu\varepsilon_r}{\left(1-\nu^2\right)s_m}\right)z\quad dz$$

$$+\int_{-\frac{hm}{2}-hp}^{-\frac{hm}{2}}\left(\frac{1}{\left(1-\nu^2\right)s_{11}^E}\left(\varepsilon_\theta+\nu\varepsilon_r\right)-\frac{1+\nu}{\left(1-\nu^2\right)s_{11}^E}d_{31}E_3\right)zdz$$

$$=-\frac{X_{31}}{12(1-\nu^2)s_{11}^E s_m}(\nu\rho_r+\rho_\theta)+\frac{d_{31}h_p\left(h_p+h_m\right)}{(1-\nu)s_{11}^E}E_3 \qquad (4.129)$$

Strains ($\varepsilon_\theta,\varepsilon_r$) are described in terms of the curvature. Substituting for strain with Eq. 4.101 and rearranging for the curvature

$$\left.\begin{aligned}\rho_r&=-\frac{12s_{11}^E s_m(M_r-\nu M_\theta)}{X_{31}}+\frac{12d_{31}s_m h_p(h_m+h_p)E_3}{X_{31}}\\ \rho_\theta&=-\frac{12s_{11}^E s_m(M_\theta-\nu M_r)}{X_{31}}+\frac{12d_{31}s_m h_p(h_m+h_p)E_3}{X_{31}}\end{aligned}\right\} \qquad (4.130)$$

where $X_{31}=6s_m h_p h_m{}^2+12s_m h_p{}^2 h_m+8s_m h_p{}^3+s_{31}^E h_m{}^3$

Thus, all the stress and the strains in the structure can be described with moments and electric fields. Energies can be solved with those stress and strain equations. The upper two layers are already shown in Equation 4.108, and the energy in the lower layer is described as

$$dU_{pl}=\frac{1}{2}\varepsilon_r\sigma_r+\frac{1}{2}\varepsilon_\theta\sigma_\theta+\frac{1}{2}d_{31}E_3(\sigma_r+\sigma_\theta)+\frac{1}{2}\epsilon^T{}_{33}E_3{}^2 \qquad (4.131)$$

Thus the total system energy can be found as

$$U=\int_0^a\int_0^{2\pi}\left(\int_{h_m/2}^{h_m/2+h_p}dU_{pu}\,dz+\int_{-h_m/2}^{h_m/2}dU_m\,dz+\int_{-h_{m/2}-h_p}^{-h_m/2}dU_{pl}\,dz\right)rd\theta dr$$

$$=\frac{\pi a^6 s_{11}^E s_m\left(1-\nu^2\right)}{32X_{31}}P_o^2+\epsilon_{33}^T\pi a^2 h_p\left(1-\frac{2}{(1-\nu)}\left(1-\frac{6s_m h_p\left(h_m+h_p\right)^2}{X_{31}}\right)K_{31}{}^2\right)E_3{}^2 \qquad (4.132)$$

where $K_{31}=d_{31}\Big/\sqrt{\epsilon_{33}^T s_{11}^E}$.

Again, replace the electric field (E_3) with $V/2h_p$ and differentiate the energy equation with respect to voltage (V) to obtain general charge generation.

$$Q=\frac{\partial U}{\partial V}=\frac{\epsilon_{33}^{T}\pi a^{2}}{2h_p}\left(1-\frac{2}{(1-\nu)}\left(1-\frac{6s_m h_p\left(h_m+h_p\right)^2}{X_{31}}\right){K_{31}}^{2}\right)V \tag{4.133}$$

Therefore, the generated charge from the pressure is

$$Q_{Gen}=0 \tag{4.134}$$

and the open circuit capacitance is

$$C_{free}=\frac{\epsilon_{33}^{T}\pi a^{2}}{2h_p}\left(1-\frac{2}{(1-\nu)}\left(1-\frac{6s_m h_p\left(h_m+h_p\right)^2}{X_{31}}\right){K_{31}}^{2}\right) \tag{4.135}$$

The voltage appeared in the electrodes is

$$V_{Gen}=0 \tag{4.136}$$

Finally, the electrical energy generated due to the constant pressure is

$$U_{Gen}=Q_{Gen}*V_{Gen}=0 \tag{4.137}$$

4.5.6 Triple-morph Interdigitated Circular Plate

The deflection shape and moment in the structure (W_{plate}, M_r and M_θ) are all the same as before. The constitutive equation used here is the same as the unimorph interdigitated diaphragm except lower layer. The electric field for the lower layer is opposite to the upper layer (Eq.4.116). That is

$$\left.\begin{aligned}\varepsilon_r&=s_{33}^{E}\left(\sigma_r-\nu\sigma_\theta\right)+d_{33}E_3\\ \varepsilon_\theta&=s_{33}^{E}\left(\sigma_\theta-\nu\sigma_r\right)+d_{33}E_3\\ D_3&=d_{33}\left(\sigma_r+\sigma_\theta\right)-\epsilon_{33}^{T}E_3\end{aligned}\right\} \tag{4.138}$$

Therefore, the stress distribution for the lower layer is

$$\left.\begin{aligned}\sigma_{ru} &= \frac{1}{(1-\nu^2)s_{33}^E}\left(\varepsilon_r + \nu\varepsilon_\theta + (1+\nu)d_{33}E_3\right)\\ \sigma_{\theta u} &= \frac{1}{(1-\nu^2)s_{33}^E}\left(\nu\varepsilon_r + \varepsilon_\theta + (1+\nu)d_{33}E_3\right)\end{aligned}\right\} \tag{4.139}$$

The stress distributions for the upper two layers are the same as the interdigitated unimorph diaphragm and are shown in Equations. 4.116, and 4.105. For the moment equations, there is not much difference from the moment equation of the 31-type triple morph diaphragm. s_{33}^E and d_{33} are used instead of s_{11}^E and d_{31}. The moment equations for the interdigitated triple layered diaphragm is

$$\begin{aligned}M_r &= \int_{\frac{h_m}{2}}^{\frac{h_m}{2}+h_p}\left(\frac{\varepsilon_r+\nu\varepsilon_\theta}{(1-\nu^2)s_{33}^E} + \frac{(1+\nu)}{(1-\nu^2)s_{33}^E}d_{33}E_3\right)zdz + \int_{-\frac{h_m}{2}}^{\frac{h_m}{2}}\frac{\varepsilon_r+\nu\varepsilon_\theta}{(1-\nu^2)s_m}zdz\\ &\quad + \int_{-\frac{h_m}{2}-h_p}^{-\frac{h_m}{2}}\left(\frac{\varepsilon_r+\nu\varepsilon_\theta}{(1-\nu^2)s_{33}^E} - \frac{(1+\nu)}{(1-\nu^2)s_{33}^E}d_{33}E_3\right)zdz\\ &= -\frac{X_{33}}{12(1-\nu^2)s_{33}^E s_m}(\rho_r+\nu\rho_\theta) + \frac{d_{33}h_p\left(h_p+h_m\right)}{(1-\nu)s_{33}^E}E_3\end{aligned} \tag{4.140}$$

$$\begin{aligned}M_\theta &= \int_{\frac{h_m}{2}}^{\frac{h_m}{2}+h_p}\left(\frac{\nu\varepsilon_r+\varepsilon_\theta}{(1-\nu^2)s_{33}^E} + \frac{(1+\nu)}{(1-\nu^2)s_{33}^E}d_{33}E_3\right)zdz + \int_{-\frac{h_m}{2}}^{\frac{h_m}{2}}\frac{\nu\varepsilon_r+\varepsilon_\theta}{(1-\nu^2)s_m}zdz\\ &\quad + \int_{-\frac{h_m}{2}-h_p}^{-\frac{h_m}{2}}\left(\frac{\nu\varepsilon_r+\varepsilon_\theta}{(1-\nu^2)s_{33}^E} - \frac{(1+\nu)}{(1-\nu^2)s_{33}^E}d_{33}E_3\right)zdz\\ &= -\frac{X_{33}}{12(1-\nu^2)s_{33}^E s_m}(\nu\rho_r+\rho_\theta) + \frac{d_{33}h_p\left(h_p+h_m\right)}{(1-\nu)s_{33}^E}E_3\end{aligned} \tag{4.141}$$

After replacing strain with strain-curvature Equation. 4.102, The curvature equations can be found from above moment Equations. 4.140, 4.141

$$\left.\begin{aligned}\rho_r &= -\frac{12 s_{33}^E s_m}{X_{33}}(M_r - \nu M_\theta) + \frac{12 d_{33} s_m h_p (h_p + h_m)}{X_{33}} E_3 \\ \rho_\theta &= -\frac{12 s_{33}^E s_m}{X_{33}}(M_\theta - \nu M_r) + \frac{12 d_{33} s_m h_p (h_p + h_m)}{X_{33}} E_3\end{aligned}\right\} \tag{4.142}$$

where $X_{33} = 6 s_m h_p h_m{}^2 + 12 s_m h_p{}^2 h_m + 8 s_m h_p{}^3 + s_{33}^E h_m{}^3$.

The energy equations in the small volume of the each layer are described as

$$dU_{pu} = \left(\frac{1}{2}\varepsilon_r \sigma_{ru} + \frac{1}{2}\varepsilon_\theta \sigma_{\theta u} + \frac{1}{2} D_3 E_3\right)$$

$$= \left(\frac{1}{2}\varepsilon_r \sigma_{ru} + \frac{1}{2}\varepsilon_\theta \sigma_{\theta u} - \frac{1}{2} d_{33} E_3 (\sigma_{ru} + \sigma_{\theta u}) + \frac{1}{2}\epsilon_{33}^T E_3{}^2\right) \tag{4.143}$$

$$dU_{pl} = \left(\frac{1}{2}\varepsilon_r \sigma_{rl} + \frac{1}{2}\varepsilon_\theta \sigma_{\theta l} + \frac{1}{2} D_3 E_3\right)$$

$$= \left(\frac{1}{2}\varepsilon_r \sigma_{rl} + \frac{1}{2}\varepsilon_\theta \sigma_{\theta l} + \frac{1}{2} d_{33} E_3 (\sigma_{rl} + \sigma_{\theta l}) + \frac{1}{2}\epsilon_{33}^T E_3{}^2\right) \tag{4.144}$$

where dU_{pu} is the energy for upper layer, and dU_{pl} is the energy for lower layer. The energy equation for the middle non-piezoelectric layer is the same as previous Eq. 4.108. Total system energy without the volume under the electrode is

$$U_{total} = \sum_{i=1}^{n} \int_{a(i-1)/n+b/2}^{ai/n-b/2} \int_0^{2\pi} \left(\int_{\frac{h_m}{2}}^{\frac{h_m}{2}+h_p} dU_{pu} dz + \int_{-\frac{h_m}{2}}^{\frac{h_m}{2}} dU_m dz + \int_{-\frac{h_m}{2}-h_p}^{-\frac{h_m}{2}} dU_{pl} dz \right) r d\theta dr$$

$$= \frac{\pi a s_{33}^E s_m \left(1-\nu^2\right)\left(a-nb\right) Y_3}{1024 n^3 X_{33}} P_o^2 - \frac{3\pi a b d_{33} s_m h_p \left(2a-nb\right)(a-nb)\left(h_m+h_p\right)\left(1+\nu\right)}{4n X_{33}} P_o E_3$$

$$+ \epsilon_{33}^T \pi h_p a\left(a-nb\right)\left(1 - \frac{2}{\left(1-\nu\right)}\left(1 - \frac{6 s_m h_p \left(h_m+h_p\right)^2}{X_{33}}\right) K_{33}^2\right) E_3{}^2 \tag{4.145}$$

where

$Y_3 = 32 n^3 a^4 - 8 a^3 b (13 n^2 + 3\nu(n^2-1) - 5) + 4 n a^2 b^2 (13 n^2 + 3\nu(n^2+2) + 10) + (3 n^3 b^4 - 12 n^2 a b^3)(3\nu + 5)$, $K_{33} = d_{33} \big/ \sqrt{s_{33}^E \epsilon_{33}^T}$.

Since the distance between the electrode is a/n, E_3 can be replaced with $V/(a/n)$. The generated charge is now

$$Q=\frac{\partial U}{\partial V}=\frac{2\pi\epsilon_{33}^{T}n^{2}\left(a-nb\right)h_{p}}{a}\left(1-\frac{2}{\left(1-\nu\right)}\left(1-\frac{6s_{m}h_{p}\left(h_{m}+h_{p}\right)^{2}}{X_{33}}\right)K_{33}^{2}\right)V$$

$$-\frac{3\pi bd_{33}s_{m}h_{p}(2a-nb)(a-nb)\left(h_{m}+h_{p}\right)\left(1+\nu\right)}{4X_{33}}P_{o} \qquad (4.146)$$

With this general charge generation, the following are solved.

Generated charge from pressure is

$$Q_{Gen}=-\frac{3\pi bd_{33}s_{m}h_{p}(2a-nb)(a-nb)\left(h_{m}+h_{p}\right)\left(1+\nu\right)}{4X_{33}}P_{o} \qquad (4.147)$$

The open circuit capacitance is

$$C_{free}=\frac{2\pi\epsilon_{33}^{T}n^{2}\left(a-nb\right)h_{p}}{a}\left(1-\frac{2}{\left(1-\nu\right)}\left(1-\frac{6s_{m}h_{p}\left(h_{m}+h_{p}\right)^{2}}{X_{33}}\right)K_{33}^{2}\right) \qquad (4.148)$$

The generated voltage becomes

$$V_{Gen}=\frac{Q_{Gen}}{C_{free}}=-\frac{3abd_{33}s_{m}(2a-nb)\left(h_{m}+h_{p}\right)\left(1+\nu\right)}{8\epsilon_{33}^{T}n^{2}X_{33}\left(1-\frac{2}{\left(1-\nu\right)}\left(1-\frac{6s_{m}h_{p}\left(h_{m}+h_{p}\right)^{2}}{X_{33}}\right)K_{33}^{2}\right)}P_{o} \qquad (4.149)$$

and the generated electrical energy is

$$U_{Gen}=Q_{Gen}*V_{Gen}$$

$$=\frac{9}{32}\frac{\pi ab^{2}d_{33}{}^{2}s_{m}{}^{2}h_{p}(a-nb)(2a-nb)^{2}\left(h_{m}+h_{p}\right)^{2}\left(1+\nu\right)^{2}}{\epsilon_{33}^{T}n^{2}X_{33}{}^{2}\left(1-\frac{2}{\left(1-\nu\right)}\left(1-\frac{6s_{m}h_{p}\left(h_{m}+h_{p}\right)^{2}}{X_{33}}\right)K_{33}^{2}\right)}P_{o}{}^{2} \qquad (4.150)$$

4.6 Diaphragm with Regrouped Electrodes

In this analysis, we will divide the diaphragm into two areas. One is the inner region where $r < a/2$ and the other is the outer region where $r > a/2$. These inner and outer regions' electric field directions will be opposite to each other in order to overcome the stress distribution from constant pressure.

The strain equations are different between inner and outer regions because the electric field condition is different. Because of this difference, two sets of strain equations are formed

For 31-type diaphragm

$$\left.\begin{array}{ll} \varepsilon_{ri} = -\rho_{ri}\left(z - z_c\right),\ \varepsilon_{\theta i} = -\rho_{\theta i}\left(z - z_c\right) & \text{when } r < a/2,\ \text{Inner region} \\ \varepsilon_{ro} = -\rho_{ro}\left(z - z_c\right),\ \varepsilon_{\theta o} = -\rho_{\theta o}\left(z - z_c\right) & \text{when } r > a/2,\ \text{Outer region} \end{array}\right\} \qquad (4.151)$$

For interdigitated diaphragm

$$\left.\begin{array}{ll} \varepsilon_{ri} = -\rho_{ri}\left(z - z_{c3}\right),\ \varepsilon_{\theta i} = -\rho_{\theta i}\left(z - z_c\right) & \text{when } r < a/2,\ \text{Inner region} \\ \varepsilon_{ro} = -\rho_{ro}\left(z - z_{c3}\right),\ \varepsilon_{\theta o} = -\rho_{\theta o}\left(z - z_c\right) & \text{when } r > a/2,\ \text{Outer region} \end{array}\right\} \qquad (4.152)$$

4.6.1 Unimorph Diaphragm with Regrouped Electrodes

All the equations are the same as previously calculated for the unimorph diaphragm except for the electric field's direction. The inner region will use the same electric field direction, and the outer region will use the opposite electric field direction. The curvature equations for inner and outer regions should be different because the electric field directions are different.

4.6.2 Regrouped 31 Unimorph Circular Plate

The middle surface where stresses are zero is almost the same as the neutral surface of the 31 unimorph cantilever beam used in Eq. 4.42. The neutral surface is not exactly the same as Eq. 4.42 because of the piezoelectric elastic parameters changes under deformation. But the change of elastic parameters is very small. The assumption that the neutral surface is described by Eq. 4.42 will not make a significant difference in calculating electric power generation. As in the previous section, the moment equations are needed to calculate a curvature. The inner region and previous 31 unimorph diaphragm are designed to be identical. The moment equations for the inner region are shown in Eqs. 4.103-4.108., The moment equations for the outer region are

$$\left.\begin{aligned} M_{ro} &= \int_0^{h_p} \left(\frac{\varepsilon_r + \nu\varepsilon_\theta}{\left(1-\nu^2\right)s_{11}^E} - \frac{\left(1+\nu\right)d_{31}E_3}{\left(1-\nu^2\right)s_{11}^E} \right)\left(z - z_c\right)dz + \int_{-h_m}^{0} \left(\frac{\varepsilon_r + \nu\varepsilon_\theta}{\left(1-\nu^2\right)s_m} \right)\left(z - z_c\right)dz \\ M_{\theta i} &= \int_0^{h_p} \left(\frac{\nu\varepsilon_r + \varepsilon_\theta}{\left(1-\nu^2\right)s_{11}^E} - \frac{\left(1+\nu\right)d_{31}E_3}{\left(1-\nu^2\right)s_{11}^E} \right)\left(z - z_c\right)dz + \int_{-h_m}^{0} \left(\frac{\nu\varepsilon_r + \varepsilon_\theta}{\left(1-\nu^2\right)s_m} \right)\left(z - z_c\right)dz \end{aligned}\right\} \quad (4.153)$$

As before, the curvature can be found in terms of moments and electric field

$$\left.\begin{aligned} \rho_{ro} &= -\frac{12 s_{11}^E s_m S_h}{B_{31}}\left(M_r - \nu M_\theta\right) - \frac{6 d_{31} s_{11}^E s_m h_p h_m \left(h_m + h_p\right)}{B_{31}} E_3 \\ \rho_{\theta o} &= -\frac{12 s_{11}^E s_m S_h}{B_{31}}\left(M_\theta - \nu M_r\right) - \frac{6 d_{31} s_{11}^E s_m h_p h_m \left(h_m + h_p\right)}{B_{31}} E_3 \end{aligned}\right\} \quad (4.154)$$

where, $B_{31} = {h_p}^4 {s_m}^2 + 6 s_{11}^E s_m {h_m}^2 {h_p}^2 + 4 s_{11}^E s_m h_m h_p \left({h_p}^2 + {h_m}^2\right) + {h_m}^4 s_{11}^2$

and partial energy equations for outer region are

$$\left.\begin{aligned} dU_{po} &= \frac{1}{2}\varepsilon_r \sigma_{rp} + \frac{1}{2}\varepsilon_\theta \sigma_{\theta p} + \frac{d_{33}\left(\sigma_{rp} + \sigma_{\theta p}\right)}{2} E_3 + \frac{1}{2}\epsilon_{33}^T E_3^2 \\ dU_{mo} &= \frac{1}{2}\varepsilon_r \sigma_{rp} + \frac{1}{2}\varepsilon_\theta \sigma_{\theta p} \end{aligned}\right\} \quad (4.155)$$

There are four curvature equations. Two are for the inner region, and the other two are for the outer region curvature. Thus the energy equations for the inner and outer regions are also different. Combining those energy equations for the inner and outer regions, the total energy in the structure can be written as

$$U = \int_0^{\frac{a}{2}} \int_0^{2\pi} \left(\int_0^{h_p} dU_{pi} dz + \int_{-h_m}^{0} dU_{mi} dz \right) r d\theta dr + \int_{\frac{a}{2}}^{a} \int_0^{2\pi} \left(\int_0^{h_p} dU_{po} dz + \int_{-h_m}^{0} dU_{mo} dz \right) r d\theta dr$$

$$= \frac{\pi a^6 s_{11}^E s_m s_h \left(1 - \nu^2\right)}{32 B_{31}} P_o^{\,2} - \frac{27 \left(1 + \nu\right) a^4 \pi d_{31} s_{11}^E s_m h_m h_p \left(h_m + h_p\right)}{64 B_{31}} P_o E_3$$

$$+ \epsilon_{33}^T \pi a^2 h_p \left(1 + \frac{1}{\left(1 - \nu\right)} \left(1 + \frac{15 s_{11}^{E2} s_m h_m^{\,2} h_p \left(h_m + h_p\right)}{S_h B_{31}} \right) K_{31}^{\,2} \right) E_3^{\,2} \tag{4.156}$$

where $B_{31} = h_p^{\,4} s_m^{\,2} + 6 s_{11}^E s_m h_m^{\,2} h_p^{\,2} + 4 s_{11}^E s_m h_m h_p \left(h_p^{\,2} + h_m^{\,2}\right) + h_m^{\,4} s_{11}^2$.

The first term is for the inner region and the second term is for the outer region. We substitute for the electric field E with V/h_p, and differentiate with respect to voltage (V) to get the charge equation.

$$Q = \frac{\epsilon_{33}^T \pi a^2}{h_p} \left(1 - \frac{2}{\left(1 - \nu\right)} \left(1 - \frac{3 s_{11}^{E2} s_m h_m^{\,2} h_p \left(h_p + h_m\right)^2}{S_h B_{31}} \right) K_{31}^{\,2} \right) V$$
$$- \frac{9}{32} \frac{\pi a^4 \left(1 + \nu\right) d_{31} s_{11}^E s_m h_m \left(h_m + h_p\right)}{B_{31}} P_o \tag{4.157}$$

Charge generated with no applied external electric field is

$$Q_{Gen} = -\frac{9}{32} \frac{\pi a^4 \left(1 + \nu\right) d_{31} s_{11}^E s_m h_m \left(h_m + h_p\right)}{B_{31}} P_o \tag{4.158}$$

From the relation $Q=CV$, open circuit capacitance is

$$C_{free} = \frac{\epsilon_{33}^T \pi a^2}{h_p} \left(1 - \frac{2}{\left(1 - \nu\right)} \left(1 - \frac{3 s_{11}^{E2} s_m h_m^{\,2} h_p \left(h_p + h_m\right)^2}{S_h B_{31}} \right) K_{31}^{\,2} \right) \tag{4.159}$$

and the voltage appears on the electrodes is

$$V_{Gen} = \frac{Q_{gen}}{C_{free}} = -\frac{9}{32}\frac{\left(1+\nu\right)a^2 d_{31}s_{11}^E s_m h_m h_p\left(h_m + h_p\right)}{\epsilon_{33}^T B_{31}\left(1-\frac{2}{\left(1-\nu\right)}\left(1-\frac{3s_{11}^{E2}s_m h_m{}^2 h_p\left(h_p+h_m\right)^2}{S_h B_{31}}\right)K_{31}{}^2\right)}P_o \quad (4.160)$$

Thus, the electric energy generated by external pressure is

$$U_{Gen} = Q_{Gen} * V_{Gen} =$$
$$= \frac{81}{1024}\frac{\pi\left(1+\nu\right)^2 a^6 d_{31}{}^2 s_{11}^{E2} s_m{}^2 h_m{}^2 h_p\left(h_m + h_p\right)^2}{\epsilon_{33}^T B_{31}{}^2\left(1-\frac{2}{\left(1-\nu\right)}\left(1-\frac{3s_{11}^{E2}s_m h_m{}^2 h_p\left(h_p+h_m\right)^2}{S_h B_{31}}\right)K_{31}{}^2\right)}P_o^2 \quad (4.161)$$

4.6.3 Unimorph Interdigitated Circular Plate

In this section, we repeat the analysis of the previous section, considering the effects of changing stress directions throughout the diaphragm. The neutral surfaces are shown in the Eqs. 4.42 and 4.65. The strain relations for the inner and outer regions are the same as in the previous section and are shown Eq. 4.151. The equations for the inner region are shown in Eqs. 4.115-4.119 and the moment equations for the outer region are

$$\left.\begin{aligned} M_{ro} &= \int_0^{h_p}\left(\frac{\varepsilon_r + \nu\varepsilon_\theta}{\left(1-\nu^2\right)S_{33}^E} - \frac{\left(1+\nu\right)d_{33}E_3}{\left(1-\nu^2\right)S_{33}^E}\right)\left(z - z_{c3}\right)dz + \int_{-h_m}^0\left(\frac{\varepsilon_r + \nu\varepsilon_\theta}{\left(1-\nu^2\right)S_m}\right)\left(z-z_{c3}\right)dz \\ M_{\theta o} &= \int_0^{h_p}\left(\frac{\nu\varepsilon_r + \varepsilon_\theta}{\left(1-\nu^2\right)s_{33}^E} - \frac{\left(1+\nu\right)d_{33}E_3}{\left(1-\nu^2\right)s_{33}^E}\right)\left(z - z_c\right)dz + \int_{-h_m}^0\left(\frac{\nu\varepsilon_r + \varepsilon_\theta}{\left(1-\nu^2\right)s_m}\right)\left(z-z_c\right)dz \end{aligned}\right\} \quad (4.162)$$

with the moment equations, the curvature can be found as

$$\left.\begin{aligned} \rho_{ro} &= -\frac{12s_{33}^E s_m S_{h3}}{B_{33}}\left(M_r - \nu M_\theta\right) - \frac{6d_{33}s_{33}^E s_m h_p h_m\left(h_m+h_p\right)}{B_{33}}E_3 \\ \rho_{\theta o} &= -\frac{12s_{33}^E s_m S_{h3}}{B_{33}}\left(M_\theta - \nu M_r\right) - \frac{6d_{33}s_{33}^E s_m h_p h_m\left(h_m+h_p\right)}{B_{33}}E_3 \end{aligned}\right\} \quad (4.163)$$

where, $B_{33} = h_p{}^4 s_m{}^2 + 4s_{33}^E s_m h_p{}^3 h_m + 6s_{33}^E s_m h_p{}^2 h_m{}^2 + 4s_{33}^E s_m h_p h_m{}^3 + h_m{}^4 s_{33}^{E\,2}$.

Energies in the small volume for each region are

$$\left.\begin{aligned} dU_{pi} &= \frac{1}{2}\varepsilon_r\sigma_{rp} + \frac{1}{2}\varepsilon_\theta\sigma_{\theta p} - \frac{d_{33}\left(\sigma_{rp}+\sigma_{\theta p}\right)}{2}E_3 + \frac{1}{2}\epsilon_{33}^T E_3^2 \quad \text{inner region} \\ dU_{po} &= \frac{1}{2}\varepsilon_r\sigma_{rp} + \frac{1}{2}\varepsilon_\theta\sigma_{\theta p} + \frac{d_{33}\left(\sigma_{rp}+\sigma_{\theta p}\right)}{2}E_3 + \frac{1}{2}\epsilon_{33}^T E_3^2 \quad \text{outer region} \end{aligned}\right\} \tag{4.164}$$

The non-piezoelectric layers' energy does not depend on the electric boundary condition, and thus the non-piezoelectric layers' energy is the same as the non-piezoelectric layer of the 31-direction diaphragm and is shown in Equation 4.155. Using all the equations above, the total energy can be described as

$$U = \sum_{i=1}^{n/2}\int_{a(i-1)/n+b/2}^{ai/n-b/2}\int_0^{2\pi}\left(\int_0^{h_p} dU_{pi}dz + \int_{-h_m}^{0} dU_m dz\right) rd\theta dr$$

$$+ \sum_{i=n/2+1}^{n}\int_{a(i-1)/n+b/2}^{ai/n-b/2}\int_0^{2\pi}\left(\int_0^{h_p} dU_{po}dz + \int_{-h_m}^{0} dU_m dz\right) rd\theta dr$$

$$= \frac{a\pi s_{33}^E s_m s_{h3}\left(1-\nu^2\right)\left(a-nb\right)Y}{1024 n^3 B_{33}} P_o^2$$

$$-\frac{3}{32}\frac{\pi a d_{33} s_{33}^E s_m h_m h_p\left(h_m+h_p\right)\left(1+\nu\right)\left(a-nb\right)(3na^2-4ab+2nb^2)}{nB_{33}} P_o E_3$$

$$+\frac{\epsilon_{33}^T \pi a\left(a-nb\right)h_p}{2}\left(1-\frac{2}{\left(1-\nu\right)}\left(1-\frac{3 s_{33}^{E\,2} s_m h_m^{\,2} h_p\left(h_p+h_m\right)^2}{S_{h3}B_{33}}\right)K_{33}^2\right)E^2 \tag{4.165}$$

where

$$Y = 32n^3a^4 - 8a^3b\left(13n^2+3\nu\left(n^2-1\right)-5\right) + 4na^2b^2\left(13n^2+3\nu\left(n^2+2\right)+10\right) + \left(3n^3b^4-12n^2ab^3\right)\left(5-3\nu\right)$$

,and $s_{h3} = s_{33}^E h_m + s_m h_p$.

The electrode areas with width b are eliminated in the calculation. Since the distance between electrodes is a/n, the electric field is now nV/a. Substitute electric field with $V/(a/n)$ and differentiate with respect to voltage (V) to get

$$Q = \frac{\epsilon_{33}^{T}\pi n^2\left(a-nb\right)h_p}{a}\left(1-\frac{2}{\left(1-\nu\right)}\left(1-\frac{3s_{33}^{E\,2}s_m h_m{}^2 h_p\left(h_p+h_m\right)^2}{S_{h3}B_{33}}\right)K_{33}^2\right)V$$

$$-\frac{3}{32}\frac{\pi d_{33}s_{33}^{E}s_m h_m h_p\left(h_m+h_p\right)\left(1+\nu\right)\left(a-nb\right)(3na^2-4ab+2nb^2)}{B_{33}}P_o \quad (4.166)$$

The first term in Eq. 4.166 is related to the capacitance of the PEG and the second term is related to the coupling between pressure and charge. The generated charge of this PEG when no external electric field is applied is

$$Q_{Gen} = -\frac{3}{32}\frac{\pi d_{33}s_{33}^{E}s_m h_m h_p\left(h_m+h_p\right)\left(1+\nu\right)\left(a-nb\right)(3na^2-4ab+2nb^2)}{B_{33}}P_o \quad (4.167)$$

From the relation $Q=CV$, the open circuit capacitance is

$$C_{free} = \frac{\epsilon_{33}^{T}\pi n^2\left(a-nb\right)h_p}{a}\left(1-\frac{2}{\left(1-\nu\right)}\left(1-\frac{3s_{33}^{E\,2}s_m h_m{}^2 h_p\left(h_p+h_m\right)^2}{S_{h3}B_{33}}\right)K_{33}^2\right) \quad (4.168)$$

and the generated voltage is

$$V_{gen} = \frac{Q_{gen}}{C_{free}} = -\frac{3}{32}\frac{a d_{33}s_{33}^{E}s_m h_m\left(h_m+h_p\right)\left(1+\nu\right)(3na^2-4ab+2nb^2)}{\epsilon_{33}^{T}n^2B_{33}\left(1-\frac{2}{\left(1-\nu\right)}\left(1-\frac{3s_{33}^{E\,2}s_m h_m{}^2 h_p\left(h_p+h_m\right)^2}{S_{h3}B_{33}}\right)K_{33}^2\right)}P_o \quad (4.169)$$

Thus, the electrical energy generated by external pressure P_o is

$$U_{Gen} = Q_{Gen} * V_{Gen}$$

$$= -\frac{9}{1024}\frac{\pi a d_{33}{}^2 s_{33}^{E\,2} s_m{}^2 h_m{}^2 h_p \left(h_m + h_p\right)^2 \left(1+\nu\right)^2 \left(a-nb\right)(3na^2 - 4ab + 2nb^2)^2}{\epsilon_{33}^T n^2 B_{33}{}^2 \left(1 - \frac{2}{\left(1-\nu\right)}\left(1 - \frac{3s_{33}^{E\,2} s_m h_m{}^2 h_p \left(h_p + h_m\right)^2}{S_{h3} B_{33}}\right) K_{33}^2\right)} P_o{}^2 \quad (4.170)$$

4.6.4 Triple-morph Diaphragm with Regrouped Electrode

In the triple morph, the neutral surface lies in the middle surface. Since the curvature is different, we need to express different curvatures for the inner and outer regions. Those curvature equations are shown in Equations 4.151-4.152. Using those relations, the following two cases will be calculated: the 31 and the 33 triple morph circular plate.

4.6.5 Triple-morph Circular Plate

The constitutive equations of the inner region are shown in Eqs. 4.126-4.131. These equations can be used here without any modification. For the outer region, the moment equations can be obtained by changing the direction of the electric field.

$$\left.\begin{aligned} M_{ro} &= -\frac{X_{31}}{12(1-\nu^2)s_{11}^E s_m}(\rho_{ro} + \nu\rho_{\theta o}) - \frac{d_{31}h_p\left(h_p + h_m\right)}{(1-\nu)s_{11}^E}E_3 \\ M_{\theta o} &= -\frac{X_{31}}{12(1-\nu^2)s_{11}^E s_m}(\nu\rho_{ro} + \rho_{\theta o}) - \frac{d_{31}h_p\left(h_p + h_m\right)}{(1-\nu)s_{11}^E}E_3 \end{aligned}\right\} \quad (4.171)$$

here $X_{31} = 6s_m h_p h_m{}^2 + 12 s_m h_p{}^2 h_m + 8 s_m h_p{}^3 + s_{31}^E h_m{}^3$, h is the thickness of the individual layer, s is the elastic compliance, subscript p shows the piezoelectric layer and m represents the non-piezoelectric middle layer. Using the above moment equations, we can get the curvature in terms of moments form classical elasticity. The curvature equation for the inner region is shown in Eqs. 4.130. The outer region curvatures are

$$\left.\begin{aligned}\rho_{ro} &= -\frac{12s_{11}^E s_m}{X_{31}}(M_{ro}-\nu M_{\theta o}) - \frac{12d_{31}s_m h_p(h_m+h_p)}{X_{31}}E_3 \\ \rho_{\theta o} &= -\frac{12S_{11}^E S_m}{X_{31}}(M_{\theta o}-\nu M_{ro}) - \frac{12d_{31}S_m h_p(h_p+h_m)}{X_{31}}E_3\end{aligned}\right\} \tag{4.172}$$

The moment used in the curvature equations are shown in Eq.4.100, which is elastic solution. With the curvature equations, stresses and strains can be found easily with constitutive Eq. 4.103 and curvature-strain Eq. 4.151. Substitute those stresses and strains with partial energy equations 4.108 and 4.131. The total system energy is

$$U_{total} = \int_0^{\frac{a}{2}}\int_0^{2\pi}(dU_i)rd\theta dr + \int_{\frac{a}{2}}^{a}\int_0^{2\pi}(dU_o)rd\theta dr$$

$$= \frac{a^6\pi s_{11}^E s_m\left(1-\nu^2\right)}{32X_{31}}P_o^2 - \frac{9}{16}\frac{\pi a^4 d_{31}s_m h_p\left(1+\nu\right)\left(h_m+h_p\right)}{X_{31}}P_o E_3$$

$$+\pi a^2\epsilon_{33}^T h_p\left(1-\frac{2}{\left(1-\nu\right)}\left(1-\frac{6s_m h_p\left(h_m+h_p\right)^2}{X_{31}}\right)K_{31}^2\right)E^2 \tag{4.173}$$

Using the curvature, the total energy in the structure is now described in terms of E_3 and P_o. E_3 is the electric field and is $V/2h_p$. We can now obtain the charge generation by partial differentiation of total energy with respect to the voltage. The charge becomes

$$Q = \frac{\pi a^2\epsilon_{33}^T}{2h_p}\left(1-\frac{2}{\left(1-\nu\right)}\left(1-\frac{6s_m h_p\left(h_m+h_p\right)^2}{X_{31}}\right)K_{31}^2\right)V - \frac{9}{32}\frac{\pi a^4 d_{31}s_m\left(1+\nu\right)\left(h_m+h_p\right)}{X_{31}}P_o \tag{4.174}$$

So, the generated charge from the applied pressure is

$$Q_{Gen} = -\frac{9}{32}\frac{\pi a^4 d_{31}s_m\left(1+\nu\right)\left(h_m+h_p\right)}{X_{31}}P_o \tag{4.175}$$

The open circuit capacitance is

$$C_{free} = \frac{\pi a^2 \epsilon_{33}^T}{2h_p}\left(1 - \frac{2}{(1-\nu)}\left(1 - \frac{6s_m h_p \left(h_m + h_p\right)^2}{X_{31}}\right)K_{31}^2\right) \tag{4.176}$$

And the generated voltage is

$$V_{Gen} = \frac{Q_{Gen}}{C_{free}} = -\frac{9}{16}\frac{a^2 d_{31} s_m h_p (1+\nu)\left(h_m + h_p\right)}{\epsilon_{33}^T X_{31}\left(1 - \frac{2}{(1-\nu)}\left(1 - \frac{6s_m h_p \left(h_m + h_p\right)^2}{X_{31}}\right)K_{31}^2\right)}P_o \tag{4.177}$$

Finally, the generated electrical energy is

$$U_{Gen} = Q_{Gen} * V_{Gen} = \frac{81}{512}\frac{\pi a^6 d_{31}{}^2 s_m{}^2 h_p (1+\nu)^2 \left(h_m + h_p\right)^2}{\epsilon_{33}^T X_{31}{}^2\left(1 - \frac{2}{(1-\nu)}\left(1 - \frac{6s_m h_p \left(h_m + h_p\right)^2}{X_{31}}\right)K_{31}^2\right)}P_o{}^2 \tag{4.178}$$

4.6.6 Triple-morph Interdigitated Circular Plate

Energy equations for the inner region are solved in the previous triple morph interdigitated circular plate section. Those equations are shown in Eqs.4.138-4.144. In this section, the energy equation for the outer region will be solved and then combine with equation for the inner region. As mentioned before, the curvature equations are needed to solve the energy equation. To solve the curvature equations of outer region, the moment equations are needed.

$$\left.\begin{aligned} M_{ro} &= -\frac{X_{33}}{12(1-\nu^2)s_{33}^E s_m}(\rho_{ro} + \nu\rho_{\theta o}) - \frac{d_{33}h_p\left(h_p + h_m\right)}{(1-\nu)s_{33}^E}E_3 \\ M_{\theta o} &= -\frac{X_{33}}{12(1-\nu^2)s_{33}^E s_m}(\nu\rho_{ro} + \rho_{\theta o}) - \frac{d_{33}h_p\left(h_p + h_m\right)}{(1-\nu)s_{33}^E}E_3 \end{aligned}\right\} \tag{4.179}$$

Those equations are almost the same as Eq. 4.140-4.141 except for the direction of the electric field. The curvature – moment relation can be found by rearranging above Eq. 4.179 . After re-arranging, the curvature equations are

$$\left.\begin{aligned}\rho_{ro} &= -\frac{12 s_{33}^E s_m}{X_{33}}(M_{ro} - \nu M_{\theta o}) - \frac{12 d_{33} s_m h_p (h_p + h_m)}{X_{33}} E_3 \\ \rho_{\theta o} &= -\frac{12 s_{33}^E s_m}{X_{33}}(M_{\theta o} - \nu M_{ro}) - \frac{12 d_{33} s_m h_p (h_p + h_m)}{X_{33}} E_3\end{aligned}\right\} \tag{4.180}$$

The moment used in curvature equations are shown in Eq. 4.100, which is elastic solution. With curvature equations, stresses and strains can be found easily with constitutive Eq. 4.115 and curvature-strain Eq. 4.151. Substituting those stresses and strains with partial energy equation 4.143-4.144 gives total system energy.

$$\begin{aligned}U_{total} &= \sum_{i=1}^{n/2} \int_{a(i-1)/n+b/2}^{ai/n-b/2} \int_0^{2\pi} (dU_i) r d\theta dr + \sum_{i=n/2}^{n} \int_{a(i-1)/n+b/2}^{ai/n-b/2} \int_0^{2\pi} (dU_o) r d\theta dr \\ &= \frac{\pi a s_{33}^E s_m \left(1-\nu^2\right)\left(a-nb\right) Y}{1024 n^3 X_{33}} P_o^{\,2} \\ &\quad - \frac{3}{16} \frac{\pi a d_{33} s_m h_p \left(1+\nu\right)\left(a-nb\right)(3na^2 - 4ab + 2nb^2)\left(h_m + h_p\right)}{n X_{33}} P_o E_3 \\ &\quad + \pi a \left(a-nb\right) h_p \epsilon_{33}^T \left(1 - \frac{2}{\left(1-\nu\right)}\left(1 - \frac{6 S_m h_p \left(h_m + h_p\right)^2}{X_{33}}\right) K_{33}^2\right) E_3^{\,2}\end{aligned} \tag{4.181}$$

where

$$Y = 32n^3a^4 - 8a^3b\left(13n^2 + 3\nu\left(n^2-1\right) - 5\right) + 4na^2b^2\left(13n^2 + 3\nu\left(n^2+2\right) + 10\right) + \left(3n^3b^4 - 12n^2ab^3\right)\left(5 - 3\nu\right)$$

The total energy in the structure is now described in terms of E_3 and P_o. E_3 is the electric field and is now V/(a/n). The partial differentiation of the total energy with respect to the voltage is the generated charge,

$$Q = \frac{2\pi n^2 (a-nb) h_p \epsilon_{33}^T}{a}\left(1 - \frac{2}{(1-\nu)}\left(1 - \frac{6S_m h_p (h_m + h_p)^2}{X_{33}}\right)K_{33}^2\right)V$$

$$-\frac{3}{16}\frac{\pi d_{33} s_m h_p (a-nb)(3na^2 - 4ab + 2nb^2)(1+\nu)(h_p + h_m)}{X_{33}} P_o \tag{4.182}$$

So, the generated charge from applied pressure is

$$Q_{Gen} = -\frac{3}{16}\frac{\pi d_{33} s_m h_p (a-nb)(3na^2 - 4ab + 2nb^2)(1+\nu)(h_p + h_m)}{X_{33}} P_o \tag{4.183}$$

and the open circuit capacitance is

$$C_{free} = \frac{2\pi n^2 (a-nb) h_p \epsilon_{33}^T}{a}\left(1 - \frac{2}{(1-\nu)}\left(1 - \frac{6S_m h_p (h_m + h_p)^2}{X_{33}}\right)K_{33}^2\right) \tag{4.184}$$

The generated voltage is

$$V_{Gen} = \frac{Q_{Gen}}{C_{free}} = -\frac{3}{32}\frac{a d_{33} s_m (3na^2 - 4ab + 2nb^2)(1+\nu)(h_p + h_m)}{n^2 \epsilon_{33}^T X_{33}\left(1 - \frac{2}{(1-\nu)}\left(1 - \frac{6S_m h_p (h_m + h_p)^2}{X_{33}}\right)K_{33}^2\right)} P_o \tag{4.185}$$

and finally the generated electrical energy is

$$U_{Gen} = Q_{Gen} * V_{Gen}$$

$$= \frac{9}{512}\frac{\pi a {d_{33}}^2 {s_m}^2 h_p (a-nb)(3na^2 - 4ab + 2nb^2)^2 (1+\nu)^2 (h_p + h_m)^2}{n^2 \epsilon_{33}^T {X_{33}}^2\left(1 - \frac{2}{(1-\nu)}\left(1 - \frac{6S_m h_p (h_m + h_p)^2}{X_{33}}\right)K_{33}^2\right)} P_o^2 \tag{4.186}$$

4.6.7 Optimal Location for Regrouped 31 Unimorph Circular Plate

The location of the regrouped electrode is also important in the power generation. To observe the optimum location of the regroup, a parameter m instead a/2 (a half of the radius) was used and calculated for the unimorph diaphragm as shown section 4.6.2.

Constitutive Equation for the inner region

$$\left.\begin{aligned} \varepsilon_r &= s_{11}^E\left(\sigma_r - \nu\sigma_\theta\right) - d_{31}E_3 \\ \varepsilon_\theta &= s_{11}^E\left(\sigma_\theta - \nu\sigma_r\right) - d_{31}E_3 \\ D_3 &= -d_{31}\left(\sigma_r + \sigma_\theta\right) + \epsilon_{33}^T E_3 \end{aligned}\right\}$$

Constitutive equation for the outer region

$$\left.\begin{aligned} \varepsilon_r &= s_{11}^E\left(\sigma_r - \nu\sigma_\theta\right) + d_{31}E_3 \\ \varepsilon_\theta &= s_{11}^E\left(\sigma_\theta - \nu\sigma_r\right) + d_{31}E_3 \\ D_3 &= d_{31}\left(\sigma_r + \sigma_\theta\right) - \epsilon_{33}^T E_3 \end{aligned}\right\}$$

Stress distribution for inner PZT layer

$$\left.\begin{aligned} \sigma_r &= \frac{1}{s_{11}^E\left(1-\nu^2\right)}\left(\varepsilon_r + \nu\varepsilon_\theta + \left(1+\nu\right)d_{31}E_3\right) \\ \sigma_\theta &= \frac{1}{s_{11}^E\left(1-\nu^2\right)}\left(\nu\varepsilon_r + \varepsilon_\theta + \left(1+\nu\right)d_{31}E_3\right) \end{aligned}\right\}$$

Stress distribution for outer PZT layer

$$\left.\begin{aligned} \sigma_r &= \frac{1}{s_{11}^E\left(1-\nu^2\right)}\left(\varepsilon_r + \nu\varepsilon_\theta - \left(1+\nu\right)d_{31}E_3\right) \\ \sigma_\theta &= \frac{1}{s_{11}^E\left(1-\nu^2\right)}\left(\nu\varepsilon_r + \varepsilon_\theta - \left(1+\nu\right)d_{31}E_3\right) \end{aligned}\right\}$$

Stress distribution for substrate layer

$$\left.\begin{aligned}\sigma_r &= \frac{1}{s_m\left(1-\nu^2\right)}\left(\varepsilon_r+\nu\varepsilon_\theta\right)\\ \sigma_\theta &= \frac{1}{s_m\left(1-\nu^2\right)}\left(\nu\varepsilon_r+\varepsilon_\theta\right)\end{aligned}\right\}$$

The moment equations for the inner region are

$$\left.\begin{aligned}M_r &= \int_0^{h_p}\left(\frac{\varepsilon_r+\nu\varepsilon_\theta}{\left(1-\nu^2\right)S_{11}^E}+\frac{\left(1+\nu\right)d_{31}E_3}{\left(1-\nu^2\right)S_{11}^E}\right)\left(z-z_c\right)dz+\int_{-h_m}^{0}\left(\frac{\varepsilon_r+\nu\varepsilon_\theta}{\left(1-\nu^2\right)S_m}\right)\left(z-z_c\right)dz\\ M_\theta &= \int_0^{h_p}\left(\frac{\nu\varepsilon_r+\varepsilon_\theta}{\left(1-\nu^2\right)S_{11}^E}+\frac{\left(1+\nu\right)d_{31}E_3}{\left(1-\nu^2\right)S_{11}^E}\right)\left(z-z_c\right)dz+\int_{-h_m}^{0}\left(\frac{\nu\varepsilon_r+\varepsilon_\theta}{\left(1-\nu^2\right)S_m}\right)\left(z-z_c\right)dz\end{aligned}\right\}$$

The moment equations for the outer region are

$$\left.\begin{aligned}M_{ro} &= \int_0^{h_p}\left(\frac{\varepsilon_r+\nu\varepsilon_\theta}{\left(1-\nu^2\right)s_{11}^E}-\frac{\left(1+\nu\right)d_{31}E_3}{\left(1-\nu^2\right)s_{11}^E}\right)\left(z-z_c\right)dz+\int_{-h_m}^{0}\left(\frac{\varepsilon_r+\nu\varepsilon_\theta}{\left(1-\nu^2\right)s_m}\right)\left(z-z_c\right)dz\\ M_{\theta i} &= \int_0^{h_p}\left(\frac{\nu\varepsilon_r+\varepsilon_\theta}{\left(1-\nu^2\right)s_{11}^E}-\frac{\left(1+\nu\right)d_{31}E_3}{\left(1-\nu^2\right)s_{11}^E}\right)\left(z-z_c\right)dz+\int_{-h_m}^{0}\left(\frac{\nu\varepsilon_r+\varepsilon_\theta}{\left(1-\nu^2\right)s_m}\right)\left(z-z_c\right)dz\end{aligned}\right\}$$

The curvature equation for the inner region

$$\left.\begin{aligned}\rho_r &= -\frac{12S_{11}^E S_m\left(s_{11}^E h_m+s_m h_p\right)}{B_{31}}\left(M_r-\nu M_\theta\right)+\frac{6d_{31}s_{11}^E s_m h_p h_m\left(h_m+h_p\right)}{B_{31}}E_3\\ \rho_\theta &= -\frac{12S_{11}^E S_m\left(s_{11}^E h_m+s_m h_p\right)}{B_{31}}\left(M_\theta-\nu M_r\right)+\frac{6d_{31}s_{11}^E s_m h_p h_m\left(h_m+h_p\right)}{B_{31}}E_3\end{aligned}\right\}$$

Curvature equation for the outer region

$$\left.\begin{aligned}\rho_{ro} &= -\frac{12s_{11}^E s_m S_h}{B_{31}}\left(M_r-\nu M_\theta\right)-\frac{6d_{31}s_{11}^E s_m h_p h_m\left(h_m+h_p\right)}{B_{31}}E_3\\ \rho_{\theta o} &= -\frac{12s_{11}^E s_m S_h}{B_{31}}\left(M_\theta-\nu M_r\right)-\frac{6d_{31}s_{11}^E s_m h_p h_m\left(h_m+h_p\right)}{B_{31}}E_3\end{aligned}\right\}$$

Partial energy equation for inner region

$$\left.\begin{aligned} dU_p &= \frac{1}{2}\varepsilon_r\sigma_{rp} + \frac{1}{2}\varepsilon_\theta\sigma_{\theta p} - \frac{d_{31}\left(\sigma_{rp}+\sigma_{\theta p}\right)}{2}E_3 + \frac{1}{2}\epsilon_{33}^{T}E_3^2 \quad &&\text{for piezoelectric} \\ dU_m &= \frac{1}{2}\varepsilon_r\sigma_{rp} + \frac{1}{2}\varepsilon_\theta\sigma_{\theta p} &&\text{for non-piezoelectric} \end{aligned}\right\}$$

Partial energy equations for outer region

$$\left.\begin{aligned} dU_{po} &= \frac{1}{2}\varepsilon_r\sigma_{rp} + \frac{1}{2}\varepsilon_\theta\sigma_{\theta p} + \frac{d_{31}\left(\sigma_{rp}+\sigma_{\theta p}\right)}{2}E_3 + \frac{1}{2}\epsilon_{33}^{T}E_3^2 \\ dU_{mo} &= \frac{1}{2}\varepsilon_r\sigma_{rp} + \frac{1}{2}\varepsilon_\theta\sigma_{\theta p} \end{aligned}\right\}$$

Total Energy

$$U = \int_0^m\int_0^{2\pi}\left(\int_0^{h_p} dU_{pi}dz + \int_{-h_m}^{0} dU_{mi}dz\right)rd\theta dr + \int_m^a\int_0^{2\pi}\left(\int_0^{h_p} dU_{po}dz + \int_{-h_m}^{0} dU_{mo}dz\right)rd\theta dr \qquad (4.187)$$

The first term is for the inner region and the second term is for the outer region. We substitute for the electric field E with V/h_p, and differentiate with respect to voltage (V) to get the charge equation.

$$Q = \frac{\epsilon_{33}^{T}\pi}{h_p}\left(a^2 + \frac{B_{fx31}}{(1-\nu)S_h B_{31}}K_{31}{}^2\right)V - \frac{9\pi d_{31}s_{11}^{E}s_m h_m m^2\left(a^2-m^2\right)(1+\nu)\left(h_m+h_p\right)}{4B_{31}}P_o$$

where

$B_{fx31} = B_{f1}a^2 - 2B_{f2}m^2$,

$B_{f1} = B_f + s_{11}^{E2}s_m h_p h_m{}^2\left(13h_p{}^2 + 14h_m{}^2 + 24h_m h_p\right)$, $B_{f2} = B_f + s_{11}^{E2}s_m h_p h_m{}^2\left(7h_p{}^2 + 8h_m{}^2 + 12h_m h_p\right)$,

$B_f = 4s_{11}^{E}s_m{}^2h_p{}^2h_m{}^3 + 6s_{11}^{E}s_m{}^2h_p{}^3h_m{}^2 + 5s_{11}^{E}s_m{}^2h_p{}^4h_m + s_{11}^{E3}h_m{}^5 + h_p{}^5s_m{}^3$,

$B_{31} = h_p{}^4s_m{}^2 + 4s_{11}^{E}s_m h_m h_p{}^3 + 6s_{11}^{E}s_m h_m{}^2h_p{}^2 + 4s_{11}^{E}s_m h_m{}^3h_p + h_m{}^4s_{11}^2$

Generated charge when no external electric field applied is

$$Q_{Gen} = -\frac{9\pi d_{31}s_{11}^{E}s_m h_m m^2\left(a^2-m^2\right)(1+\nu)\left(h_m+h_p\right)}{4B_{31}}P_o$$

From the relation $Q=CV$, open circuit capacitance is

$$C_{free} = \frac{\epsilon_{33}^{T}\pi}{h_p}\left(a^2 + \frac{B_{fx31}}{(1-\nu)S_h B_{31}}{K_{31}}^2\right)$$

and the voltage appears on the electrodes is

$$V_{Gen} = \frac{Q_{gen}}{C_{free}} = -\frac{9d_{31}s_{11}^{E}s_m s_h h_m h_p m^2\left(a^2-m^2\right)\left(1-\nu^2\right)\left(h_m+h_p\right)}{4\epsilon_{33}^{T}\left(\left(1-\nu\right)a^2 s_h B_{31}+2B_{fx31}{K_{31}}^2\right)}P_o$$

Thus, the electric energy generated by external pressure is

$$U_{Gen} = Q_{Gen} * V_{Gen} = -\frac{81\pi m^4 {d_{31}}^2 s_{11}^{E2} {s_m}^2 s_h {h_m}^2 h_p\left(1-\nu^2\right)\left(a^2-m^2\right)\left(h_m+h_p\right)^2}{16\epsilon_{33}^{T}B_{31}\left(2B_{fx31}{K_{31}}^2+a^2\left(1-\nu\right)s_h B_{31}\right)}P_o^2 \qquad (4.188)$$

5.0 NUMERICAL RESULTS

The expressions for generated energy developed in chapter 4 provide a basis for studying the different PEG configurations. Using those equations, a set of numerical calculations has been carried out to determine how the generated charge, voltage, and energy vary with different substrate (non-piezoelectric) materials and thickness.

The results of those calculations are shown in Figure 29- Figure 30. Shown on the left side of each figure configuration are the energy, voltage, and charge results for the 31-mode bender system, and on the right the same values are shown for the corresponding 33-mode bender configuration.

In each case, the general trend is that the generated voltage and charge are relatively small for the extremes of piezoelectric layer thickness (near 90% or 10% of the total thickness), and they reach a peak near the centers (where the thickness of the piezoelectric and non-piezoelectric layers are approximately equal). In some cases (especially for charge) there is no peak, but the charge monotonically decreases with decreasing PZT thickness. The energy curve is the product of voltage and charge, so it too shows a peak, since the generated energy is highly dependent on the location of the neutral surface (which itself is dependent on the Young's modulus of the non-piezoelectric material) the peak energy occurs at different thickness ratios for the various substrate materials.

The results shown in Figure 31-Figure 32 are the diaphragm comparison. Shown on the left side of each figure configuration are the energy, voltage, and charge results for the 31-mode unmodified system, and on the right the same values are shown for the corresponding 31-mode regrouped configuration. Due to the stress distribution, the unmodified diaphragm did not generate electrical energy but in the regrouped diaphragm, trends are similar to those of the cantilever bender.

The explanation for the shape of the curves is as follows. As the piezoelectric material makes up a thicker portion of the system, the generated energy decreases for the unimorph because the neutral axis moves farther into the piezoelectric layer On the other hand, as the piezoelectric layer becomes thinner relative to the non-piezoelectric layer, it moves farther from the neutral axis and the stresses become larger, so the energy conversion increases. At some point; however, the volume of piezoelectric material itself becomes small enough such that it cannot maintain high energy conversion in spite of the higher stresses, so the electrical energy generation begins to decrease. This explanation for energy reduction for thin piezoelectric layer is believed to hold for both the unimorph and the triple layer systems.

In most of the configuration cases, interdigitated PEGs show better performance but, it is very hard to declare that the interdigitated PEGs are always better than conventional 31-direction PEGs. The PEG's parameters are coupled and also affect the electric power generation. Among those parameters, more significantly affecting parameters are the thickness of each layer and the elastic stiffness of the non-piezoelectric layer. In the unimorph PEGs, the thicker piezoelectric layer does not always increase the electric energy generation. If the neutral surface lies in the piezoelectric layer, the piezoelectric volume below the neutral surface and the same amount of the piezoelectric volume above the neutral surface will not generate the electric energy.

The interdigitated electrode configurations increase the voltage generation while reducing charge generation to a small degree. The voltage is related to the number of segments n. If the number of the segments is large, which means the electrode is not far away, the voltage will decrease. This voltage magnification can also be an advantage for sensor applications.

In Figure 31-Figure 32, it is clear that just disconnecting the original electrode on the piezoelectric plate and regrouping can increase performance. These results were based on the configurations where the electrodes were not regrouped and also regrouped at a radius of *a/2*. This regrouping location also affects the performance. Figure 35-Figure 37 shows charge, voltage, and energy vary with different regroup location and thickness. It is clearly seen that near three-quarter of the radius is the optimum regroup location and the capacitance is not affected by the regrouping.

Figure 33-Figure 34 shows the ratio between applied mechanical energy and generated output energy. The ratio also depends on the thickness and elastic properties of substrate. It clearly can be seen that the conversion rates of the cantilever type PEGs are much higher than that of diaphragm PEGs. The maximum conversion ratio for the diaphragm (regrouped diaphragm) is about 39% while the maximum theoretical conversion ratio of the interdigitated unimorph cantilever beam is 52%. The energy ratios and optimal thickness ratios are summarized in Table 2 and Table 3

In summary, it appears that the regrouped configuration is best for the diaphragm type PEGs, and the interdigitated configuration is best for cantilever type PEGs in generating electrical energy.

Table 2. Optimum PEG thickness ratio and energy conversion ratio for several different non piezoelectric layer (Cantilever Beam)

	31 Unimorph cantilever		33 Unimorph cantilever	
	h_p / h_m	U_{Gen} / U_{mech}	h_p / h_m	U_{Gen} / U_{mech}
Steel	1.13	9.91	1.23	51.58
Aluminum	0.56	8.62	0.61	46.75
Brass	2.55	5.32	0.82	48.67
Titanium	0.78	9.22	0.86	49.06
Silicon	0.56	8.53	1.07	50.6

Table 3. Optimum PEG thickness ratio and energy conversion ratio for several different non piezoelectric layer and regrouped location (Diaphragm)

	Unmodified		M=a/2		M=3*a/4	
	h_p / h_m	U_{Gen} / U_{mech}	h_p / h_m	U_{Gen} / U_{mech}	h_p / h_m	U_{Gen} / U_{mech}
Steel	-	0%	2.25	23.98%	2.25	39.43%
Aluminum	-	0%	1.10	21.94%	1.10	36.08%
Brass	-	0%	1.47	22.75%	1.47	37.41%
Titanium	-	0%	1.56	22.91%	1.56	37.68%
Silicon	-	0%	1.95	23.57%	1.95	38.75%

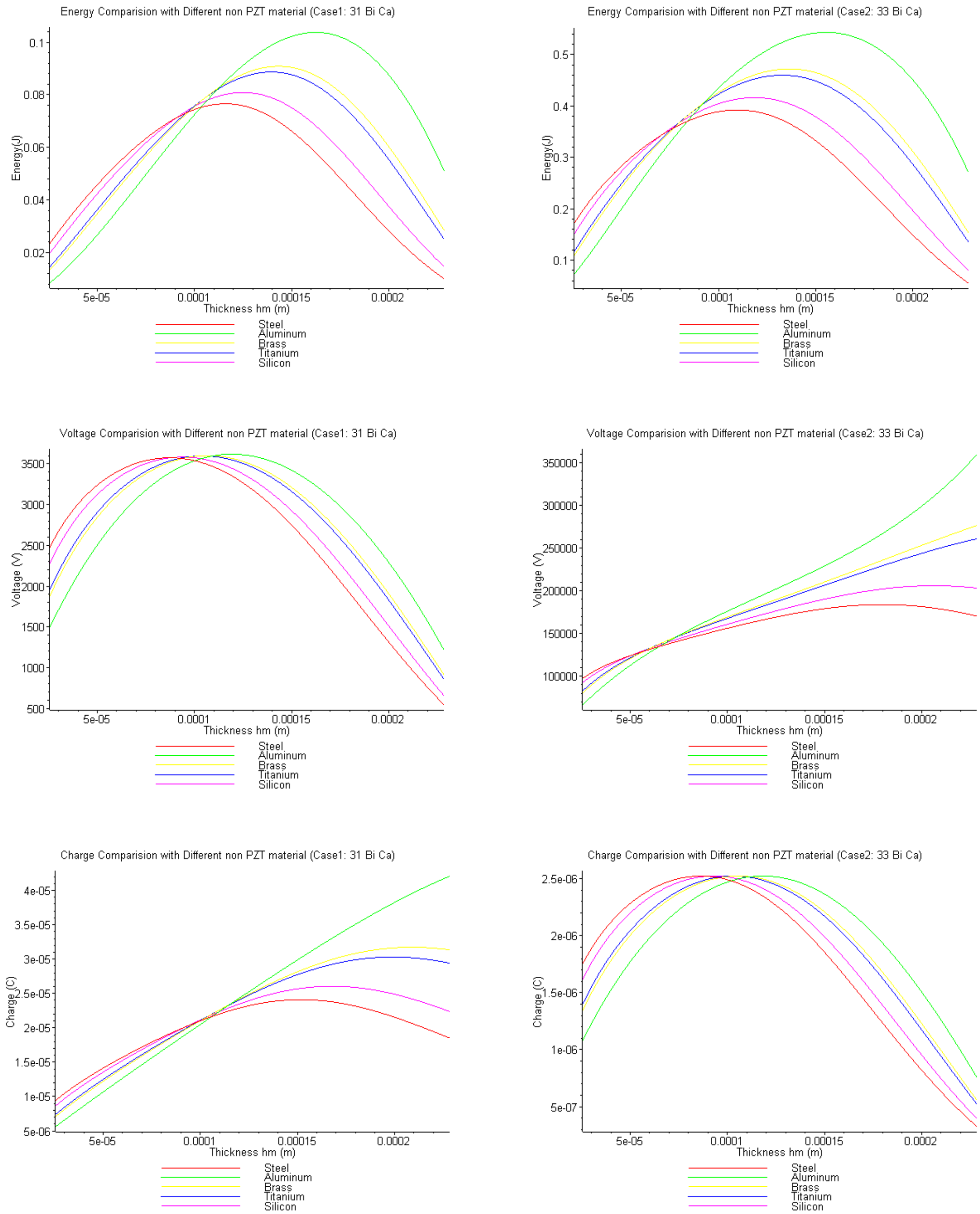

Figure 29. Unimorph cantilever beam with left) 31 type right) Interdigitated. First row : Energy generation, Second row: voltage generation, Third row: charge generation

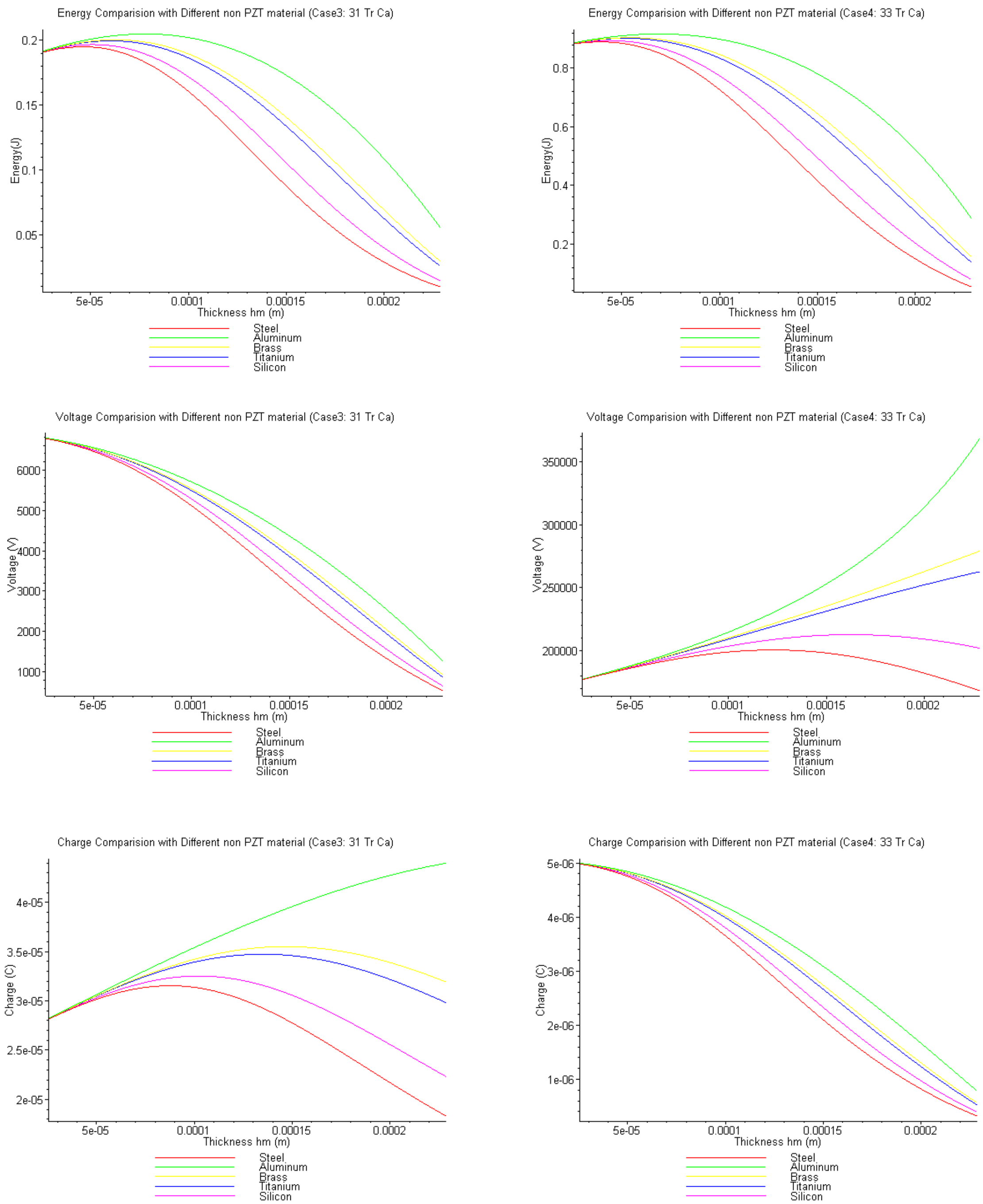

Figure 30. Triple morph cantilever beam with left) 31 type right) Interdigitated. First row : Energy generation, Second row: voltage generation, Third row: charge generation

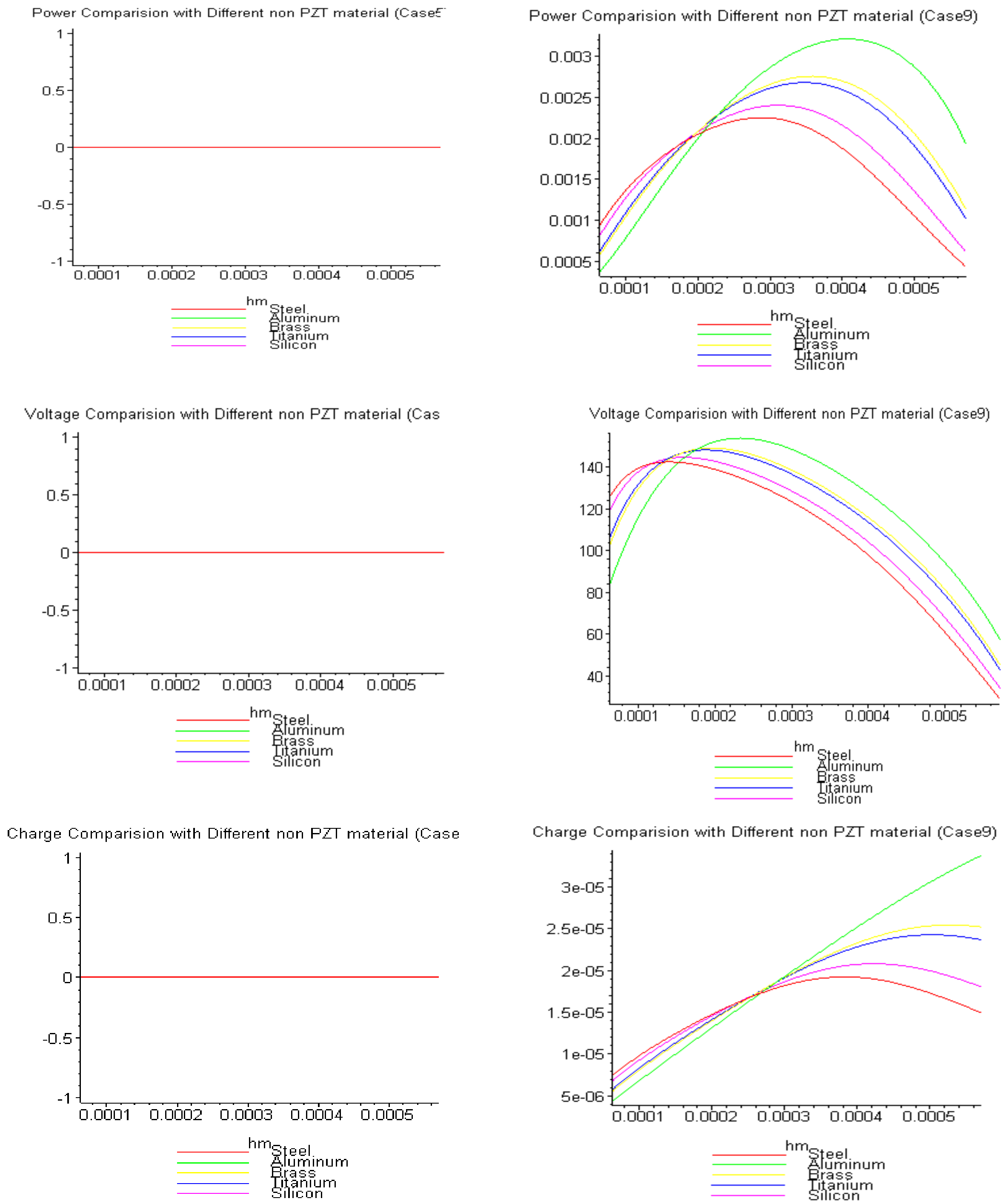

Figure 31.Unimorph diaphragm with left) unregrouped 31 type; right) Regrouped at radius of a/2. First row : Energy generation, Second row: voltage generation, Third row: charge generation

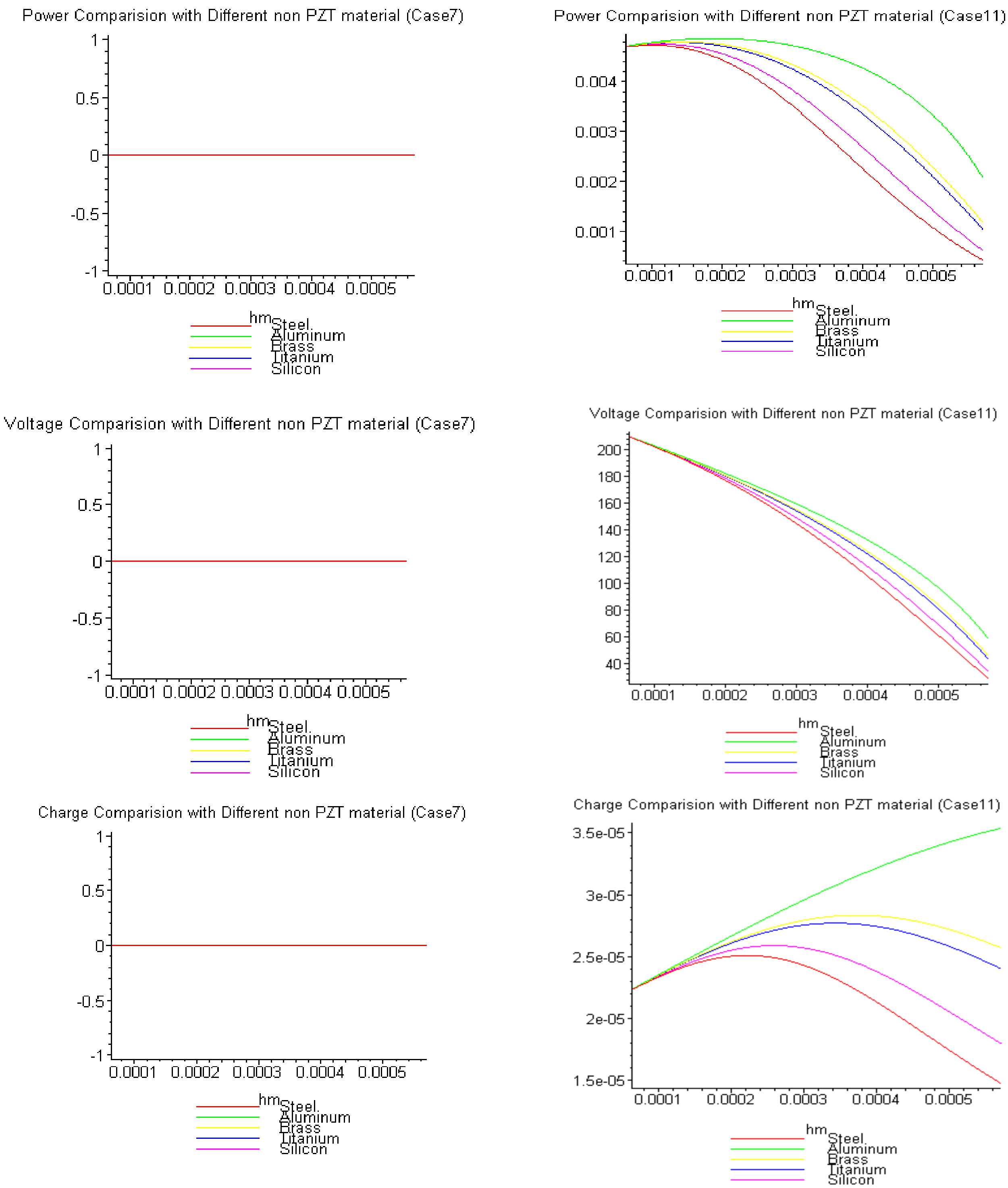

Figure 32. Triple morph diaphragm with left) unregrouped 31 type; right) Regrouped at radius of a/2. First row : Energy generation, Second row: voltage generation, Third row: charge generation

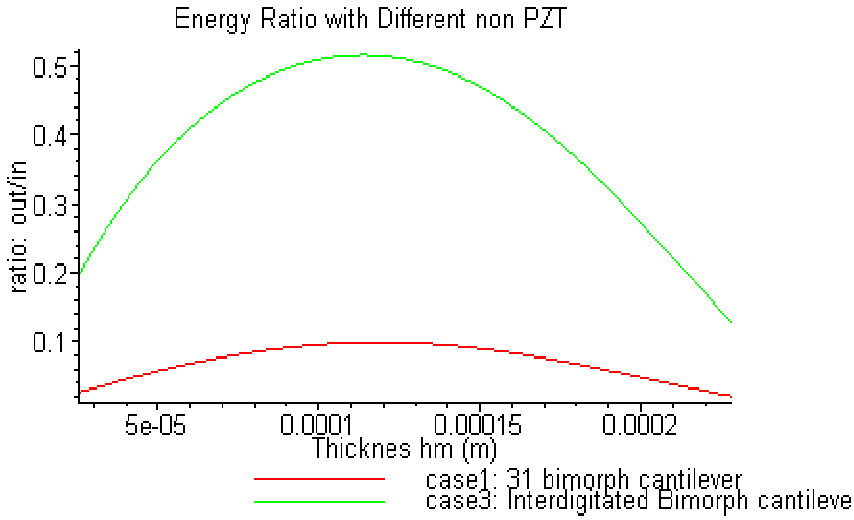

Figure 33. Energy ratio difference between 31 unimorph cantilever beam and interdigitated unimorph cantilever beam

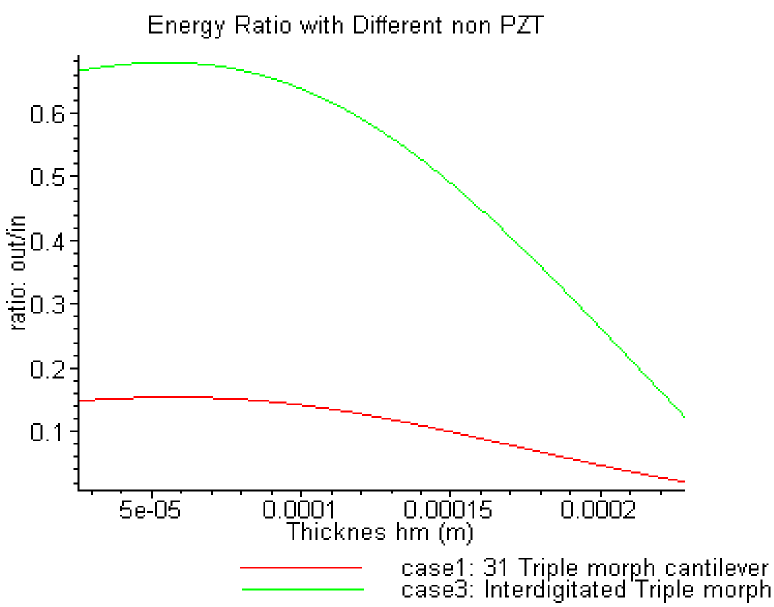

Figure 34. Energy ratio difference between 31 triple morph cantilever beam and interdigitated triple-morph cantilever beam

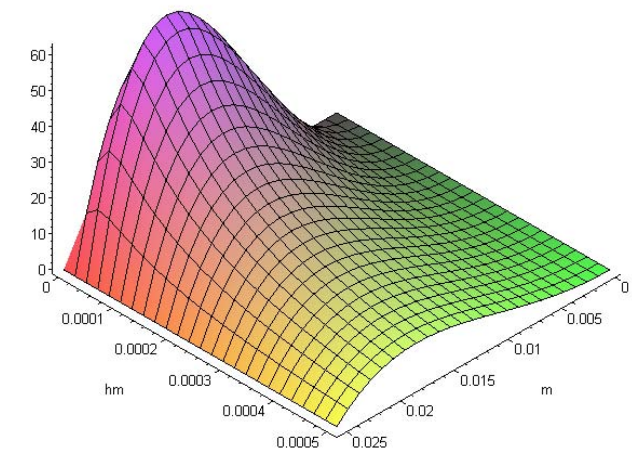

Figure 35. Voltage output. hm is the thickness of the substrate layer and m is the boundary of each grouped electrode

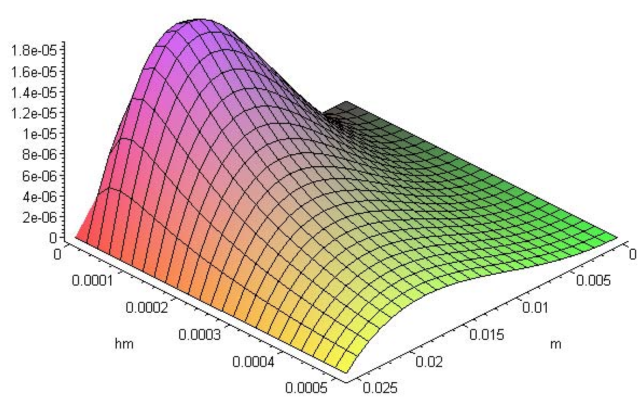

Figure 36. Charge output. hm is the thickness of the substrate layer and m is the boundary of each grouped electrode

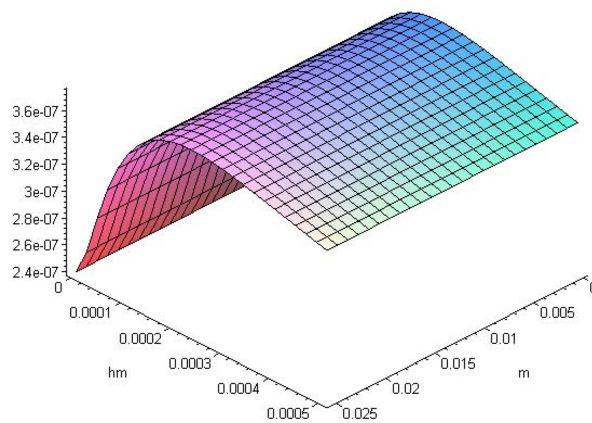

Figure 37. Capacitor changes. hm is the thickness of the substrate layer and m is the boundary of each grouped electrode

6.0 EXPERIMENTS

In this section, three diaphragm cases were verified with experiments. One unmodified unimorph diaphragm and two regrouped unimorph diaphragm cases which were regrouped at radii of *a/2* and *3a/4*. Three unmodified specimens, and two each of the regrouped specimens were prepared and tested.

6.1 Specimen Preparation

The piezoelectric diaphragms were constructed as shown in Figure 26. The unimorph diaphragms were made up of an aluminum substrate (thickness 0.508mm) and a PZT layer. In these experiments, PZT type 5H (Piezo systems, Inc., model# PSI-5H-S4-ENH) of 0.127mm thickness was used. Both flat surfaces of the piezoelectric wafer were originally covered with nickel electrodes.

The fabrication process involved first etching the PZT electrodes to form the desired regrouped pattern, poling the PZT as necessary, and finally bonding the PZT to the aluminum substrate.

6.1.1 Electrode Etching

In this research, the main reason for etching the electrode on the PZT was to disconnect and localize the electrodes to modify the poling direction of certain areas. Ferric Chloride acid ($FeCl_3$) was used to etch the nickel electrode. For the mask, acid resistive ink was used.

The specimen was etched at precise areas on the electrode surface. After etching, those electrodes should be disconnected from each other.

6.1.2 Poling and Bonding

The PZT wafers used in this research are poled by the manufacturer. Because of the regrouping idea, alternate electrode regions must be oppositely poled. In order to achieve this poling pattern, some of the sections must be re-poled to reverse their polarity.

Usually poling is done at high temperature (above Curie temperature) and high electric field. The poling direction of the PZT tends to move freely above the Curie temperature such as how ice melts and flows freely above 0°C. The Curie temperature of the PZT used in this work is 250°C. Electric fields of up to 2000V/mm are commonly used to pole PZT material. The Curie temperature is important but the electric field itself can change the poling direction of the PZT. The given thickness of the PZT wafer was 0.127mm and 200V poling voltage was applied across to the PZT to provide ~1574V/mm electric field. A Lambda model LLS9300 high voltage power supply, which can supply up to 300V, was used for the poling.

PZT wafers usually have some indication of the poling direction. This is done with a marking that shows which surface is positively charged when poled. Therefore, when received from the manufacturer the poling direction is away from the marked surface.

After poling, the poling direction was checked with a phase test. This test is derived from the operation of a PZT transformer. PZT transformers involve three steps and two segments of PZT that are coupled mechanically but not electrically. First, an electrical signal is applied to one PZT segment. The electrical signal is converted to mechanical deformation. Because of the mechanical coupling between PZT segments, this deformation illicits a response in the second PZT segment that generates an electrical output. The diaphragm with regrouped electrodes acts similar to the transformer. Exciting one electrode segment will induce an electrical response in the other electrode segment. This process can be used to determine the poling directions of the segments. The PZT beneath the input electrode acts as an actuator and the PZT beneath the output electrode works as a sensor. If the poling direction is the same, the phase difference should be 180° because in the diaphragm, if the actuator expands, the sensor compresses. Therefore, if the poling direction is the same for the input and the output, the phase should be 180° different due to the opposing stresses. The opposite is true if the phase difference between the input and the output signal is zero. In other words, if the phases are the same, the poling directions of the input side and the output side are opposite each other. Poling strength was also measured by comparing the voltage output. A 1 volt, 1kHz sinusoidal signal was used as a reference signal to check the poling direction and the strength of the regrouped PZT segments. If the poling was successful, only the phase of the output should be changed and not the magnitude.

6.1.3 Specimen Configuration

Three types of specimen were compared as shown in Figure 38. The specimens included an unmodified PEG, a PEG with electrodes regrouped at one half the radius, and a PEG with electrodes regrouped at three quarter of the radius.

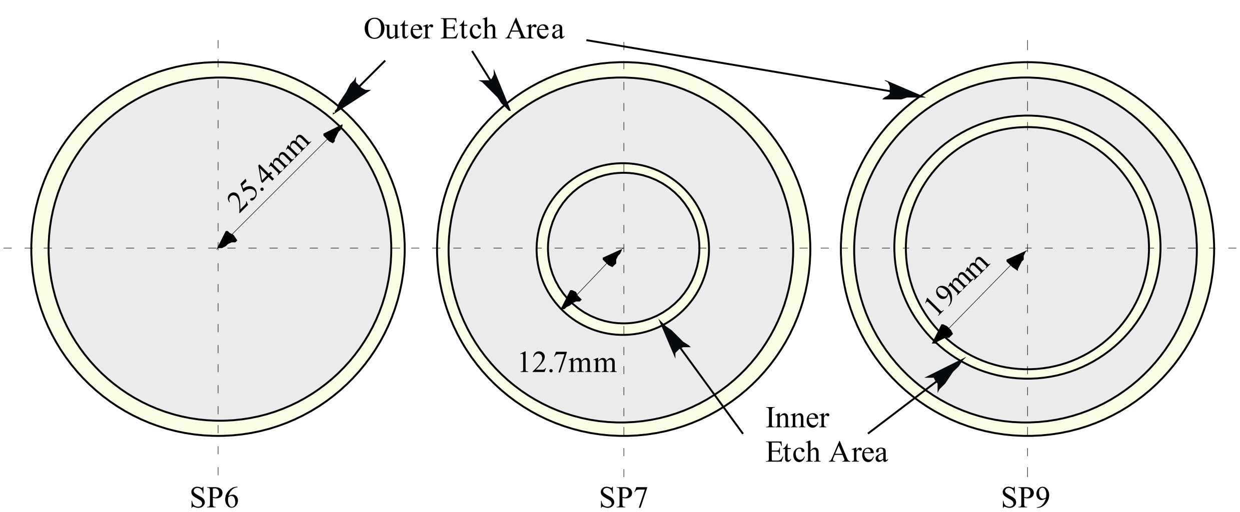

Figure 38. Specimen description. SP6:unmodified, SP7: regrouped, etched in the middle and repoled outside, SP9: regrouped, etched in 3/4 of the radius and repoled outside

Specimen 6 (SP6) is an unmodified case, so there is no need to re-pole. But for specimens SP7 and SP9, the poling directions should be different between the inside and the outside electrodes. To do that, the electrodes were disconnected at the border of opposite poling direction. The electrode was etched away at the border area with $FeCl_3$, which removed the nickel electrode. This disconnected electrode gap was refilled with conductive paint after poling, so a minimum etch area was preferable. For the specimen 7 (SP7), three circular masks were drawn at radii of 25.4 mm, 12.7 mm, and 10 mm with an etch resistant ink. For the SP9 specimen, the masks were drawn at radii of 25.4 mm, 20.4 mm, and 18 mm. Finally, specimen SP6 required only a mask of 25.4 mm.

The region beyond the 25.4 mm radius in each specimen was used for clamping to achieve the clamped boundary condition. The electrodes were etched out in the area under the clamp to minimize the experimental error. If there is no PZT under the clamp, then the boundary condition is no longer a clamped piezoelectric diaphragm, which will result in errors. However, if the PZT under the clamp has an electrode, then excess charge can be generated, also causing error. So the best approach is to leave the PZT under the clamp, but to etch away its electrode in that region.

The circular masks are essentially lines of etch-resistant ink that contain the etchant within the region required to remove electrode material as desired. Etching has been done between two inner circle masks. The etchant $FeCl_3$ is not a strong acid but is sufficient to remove the nickel electrode. $FeCl_3$ was applied between the inner masks using Q-Tips. The nickel electrodes melt away as soon as the $FeCl_3$ is applied. The etchant does not go beyond the areas covered by etch-resistant ink because of the surface tension of the etchant (Figure 39).

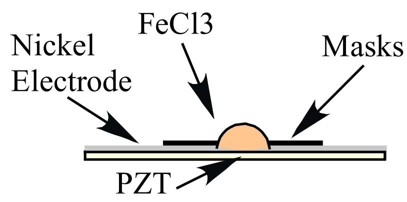

Figure 39. Electrode etching with FeCl3

Before poling, only the inner etch area should be etched. If the outer area (clamped area) is also etched, stress concentration problems occur and the PZT will break while re-poling.

After the inner etch area was etched, the PZT specimen was washed and air-dried. The resistance value between electrodes was measured to verify that those electrodes were fully disconnected. After that, the outside electrode area was re-poled, as shown in Figure 40.

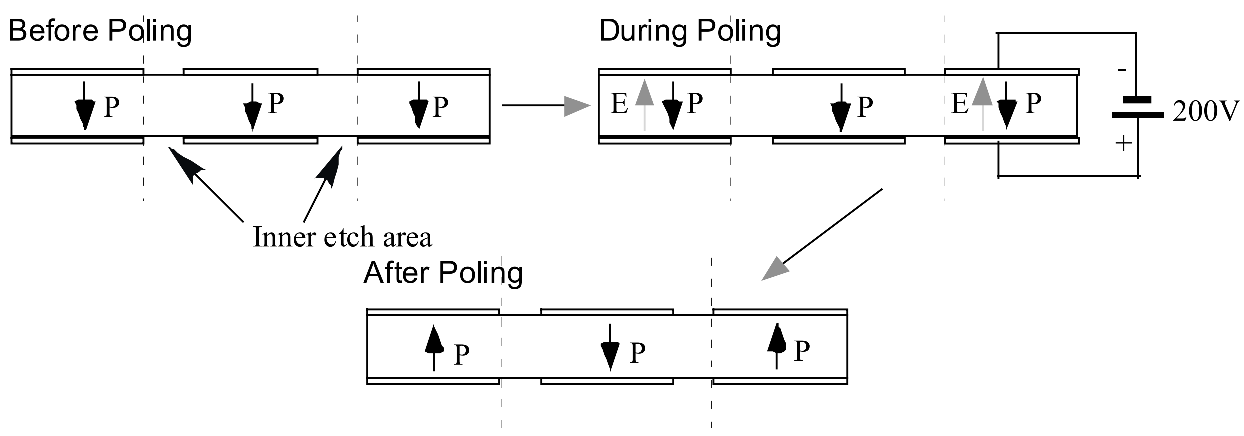

Figure 40. Repoling of the specimen

Before etching the outer etch area, the PZT was bonded to the aluminum substrate layer with conductive epoxy and cured for 24 hrs. Since at this point the outer electrode extended to the edge, the lower and upper surfaces of the PZT could have been electrically shorted to each other due to leftover epoxy. Etching the outer etch area ensures that the upper and the lower electrodes are disconnected, leaving the electrode only where energy will be harvested.

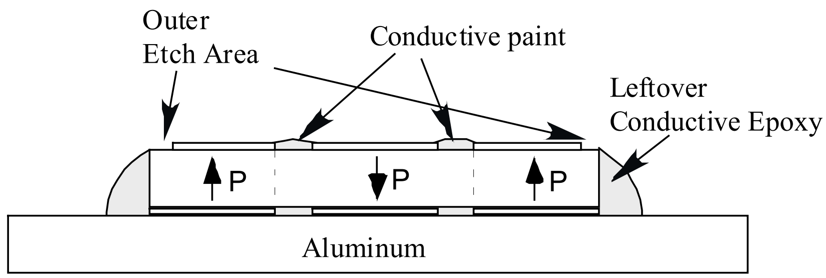

Figure 41. Outer etch area and filling up the electrode

The final step of the specimen preparation was to replace the electrode on the etched surface. If the etched area were left alone without refilling with conductive material, the total capacitance would be lowered and energy generation at that area would be lost. Using silver conductive ink (Chemitronics® conductive pen), the electrode of the inner etched area was reconstructed. The bottom surface was already filled with conductive epoxy, so all the bottom substrate area becomes the bottom electrode for the PZT. Figure 42 shows a schematic of the final PEG, bonded to the aluminum substrate and ready for clamping in the test rig. In the Figure 42, there is no inner etch area shown since the inner etch area was filled with conductive ink. Figure 43 shows photographs of three of the diaphragm specimens, one unmodified (SP-6), one regrouped at radius *a/2* (SP-7), and one regrouped at radius *3a/4* (SP-9).

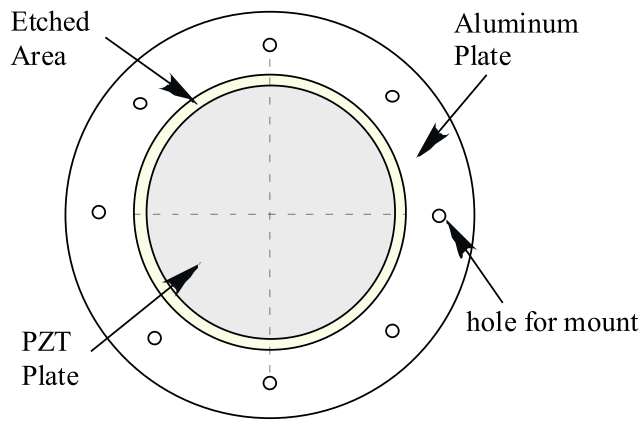

Figure 42. Final View of the PEG

As discussed in the previous sections, SP6, which has modified poling direction should yield no net harvested electrical energy, and SP9 which is regrouped at the best location should harvest the largest energy among the clamped diaphragm structures.

6.2 Test Rig for Unimorph Diaphragm

The diaphragm device used in this work is motivated by an application in air tanks which are essential to fire fighters and scuba divers. Highly compressed air is filled inside the air tank and is released through a regulating device. During regulation of the air pressure, pressure drops approximately 1 atm (96.5kPa). If that pressure difference can generate enough electric energy to support essential devices such as a communication device or the sensor which measures the remaining air in the tank, it will be beneficial by reducing the extra weight of batteries. The test rig, then is developed to apply predetermined amounts of pressure to the diaphragm so that the generated charge can be measured.

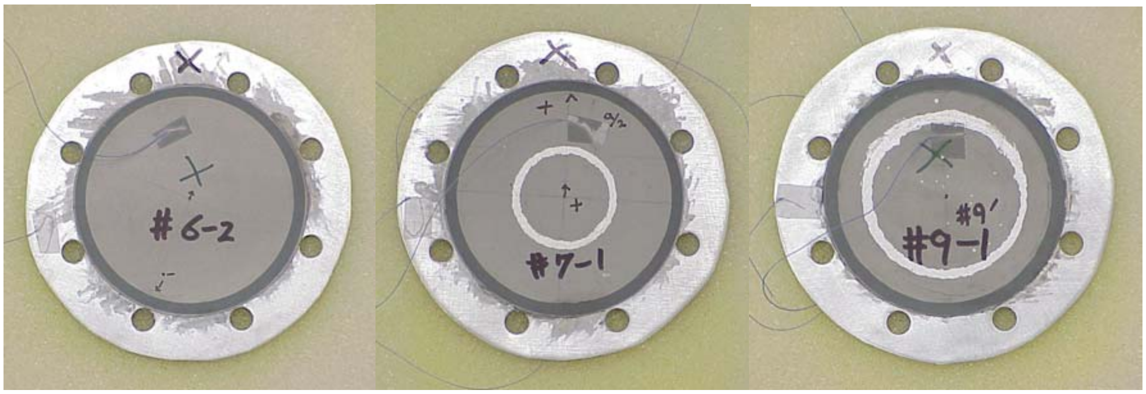

Figure 43. Picture of Three Types of The Diaphragm

6.2.1 Test Rig Configuration

A schematic of the test rig is shown in Figure 44, and a photo is shown in Figure 45. The air chamber (shown in close-up in Figure 46) used to supply pressure to the diaphragm was a Plexiglas cylinder. The diaphragm was mounted to one end of the cylinder by a ring of bolts that ensured a tight seal (with LOCTITE™ silicon adhesive sealant 59530) and also approximated the required clamped boundary condition. The other end of the closed cylinder contained a fitting for the air inlet and release. The cylinder's outer diameter was 76.2 mm and the wall thickness was 12.7 mm. Supplied house air pressure (approx. 690 kPa) was reduced to 9.65kPa with a pressure regulator (SPEEDAIRE 4Z029) and a pressure sensor (OMEGA PX137) was used to measure the pressure inside the chamber.

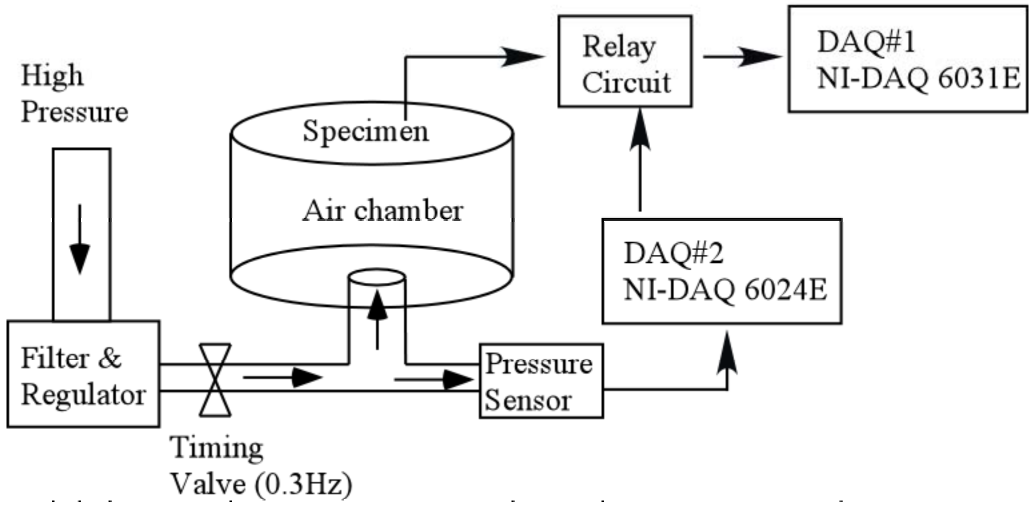

Figure 44. Schematics of the test rig

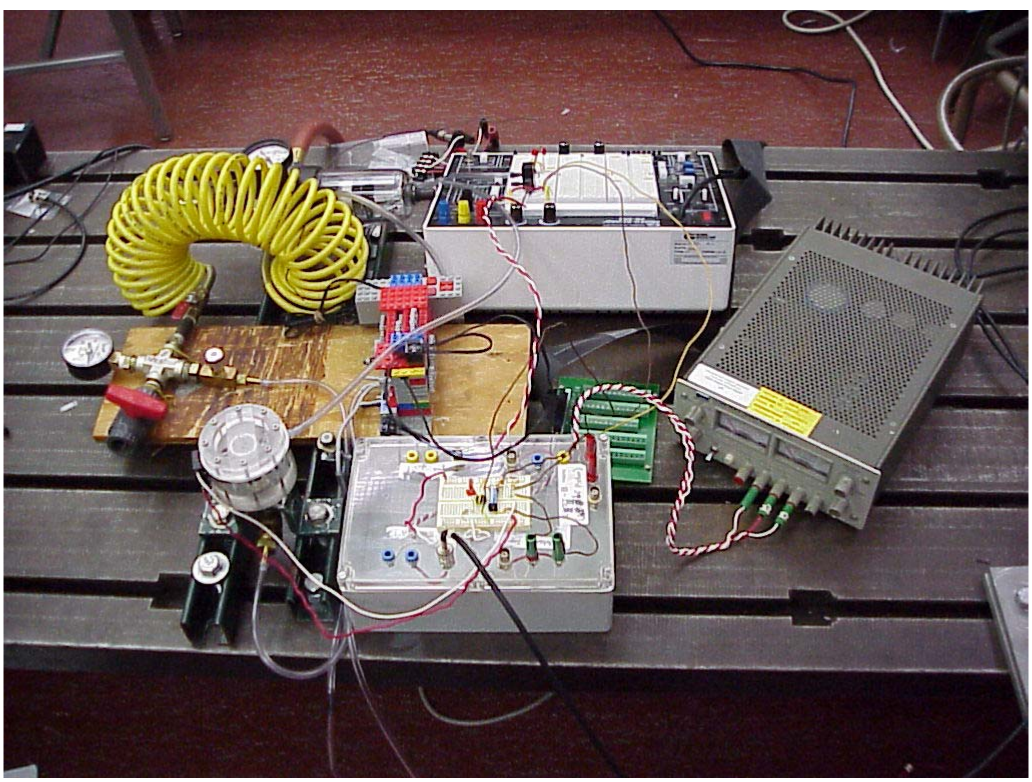

Figure 45. Picture of the test rig

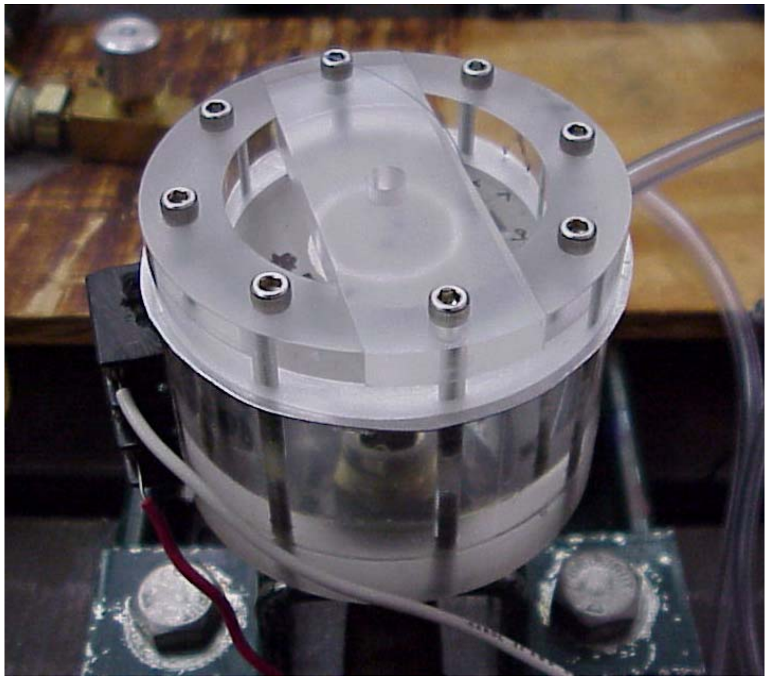

Figure 46. Pressure Chamber with PEG

The pressure applied to the chamber was controlled by a timing valve (Figure 47), which changed air direction in a predefined schedule. This valve has two positions. In one position, the valve connects the regulator to the chamber to allow the chamber to be pressurized. In the other position, the pipeline is disconnected from the regulator and is opened to the atmosphere such that the chamber is exhausted. In this research, the valve is opened and closed at a frequency of approximately 0.3 Hz to allow repeated measurements.

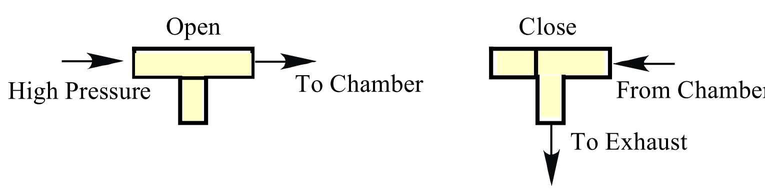

Figure 47. Timing valve operation

Due to the small charge generation, cross talk between channels in the data acquisition system was considerably high and one data acquisition board could not be used for measuring both pressure and power generation. Two separate computers and two separate data acquisition board were used, a National Instrument PCI-6024E board measured applied pressure and a National Instrument 6031E board was used to measure generated energy. Each board was operated by LabView® software.

6.3 TESTING PROCEDURE

The main target for this experiment was to measure the electrical energy generated by the PEG and compare to the theoretical values that were calculated in the previous chapters. Two different types of measurements were conducted. In the first set of tests, the open circuit voltage generation of the piezoelectric diaphragm was measured. In the second set, the voltage drop across a load resistor was measured.

6.3.1 Open Circuit Voltage Measurement

To find the open circuit voltage, a relay circuit was introduced, as shown in Figure 48. This circuit measures voltage across the resistor using the data acquisition board. The relay in the following circuit is controlled by the other pressure monitoring computer.

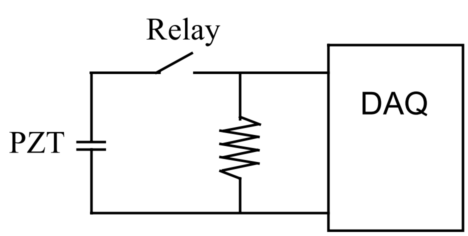

Figure 48. Relay circuit: mechanical reed relay driven by 741 op-amp

The operation of the test involves loading the chamber with high pressure air, measuring the voltage on the fully charged PZT, and then releasing the air from the chamber. The timing of the air valve, the relay, and the PZT voltage are shown in Figure 49.

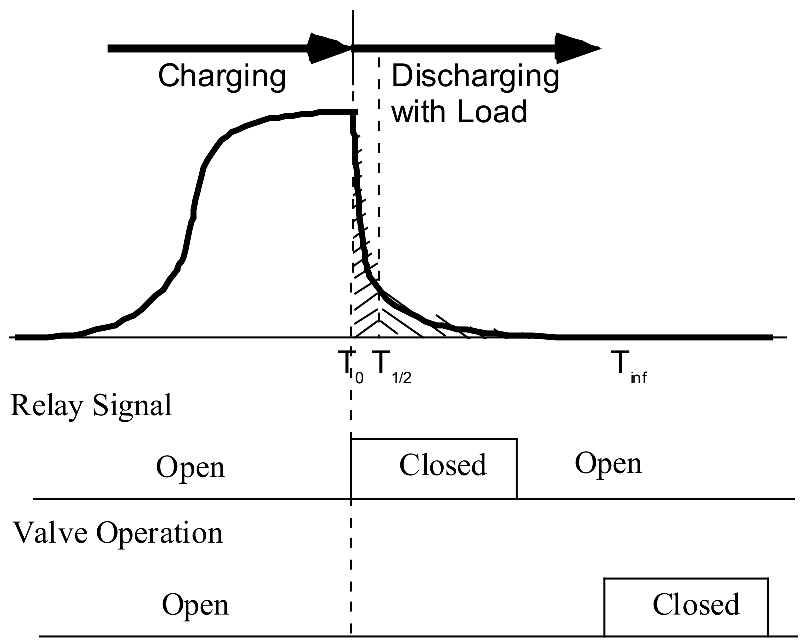

Figure 49. Charge discharging sequence and relay circuit timing

When the relay is open, no current flows in the resistor of Figure 48 and therefore no voltages appear to the data acquisition channel, however, the actual voltage on the PZT builds to a peak value as the chamber pressure increases. The resistor located across the input channel of the data acquisition device prevents drift of the channel. When the relay closes, the accumulated charge in the PZT instantaneously flows through the resistor and dissipates energy. During this period, the voltage drop across the resistor can be measured. The open circuit voltage is the peak voltage measured from the relay circuit. Figure 49 shows the charge vs. time according to the relay position.

In the actual experiment, generated charges disappear very rapidly even if the relay is not closed. Therefore, the relay must close as soon as the charge reaches its peak as in Figure 49. However, if the relay is closed before the PEG generates full charge, the full effect of applied pressure on the PZT charge will not be realized. Suppose that 10kPa pressure is applied to the PEG and the relay is closed when the measured pressure has only reached 5kPa. Then the discharge slope is not as sharp as if the relay were to close at the full 10kPa pressure, and the measured peak voltage would indicate the open circuit voltage generation was only 5kPa. Therefore, the relay timing was adjusted such that the relay was closed just before the pressure reached its maximum, as indicated by the pressure sensor.

Even though the response time of the PZT was very fast, the sampling rate used in this research (55 kHz) was sufficiently fast to capture the voltage response. The measured voltage when the relay close at a 10 kPa was acceptable to use as the generated open circuit voltage at a 10 kPa pressure.

Using the simple relation, $Q=CV$, the generated charge can be calculated with the measured open circuit voltage and the measured capacitance. Another way of measuring generated charge is to integrate the current graph. The shape of the voltage and the current graph are the same and only the magnitudes are different. Both voltage and current output graphs should look a like Figure 49. The generated charge could be obtained by integrating the dissipating current graph. However, given the rapid decay of the voltage and current graphs and the fact that they do not settle to zero at a definitive point in time (T_{inf}), it is very difficult to numerically integrate to find the area under the curve with suitable accuracy. Therefore, it was found that the most accurate and repeatable method for determining charge was to calculate it based on open circuit voltage and capacitance.

As mentioned before, two different measurements are made in the test. One measurement was the voltage across the resistor, and the other was the chamber pressure to determine when the relay should be closed.

6.3.2 Voltage Measurement Across Load Resistance with No Relay

An alternative set of tests was carried out to obtain data on instantaneous power generation by the PEG. In these tests, the piezoelectric generator was short circuited with a small load resistor and the voltage drop across the resistor was measured while the PEG was cycled with pressure. A 12 kΩ single resistor was used to perform the loading case experiment (Figure 50).

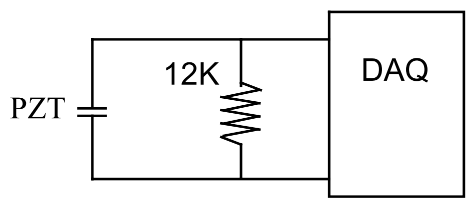

Figure 50. Loading case circuit

The exact power generation from this piezoelectric generator can not be calculated from the load resistor voltage, which is measured from the loading case because of internal losses in the piezoelectric material. But the power calculated from the voltage across the 12kOhm resistor will be a good indication of how much power was generated from the piezoelectric generator.

Figure 51 shows a representative sketch of the voltage drop across the load resistor as pressure is cycled to the PEG. With this voltage response, the current flowing through the load resistor can be calculated using the simple relation $I=V/R$, and the power is $P=VI=V^2R$. Therefore, the maximum peak power can be calculated, and used to compare the performance of the each piezoelectric generator.

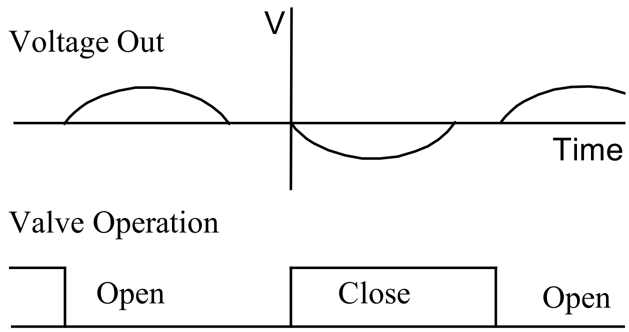

Figure 51. Loading case response. Voltage output across the 12KOhm resistor and valve position

7.0 RESULTS AND DISCUSSION

7.1 Comparison Between Theoretical and Experimental Energy generation

This section presents the theoretical and experimental results. Three cases were introduced; unmodified diaphragm, regrouped at one-half the radius, and regrouped at three quarters of the radius. For the unmodified case, three samples were tested, while two each of the regrouped cases were tested. Table 2 summarizes the comparison between theoretical and experimental results.

Table 4. Generated Open Circuit Voltage and Capacitor comparison at 9.65 kPa.
*(* indicate 1 kHz measurement.)*

Specimen			Numerical Calculation	Experimental Data
31 unmodified	Sp6	V	0	1.17±0.006
		nF	350.8	292*
	Sp6_1	V	0	1.63±0.006
		nF	350.8	348*
	Sp6_2	V	0	1.61±0.003
		nF	350.8	328*
31 Regrouped	Sp7	V	6.176	5.31±0.014
		nF	350.8	365*
	Sp7_1	V	6.176	5.61±0.014
		nF	350.8	343*
31 Regrouped	Sp9	V	10.174	8.84±0.039
		nF	350.8	338*
	Sp9_1	V	10.174	9.26±0.010
		nF	350.8	335*

Each experimental data point for pressure shown in Table 4 is a result of 1000 pressure loadings of the diaphragm. The data are presented as mean ± uncertainty using the 95%

probability t-distribution. A sample of the actual data is shown in Figure 52 and Figure 53 shows the collected peak voltage data for a large sample of the tests. As shown in Table 4, the measured open circuit voltages agree with the predicted values except for the unmodified case which shows an unexpected non zero voltage. For the unmodified open circuit voltage case, there are several possible explanations. The numerical calculation is based on the “perfectly symmetric” case and in the real experiment, that perfect symmetry might not be achieved. Another possibility is the width difference between top and bottom electrode. As mentioned before, the lower electrode of the PZT is the aluminum substrate itself because of the conductive epoxy. The wiring can also be a problem. The lead wire was attached to the upper electrode of the piezoelectric material using adhesive tape, which might have altered the stress distribution.

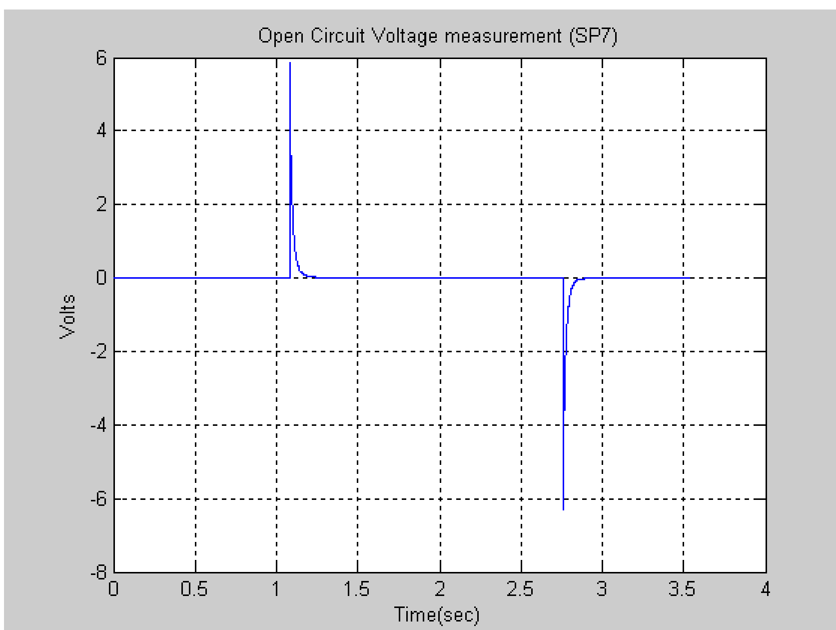

Figure 52. Open circuit voltage measurement (single cycle, SP7)

The static capacitance measurement of the PEG was done with an LCD meter (BK Precision 875B). This meter measures capacitance with 1 kHz sinusoidal signal and measures impedance across the specimen. This measured value at 1 kHz is not the static capacitance but is very close to the real one. The definition of the coupling factors are also defined for the 1kHz case, therefore, 1KHz data is also acceptable for the quasi-static case.

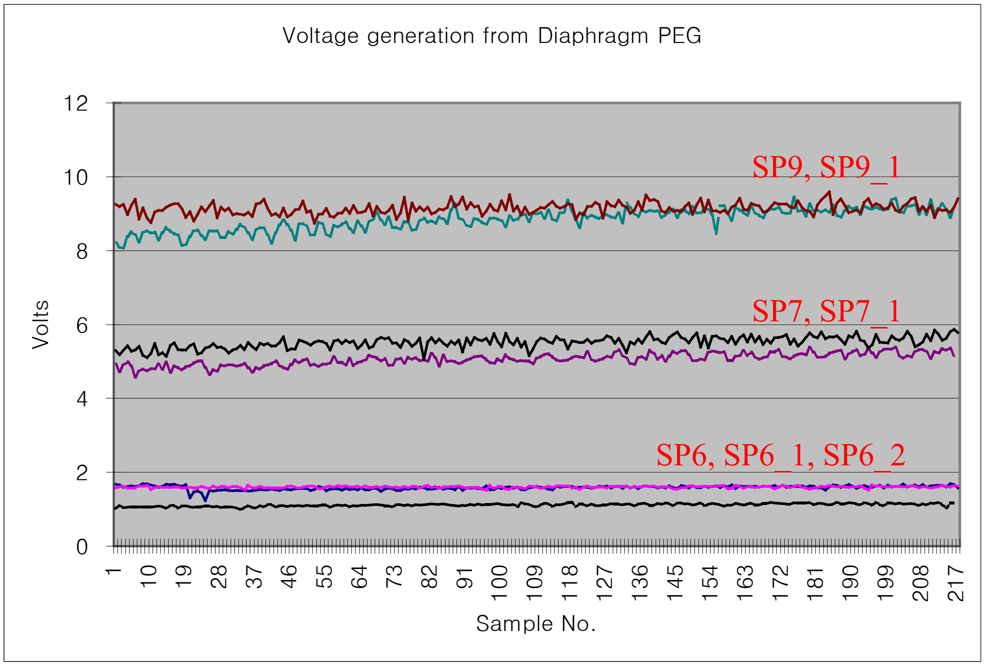

Figure 53. Open circuit voltage measurement for each specimen

With the generated open circuit voltage and measured capacitance, the generated electrical energy can be calculated using a simple equation. The generated charge is

$$Q_{Gen} = CV_{open} \tag{4.189}$$

and the generated energy is

$$Energy_{gen} = Q_{Gen}V_{open} \tag{4.190}$$

Using the above two relations, experimental energy and charge can be calculated and compared with the analytical values. This information is shown in Figure 54 & Figure 55, and summarized numerically in Table 5.

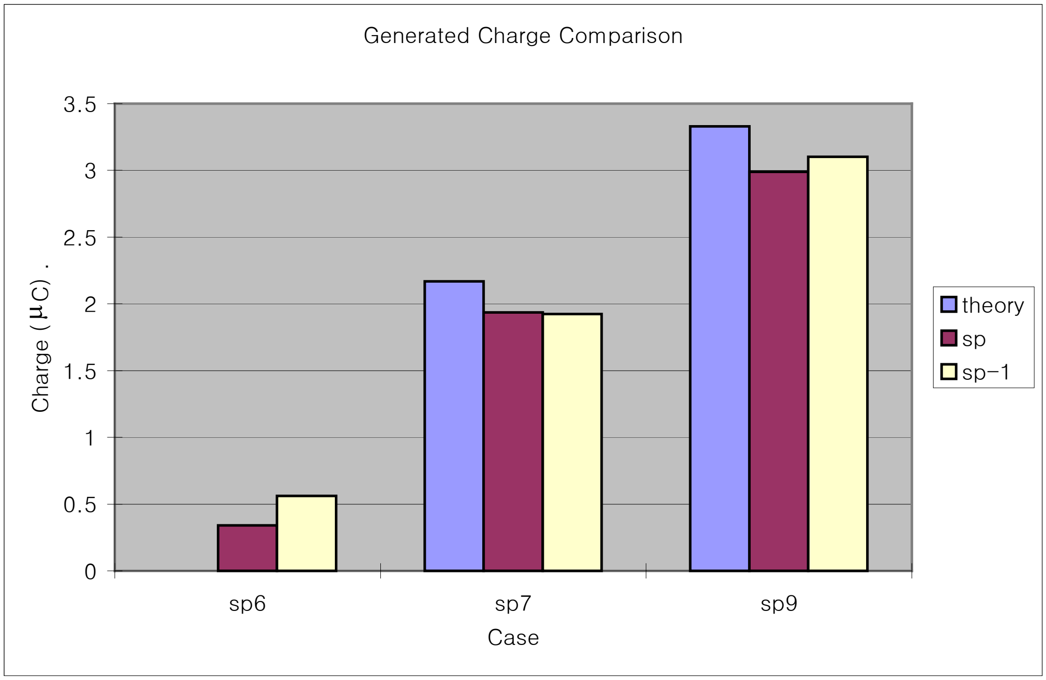

Figure 54. Experimentally generated charge comparison with theoretical calculation.

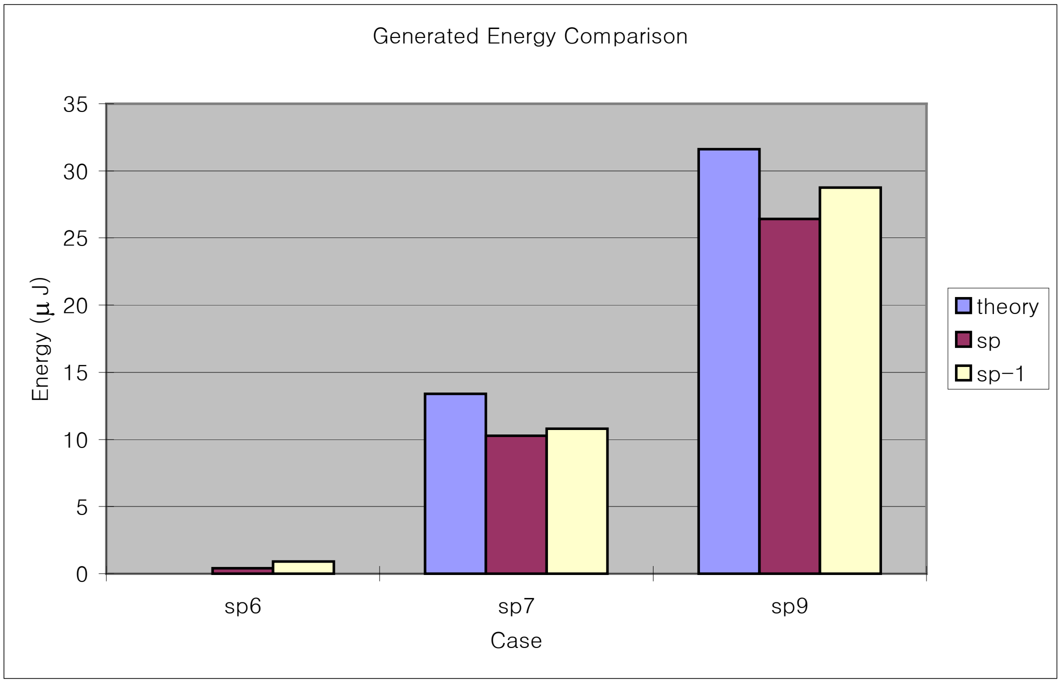

Figure 55. Experimentally generated energy comparison with theoretical calculation

Table 5. Charge and energy generation comparison between numerical value and experimental value

	Numerical Calculation			Experimental Data						
	Unmodified	Regroup		Unmodified			Regroup			
		SP7	SP9	sp6	sp6-1	sp6-2	sp7	sp7-1	sp9	sp9-1
Q (μC)	0	2.2	3.3	0.3± 0.0008	0.5± 0.0019	0.6± 0.0010	1.9± 0.0053	1.9± 0.0047	3.0± 0.0130	3.1± 0.0035
E (μJ)	0	13.4	31.6	0.4± 0.0000	0.9± 0.0000	0.9± 0.0000	10.3± 0.0001	10.8± 0.0001	26.4± 0.0005	28.7± 0.0000

7.2 Comparison Between Theoretical and Experimental Power Generation using Load Resistor

In the previous section's measurements, the open circuit voltage could be measured, but independent measurement of generated charge (or current) could not be made. The piezoelectric generator with 9.65 kPa pressure creates very small charge and it is hard to measure the generated power. In this section, a resistor was attached directly to the diaphragm PEG and the voltage drop across the resistor was measured as the diaphragm was loaded and unloaded.

With a large resistor load, the generated current could not flow well through the resistor and the measurement would not provide acceptable data. If too small of a resistor were used, the voltage drop across the load resistor would be very small to measure. Therefore, choosing the proper load resistor was important. In this measurement, a 12 kΩ resistor was used which was as small as possible to produce acceptable results. Below 12 kΩ, the measured voltage was too small for the resolution of the DAQ board. The resolution of the DAQ board was 0.15 mV at ±0.5 V range measurement.

Table 6 shows the voltage measurements across the 12 kΩ load resistor. All these data were measured more than 100 times and the uncertainties shown are found using 95% confidence t-distribution.

Recall that the process used to generate the data shown in Table 6 involved pressurizing and depressurizing the chamber while measuring the voltage drop across the load resistor. A sample of the pressure cycle is shown in Figure 56. The resulting voltage drop across the load resistor is shown in Figure 57. When the pressure increases, a positive voltage is measured as charge begins to flow across the load resistor. When the chamber pressure is released, the stress in the PZT is released, and charge once again moves in the piezoelectric material, but in the opposite direction, given the fact that the original charge was dissipated through the load resistor, a new reference point is created in terms of charge generation vs. material strain. So during depressurization, charge is generated with opposite polarity of the pressurization phase. This causes current to flow in the opposite direction through the load resistor, as shown by the negative voltages on the right side of Table 6.

Table 6. Measured voltage across 12 kΩ load resistor

Specimen	Max Voltage (Pressurized, 0→9.65KPa)	Min Voltage (Depressurized, 9.65KPa→0)
SP6	0.017±0.0007	−0.029±0.0013
SP6−1	0.028±0.0010	−0.043±0.0016
SP6−2	0.028±0.0010	−0.044±0.0017
SP7	0.112±0.0038	−0.164±0.0053
SP7−1	0.120±0.0048	−0.174±0.0067
SP9	0.167±0.0058	−0.242±0.0086
SP9−1	0.179±0.0090	−0.259±0.0125

In Table 6, we can observe that the voltage drop across the 12 kΩ load is different for the various cases as expected. More voltage drop occurs when regrouped diaphragms were used. An additional feature is that the voltage drop is higher when the diaphragm was depressurized as shown in Figure 57. This is because the releasing time of the air in this test rig is much quicker than the pressurizing time, by a factor of approximately 1.5 (Figure 56). The magnitude of the current generation is in the form of frequency times charge magnitude. Therefore, faster time of compression will generate more current. This is verified in the experimental data.

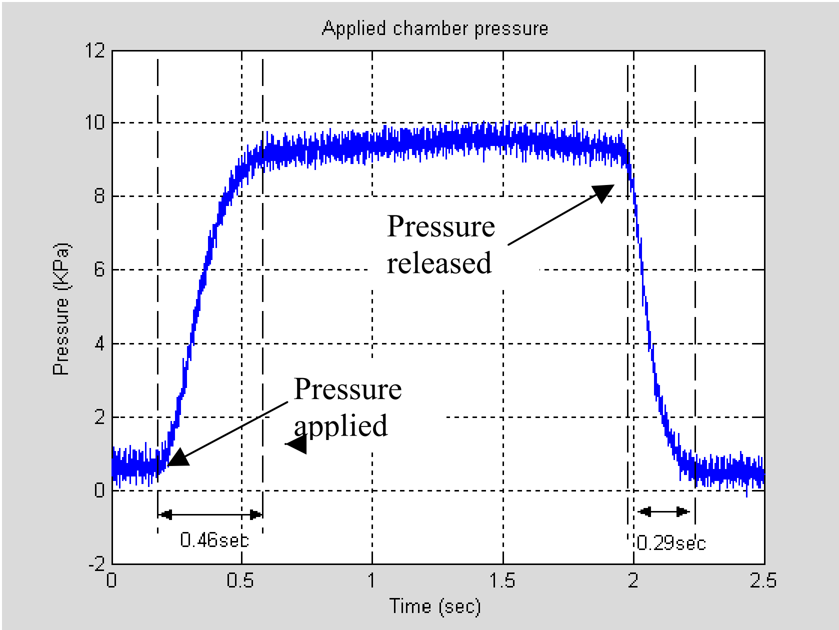

Figure 56. Applied chamber pressure

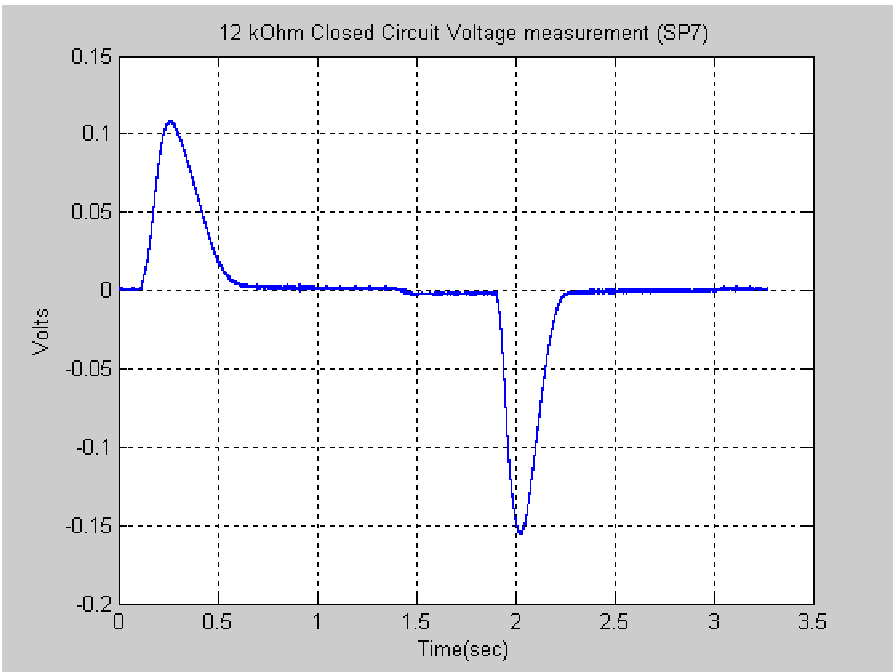

Figure 57. Measured voltage across 12 kΩ load resistor (single cycle, SP7)

The measured voltages were converted to current and power using classic electrical equations. The current was calculated using Ohm's law, $V=IR$, with the measured voltage across the resistor. The instantaneous power was calculated with $P=VI=V^2/R$. Using the max and min voltage values from Table 6, the peak current and power values are calculated and listed in a Table 7. These calculated current and power values do not exactly mean the generated current and power from piezoelectric generator because of internal losses, but are the consumed power and current at the load. Even though the consumed power is not the generated power, it is correct to say that more power is generated by the piezoelectric generator than is consumed at the load. Figure 58-54 show bar graphs comparing voltage, charge and consumed power for the three types of PEG's tested.

Table 7. Calculated peak current and power from the measured voltage at the 12KOhm load

Specimen	Calculated Current (mA)		Calculated Power (μW)	
	Pressure	Release	Pressure	Release
SP6	0.0014±0.0001	0.0024±0.0001	0.0252±0.0000	0.0676±0.0001
SP6-1	0.0023±0.0001	0.0036±0.0001	0.0664±0.0001	0.1549±0.0002
SP6-2	0.0023±0.0001	0.0036±0.0001	0.0657±0.0001	0.1574±0.0003
SP7	0.0094±0.0003	0.0136±0.0004	1.0611±0.0012	2.2332±0.0023
SP7-1	0.0100±0.0004	0.0145±0.0006	1.2124±0.0019	2.5212±0.0037
SP9	0.0139±0.0005	0.0201±0.0007	2.3124±00027	4.8497±0.0061
SP9-1	0.0149±0.0007	0.0215±0.0010	2.6532±0.0067	5.5748±0.0130

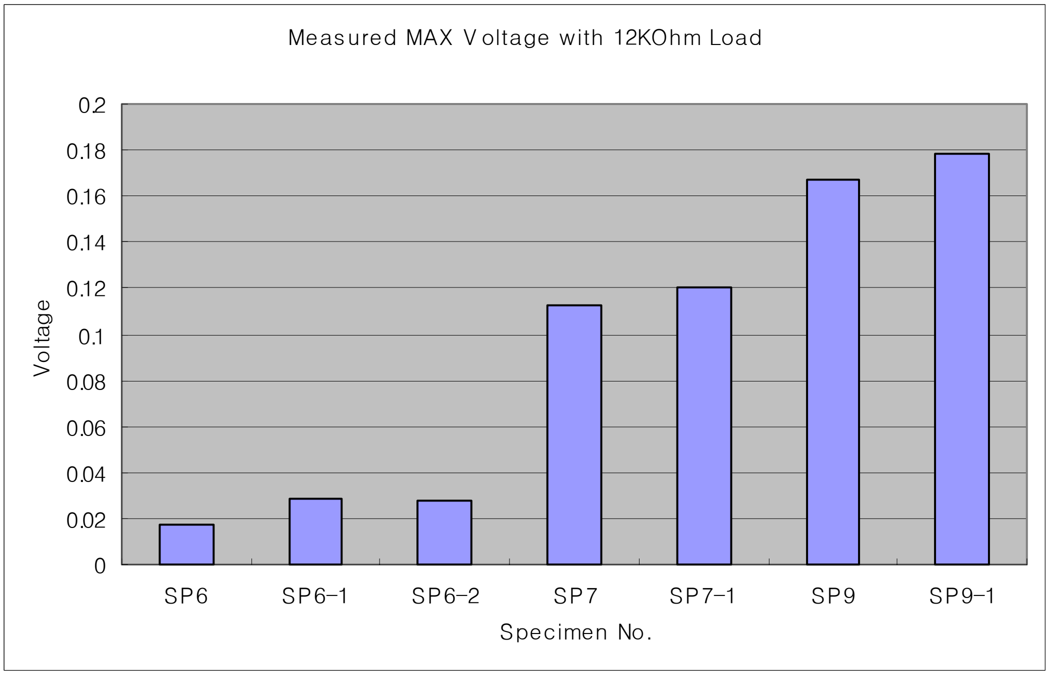

Figure 58. Comparison of the voltage measurements across 12 kΩ resistor for all PEG specimens.

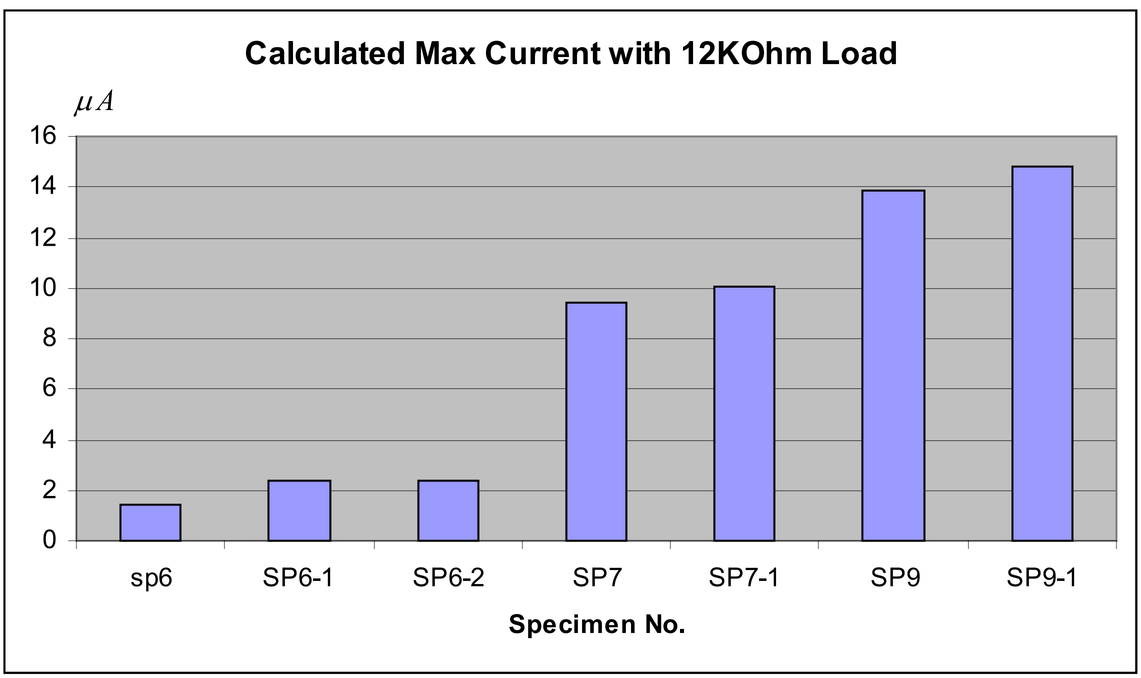

Figure 59. Comparison of the calculated maximum current from measured voltage

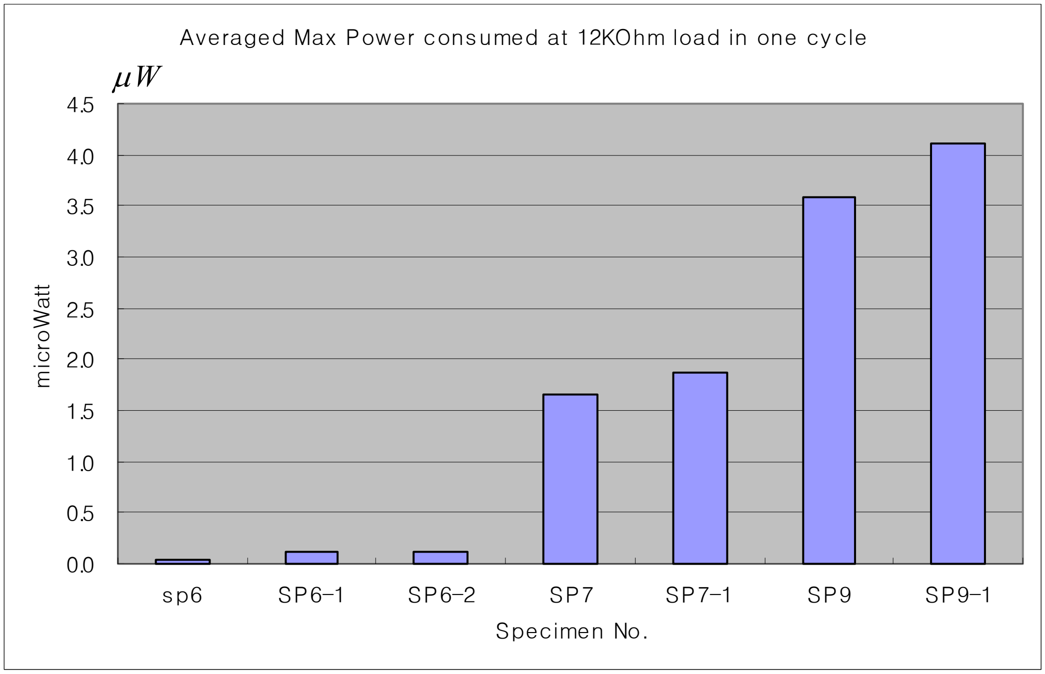

Figure 60. Experimental peak power generation for each PEGs

7.3 Discussion

Experimental and theoretical calculations show that the change in stress polarity in a loaded structure can be utilized to enhance or optimize energy harvesting by properly poling segments of the piezoelectric material. The experimental data show that regrouped diaphragm PEGs are superior to the un-modified diaphragm support this concept. The optimal location of the regrouped electrode interface was found theoretically and was verified with the experiments. Regrouping at three-quarters of the radius generated about twice as much power as regrouping at half the diaphragm radius, and about ten times more power than the un-modified diaphragm (although theory predicts zero power in the un-modified case).

The capacitance value of the PEG has a very important role in the piezoelectric energy harvesting device design because the PEG can not sustain high voltage. If the capacitance is small, voltage generation increases and can eventually damage the PEG itself. Therefore in the power generation, minimizing voltage while maximizing capacitance by changing boundary conditions is preferable.

The measured capacitances values shown in the previous section are measured at 1 kHz and do not precisely match the theoretical values. Since the capacitance does not change with the poling direction but is highly dependent on piezoelectric and substrate thickness and boundary conditions, the differences may be due to uncertainty in the actual material thicknesses and boundary conditions in the specimens. Additional causes for the differences may be conductive epoxy layers' thicknesses or the fact that quasi-static values are different than those found with the 1 kHz measurement.

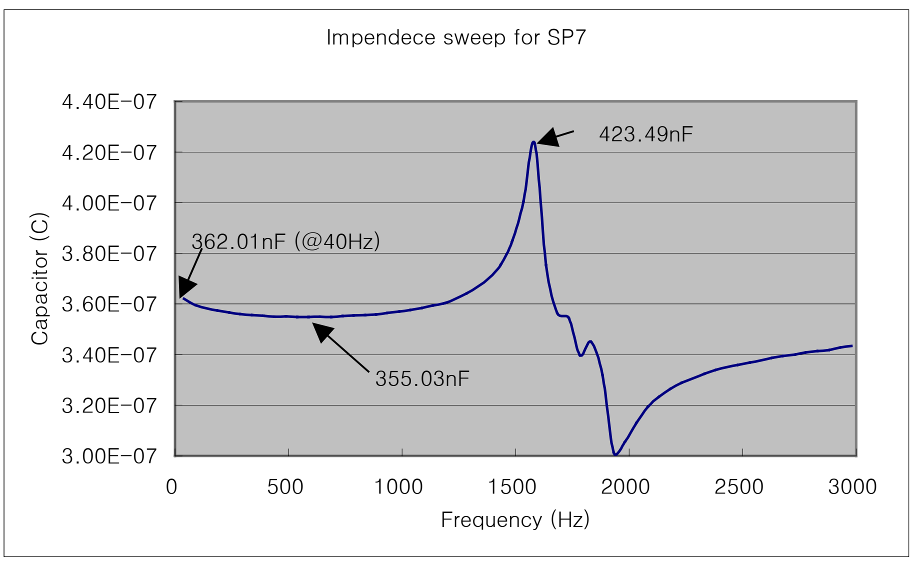

Figure 61. Capacitor VS. frequency

The capacitance values are a function of frequency, as shown in Figure 61. This measurement has been done using an impedance meter (Agilent 6294A Precision impedance

Analyzer) with specimen SP7. The calculated capacitance of SP7 is 350.8 nF, and the measured capacitance is 362.01 nF @ 40Hz and 365nF @ 1 kHz. In between 40 Hz and 1 kHz the minimum capacitance value was 355 nF.

Static capacitance measurement was hard to obtain with common measurement devices. A possible measurement method for the static capacitance is to measure the slope of the discharging graph and calculate the time constant. In the systems tested, however, the discharging time is too fast and the measurement error is large. Therefore, precise measurement of the static capacitance was not possible with the instrumentation available because the errors were larger than those measured at 1 kHz.

According to the data, the calculated capacitances are in general lower than the experimentally-measured values. However, given the assumptions about the diaphragm, such as an isotropic diaphragm, this small difference does not greatly affect the results.

The diaphragm analysis and experiment shows that the piezoelectric generation is very small when compared to other generation techniques (shown in chapter 3) even if the performance can be improved about 5 times through electrode regrouping. Of course, the input force and frequency were very small but with this volume of PEG device, more than 90 kPa cannot be applied because of the limitation of the PZT materials' extensional stress. With 90 kPa, barely 0.5 mW of electrical power was obtained. If the specimen was made to sustain more pressure, such as through pre-compression, and was excited with 1 MPa of pressure, 50 mW of peak power could be obtained with a 50 mm diameter diaphragm.

Another possible way of increasing power generation is that, since the deflection of this 50 mm diaphragm is very small, one could stack up a large number of diaphragms in one PEG. For example, a 50 mm diameter by 50 mm long structure could contain approximately 16 diaphragms (assuming each diaphragm's deflection is 2mm) and could create 0.5 x 16 = 8 mW peak power.

Increasing frequency is also a useful way to increase power generation with the PEG. However, for continuous power delivery at a given frequency, one must use an RMS calculation, which will be lower than the peak value given here. On the other hand, increasing frequency will result in higher voltages caused by the more rapid pressure charge and stress change in the PZT. This will increase total RMS power.

This regrouped diaphragm analysis also can help to fabricate an active device. The regrouped diaphragm is easy to fabricate compared to the 33 interdigitated diaphragms and it can generate more deflection and more force since the diaphragm follows its natural stress distribution. Therefore, the regrouped diaphragm can be utilized in the actuator case, which requires large force and deflection.

8.0 FUTURE WORK

This section briefly discusses some of the unsolved problems with this research. The first issue is the assumption of isotropy in the analysis. Piezoelectric material is not isotropic, and there might be some numerical differences if an anisotropic analysis is used. The stiffness differs slightly in the 1 and 2 directions, and the Poisson's ratio differs by a very small amount. It is unlikely that this anisotropic problem causes a major difference in the power generation from the previous analysis with an isotropic plate assumption, but there is an argument for carrying out the analysis.

Another unsolved question is that the un-modified (un-regrouped) diaphragm should generate no electrical energy, but a noticeable amount of energy was converted in the experiment. The effect of an off-centered diaphragm was raised, but that effect was very small compared to the voltage generation. The diaphragm was moved off centered by about 1mm, but the voltage difference was within 10% of the original generated voltage. So being off center does cause this problem, but there exists a bigger problem to be solved. The current best guess is that the electrode width of the bonding layer is wider than the pressurized area. Conductive epoxy has been used to bond the aluminum plate and the whole substrate aluminum layer is also the bottom electrode of the piezoelectric material. Theoretically, the capacitance area of the electrode is a smaller area but there might be some effect with the larger electrode on one side. Since, at the clamped area, the piezoelectric material still creates electric field, and since one side of the electrode still remains, this remaining electrode might cause this kind of problem.

Based on earlier discussions, it would appear that continuous power generation by the PEG can be significantly increased by increasing the frequency of application of the mechanical excitation. A study of the tradeoffs between dynamic and quasi-static operation of the PEG is in order, and may lead to an understanding of optimal operating conditions.

Finally a further area of exploration is the 33-mode diaphragm. Robust numerical calculations and experimental confirmation is needed.

APPENDICES

APPENDIX A

Properties of PSI-5H4E ceramic

Part Number		T107-H4E-602	
Electrode type		Nickel	
Composition		Lead Zirconate Titanate	
Material Designation		PSI-5H-S4-ENH (Industry Type 5H, Navy Type VI)	
Capacitance		850	nF (±10%)
Relative Dielectric Constant (@ 1 KHz)	K^T_3	3800	
Piezoelectric Strain Coefficient	d_{33}	650×10^{-12}	m/V
	d_{31}	-320×10^{-12}	m/V
Piezoelectric Voltage Coefficient	g_{33}	19.0×10^{-3}	V m/N
	g_{31}	-9.5×10^{-3}	V m/N
Coupling Coefficient	k_{33}	0.75	
	k_{31}	0.44	
Polarization Field	Ep	1.5×10^6	V/m
Initial Depolarization Field	Ec	3.0×10^5	V/m
MECHANICAL			
Dimension		72.4 x 72.4 x 0.191	Mm^3
Density		7800	Kg/m^3
Mechanical Q		30	
Elastic Modulus	Y^E_3	5.0×10^{10}	N/m^2
	Y^E_1	6.2×10^{10}	N/m^2
THERMAL			
Thermal Expansion Coefficient		$\sim 3 \times 10^{-6}$	m/m °C
Curie Temperature		250	°C

$$\epsilon_o = 8.854 \times 10^{-12} F/m$$

APPENDIX B

Testrig Drawings

PARTS

THIS TEST RIG IS CONSISTS OF 4 PARTS

1 OF BODY SECTION

2 OF TOP SECTION

1 OF BOTTOM SECTION

TABLE OF CONTENTS

*NOTE : ALL DRAWINGS ARE IN BTU (INCH)

Figure 62. Assembled testrig

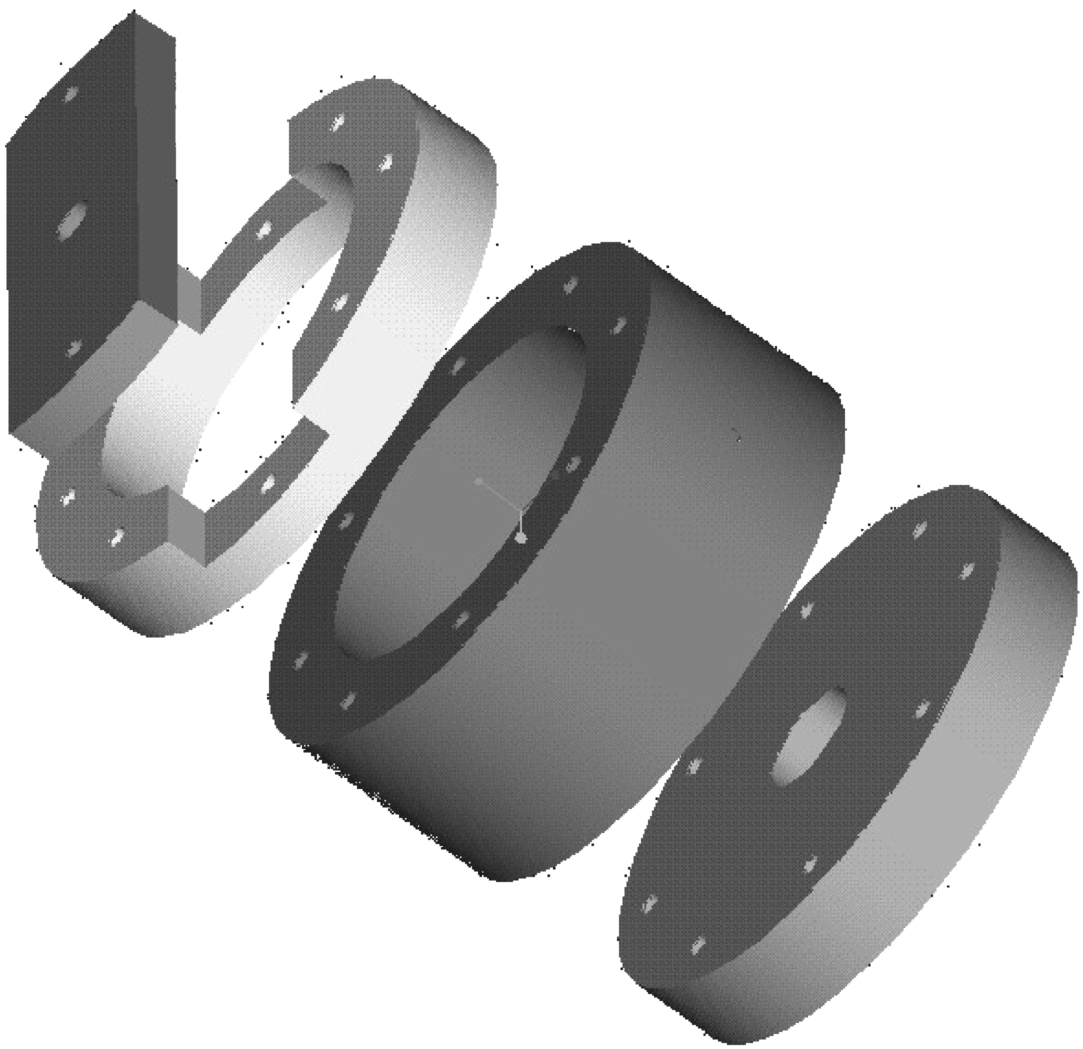

Figure 63. Assembly figure #2

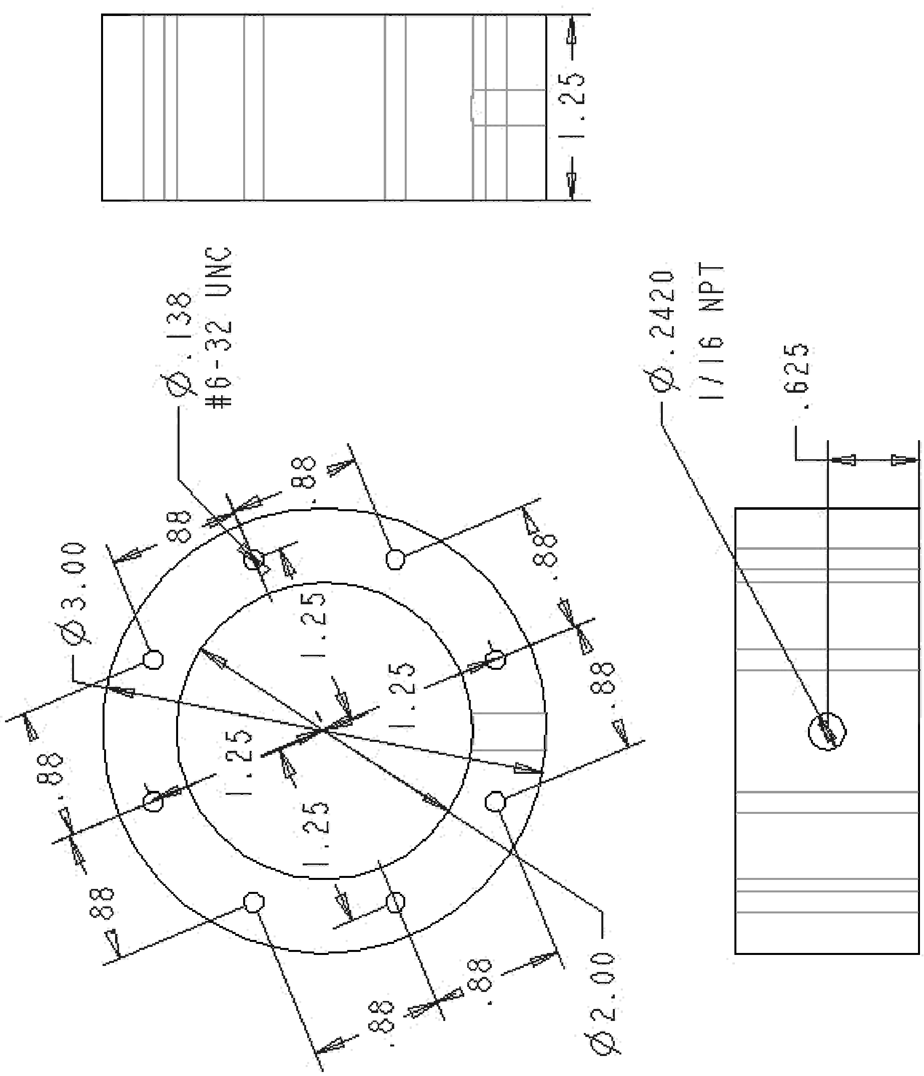

Figure 64. Air chamber part, Plexiglas

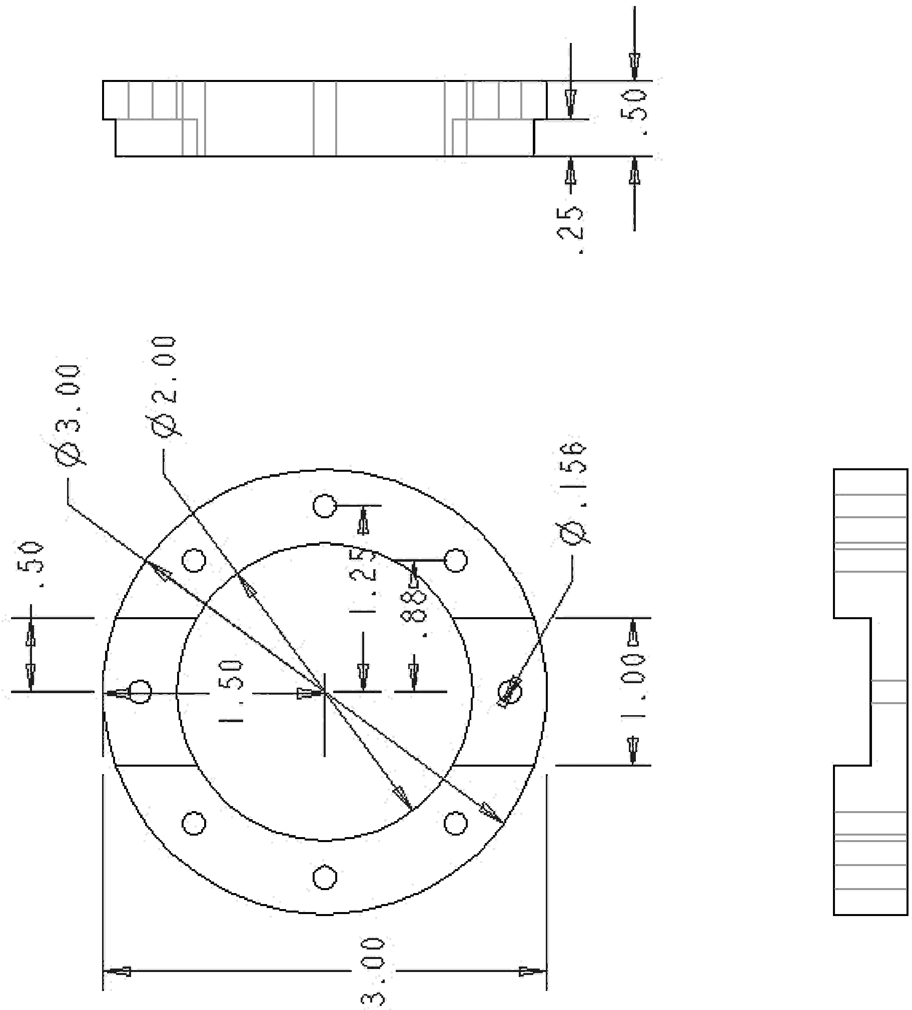

Figure 65. Top plate #1, Plexiglas

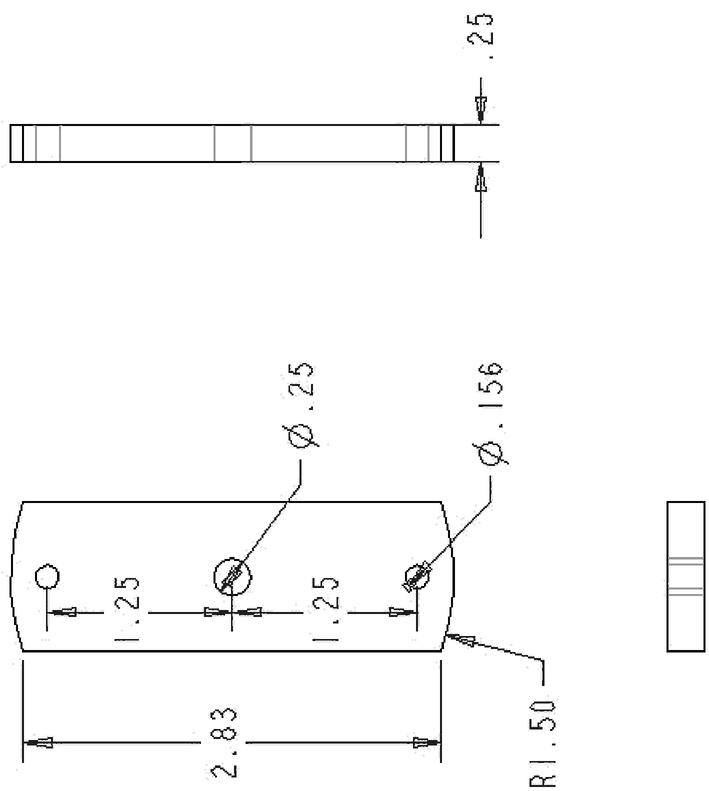

Figure 66. Top Plate #2, Plexiglas

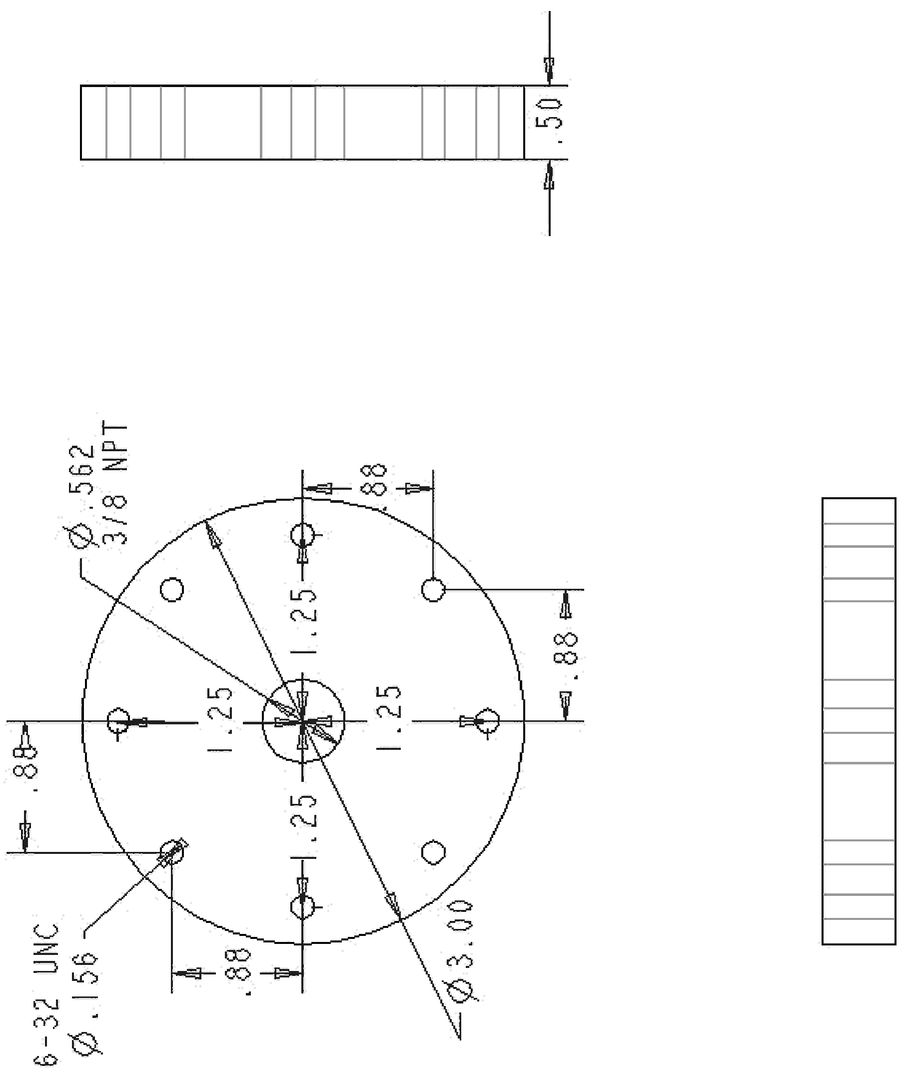

Figure 67. Bottom Plate, Plexiglas

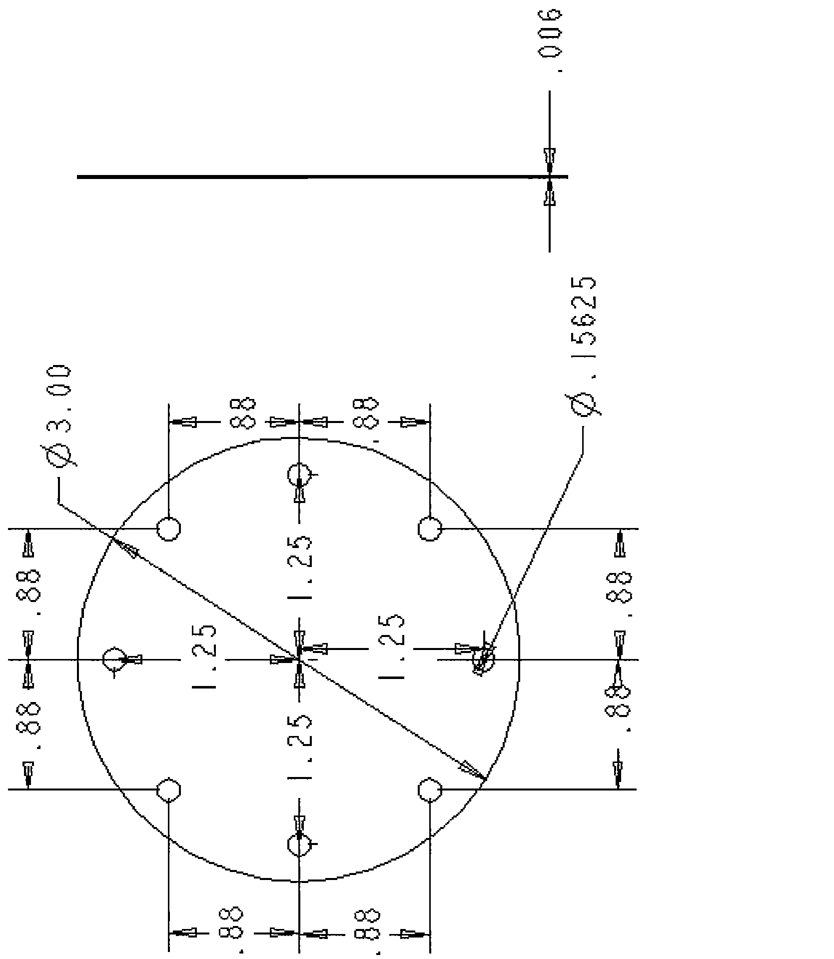

Figure 68. Diaphragm Section

BIBLIOGRAPHY

BIBLIOGRAPHY

1. Xu,C., Akiyama, M., Nonaka, K., Shobu, K., and Watanabe, T., **Electrical Output Performance of PZT-Based Piezoelectric Ceramics**, IEEE 1996,pp.967-970

2. Josheph M. Crowley, Christopher Snelling and Dale R. Mashtare, **Output Characteristics of a Xeromorph High-Voltage Generator**, Journal of Electrostatics, Vol.42, Issues1-2, October 1997, PP. 33-42

3. Durkan,C., Welland,M.E., Chu,D.P., Migliorato,P., **Scaling of piezoelectric properties in nanometre to micrometre scale**, Electronics Letters, Vol.36, Issue 18, Auguest 2000, PP. 1538-1539

4. Chao-Nan Xu, Morito Akiyama, Kazuhiro Nonaka, and Tadahiko Watanabe, **Electrical Power Generation Characteristics of PZT Piezoelectric Ceramics**, IEEE Trans. Ultrason.,Vol.,45, No.4, July 1998,pp1065-1998

5. Kymissis, J., Kendall, C., Paradiso, J., Gershenfeld, N., **Parasitic Power Harvesting in Shoes**, Wearable Computers, 1998. Digest of Papers. Second International Symposium on , 1998, pp132-139

6. Goldfarb, M.., Jones, L.D. **On the Efficiency of Electric Power Generation with Piezoelectric Ceramic**, To appear in the ASME Journal of Dynamic System, Measurement, and Control, Version: May 6, 1999

7. Shenck, N., **A Demonstration of Useful Electric Energy Generation from Piezoceramics in a Shoe**, MS Thesis, Dept. of Electric Engineering and Computer Science, Massachusetts Institute of Technology, April 1998

8. Engel, T.G., Nunnally, W.C., and VanKirk,N.B., **COMPACT KINETIC-TO-ELECTRICAL ENERGY CONVERSION**, Pulsed Power Conference, 1997.Digest of Technical Papers. 1997 11th IEEE International, Volume: 2 , 1997. PP.1503-1507

9. IEEE standard 176, **IEEE Standards on Piezoelectricity**, The Institute of Electrical and Electronics Engineers, 1978

10. Levy, G.C.; Hunt, T.K.; Sievers, R.K., **AMTEC: current status and vision**, Energy Conversion Engineering Conference, 1997. IECEC-97., Proceedings of the 32nd Intersociety , 1997, PP.1152-1155

11. Johnson, G.; Hunt, M.E.; Determan, W.R.; HoSang, P.A.; Ivanenok, J.; Schuller, M., **Design and integration of a solar AMTEC power system with an advanced global positioning satellite**, IEEE Aerospace and Electronics Systems Magazine , Volume: 12 Issue: 2 , Feb. 1997,PP.33-40

12. Rowe, D.M., **Miniature Semiconductor Thermoelectric Devices**, Handbook of Thermoelectrics, CRC Press, 441,1995

13. Kishi,M., Yoshida,Y.,Okano,H., **Fabrication of miniature thermoelectric module with elements composed of sintered Bi-Te compound**, Proceedings of 16th International Conference on Thermoelectrics, IEEE, Dresden, 1997, pp.653-656

14. Kiely,J.H., Morgan,D.V. and Rowe,D.M., **The design and fabrication of a miniature themoelectric generator using MOS processing techniques**, Meas. Sci. Technol. V.8, 1994, pp182-189

15. Stolzer,M.,Stordeur,M. and Stark,I., **Optimization of p-$(Bi_{0.25}SB_{0.75})_2Te_3$ and n-$Bi_2(Te_{0.9}Se_{0.1})_3$ Films for Thermoelectric Thin Film Components**, Proceedings of 2nd Symposium on Thermoelectrics - Materials, Processing Techniques and Applications, FAT, Dresden, 1994, pp.81-85

16. Glosch, H., Ashauer,M.,Pfeiffer,U. and Lang,W., **A Thermoelectric converter for energy supply**,Sensors and Actuators v.74, 1999, pp.246-250

17. Coutts,T.J., Wanlass, M.W., Ward, J.S., and Johnson, S., **A Review of Recent Advances in Thermophotovoltaics**, Photovoltaic Specialists Conference, Conference Record of the Twenty Fifth IEEE , 1996, PP.25-30

18. Fry, D., Holcomb,D., Munro,J., Oakes,L., and Maston, M., **Compact Portable Electric Power Sources**, Oak Ridge National Laboratory, ORNL/TM-13360, 1997

19. Zelenka, J., **Piezoelectric resonators and their applications**, New York, Elsevier, 1986.

20. Vinson, J.R., **Structural Mechanics: The Behavior of Plates and Shells**, A Wiley-Interscience publication, 1974

21. Starner, Thad. "**Human-Powered Wearable Computing**" *IBM Systems Journal* Vol. 35, 1996, pp. 618-629

22. Stark, I.; Stordeur, M., **New micro thermoelectric devices based on bismuth telluride-type thin solid films,** Thermoelectrics, 1999. Eighteenth International Conference on, 1999, pp: 465 -472

23. Ohta, T., **Energy technology: sources, systems, and frontier conversion**, 1st ED, PERGAMON, 1994

24. Wang, Q. M., Cross, L. E., **Constitutive Equations of Symmetrical Triple Layer Piezoelectric Benders**, IEEE Transactions on Ultrasonics, Ferroelectrics, and Frequency control, Vol. 46, No.6, 1999, pp.1343-1351

25. Wang, Q. M., Du, X. H., Xu, B. Cross, L.E., **Theoretical analysis of the sensor effect of cantilever piezoelectric benders**, Journal of Applied Physics, Vol.85, No.3, 1999, pp. 1702-1712

26. Wang, Q. M., Du, X. H., Xu, B. Cross, L.E., **Electromechanical Coupling and Output Efficiency of Piezoelectric Bending Actuators**, IEEE Transactions on Ultrasonics, Ferroelectrics, and Frequency control, Vol. 46, No.3, 1999, pp.638-646

27. Smits, J. G., Choi, W., **The Constituent Equations of Piezoelectric Heterogeneous Bimorphs**, IEEE Transactions on Ultrasonics, Ferroelectrics, and Frequency control, Vol. 38, No.3, 1991, pp. 256-270

28. Smits, J. G., **Dynamic Admittance Matrix of Piezoelectric Cantilever Bimorphs**, Journal of Microelectromechanical systems, Vol.3, No.3, pp:105-112, 1994

29. Mason, W. P., **Electrostrictive Effect in Barium Titanate Ceramics**, Physical Review, Vol. 74, No. 9, 1948, pp.1134-1147

30. Mandurino. P., Bianc. G. B., Garbin, R., **Energy Recovering PZT-Panel for Noise Reduction: Numerical Analysis for Fully Coupled Fluid-PZT Structure-Electric Interaction, Experimental Verification**, SPIE 8th annual international conference on Smart structures and smart materials, Los Angeles, CA., 2001, March, 4-8

31. Schmidt, V.H., **Piezoelectric Energy Conversion in Windmills**, Ultrasonics symposium, 1992, pp.897-904

32. Stone, K.W., Drubka, R.E., Kusek, S.M., **A Space Solar Thermophtovoltaic Power System, Energy conversion engineering conference**, Vol.2, 1996, pp 1001-1006